UNIVERSITÀ DELLA CALABRIA

Dipartimento di Chimica
CHIM/03 Chimica Generale e Inorganica

Scuola Dottorale Scienza e Tecnica "Bernardino Telesio"
Metodologie Chimiche Inorganiche (ICM) - XXV Ciclo

Tesi di Dottorato

Applicazioni Bio-Mediche di Composti di Coordinazione: uno Studio Fotofisico

SUPERVISORE
Dr. Massimo LA DEDA

CANDIDATA
Loredana RICCIARDI

COORDINATORE DEL CURRICULUM
Prof. Nino RUSSO

DIRETTORE DELLA SCUOLA
Prof. Roberto BARTOLINO

Anno Accademico 2011-2012

UNIVERSITY OF CALABRIA

Department of Chemistry
CHIM/03 General and Inorganic Chemistry

Bernardino Telesio - Doctorate School of Science and Technique
Inorganic Chemistry Methods (ICM) - XXV Cycle

PhD Thesis

Bio-Medicinal Applications of Coordination Compounds: a Photophysical Point of View

SUPERVISOR
Dr. Massimo LA DEDA

PhD CANDIDATE
Loredana RICCIARDI

CURRICULUM COORDINATOR
Prof. Nino RUSSO

SCHOOL DIRECTOR
Prof. Roberto BARTOLINO

Academic Year 2011-2012

Sommario

Il presente lavoro di ricerca, svolto presso il Laboratorio di Chimica Inorganica e di Coordinazione (LaCIC) dell'Università della Calabria, sotto la supervisione del Dott. Massimo La Deda, e in parte nel Laboratoire de Physico-Chimie des Matériaux Luminescents (Université Claude Bernard, Lyon, France), si colloca all'interfaccia tra la Biomedicina, la Chimica di Coordinazione e la Fotochimica, alla ricerca di un comune denominatore.

L'obiettivo del nostro lavoro è stato quello di sviluppare una metodologia ed un set-up sperimentale per collegare l'esperienza del LaCIC nella sintesi organometallica, con le applicazioni di composti di coordinazione in campo biomedico.

Abbiamo scelto tre aree di ricerca in grado di mettere in evidenza la relazione tra "composti di coordinazione", "luce" e "biomedicina": l'applicazione di complessi metallici incapsulati in polimeri o in nanoparticelle di oro e silice per la generazione di ossigeno di singoletto nella Terapia Fotodinamica (Capitoli 3 e 4), l'utilizzo dei processi a trasferimento di energia che coinvolgono i composti di coordinazione per lo studio delle interazioni farmaco-proteina (applicazioni di “sensing”, capitolo 2), l'utilizzo della luminescenza di nanoparticelle contenenti complessi di metalli di transizione nell’imaging cellulare.

Le proprietà uniche dei composti metallici, soprattutto la rilevante fotochimica e fotofisica dei composti di metalli di transizione, li rendono idonei per applicazioni in fotomedicina.

Capitolo 2 - Applicazione di “sensing” dei composti di coordinazione: interazione farmaco-proteina. Un nuovo complesso di zinco, recentemente sintetizzato presso il LaCIC, ha evidenziato un’interessante attività antiproliferativa *in vitro* nei confronti di alcune linee cellulari tumorali. Tuttavia, i test *in vitro* rappresentano solo il primo step per l’applicazione di questo complesso come farmaco antineoplastico; una fase successiva richiede uno studio della sua biodistribuzione, dunque la sua interazione con biomolecole quali l’ Albumina sierica umana, la proteina più abbondante presente nel torrente circolatorio, la quale aumenta la solubilità di farmaci idrofobici nel plasma e ne modula il rilascio a livello cellulare.

Grazie alla fluorescenza della proteina, è stato possibile studiarne il fenomeno di quenching della luminescenza, correlandolo all'interazione di legame con il complesso metallico. Inoltre, la "struttura speciale" del composto di coordinazione, la sua luminescenza intrinseca, ha reso possibile lo studio dell'interazione di legame da un'altra prospettiva, giungendo ad una interessante conclusione, che evidenzia l'aspetto multifattoriale del complesso: terapeutico e sensoristico.

Capitolo 3 - Processi attivati dalla luce in composti di coordinazione: fotogenerazione di ossigeno di singoletto. La Terapia Fotodinamica (PDT) fa riferimento all'applicazione di luce al fine di ottenere un effetto terapeutico, in particolare fa riferimento alla capacità di fotogenerare $^1O_2$, una specie altamente reattiva (il "vero" agente terapeutico) da una molecola cosiddetta "fotosensibilizzante". Tra gli effetti terapeutici dell' $^1O_2$ si pongono in evidenza la terapia antimicrobica e, soprattutto, la terapia antitumorale: in entrambe è preferibilmente richiesto l'utilizzo di fotosensibilizzanti solubili in acqua.

I Complessi di Metalli di Transizione (TMC), grazie alle loro "speciali" proprietà fotofisiche, sono fotosensibilizzanti eccellenti, ma per la maggior parte scarsamente idrofilici. Per rendere TMC solubili in acqua si può procedere per esempio inserendoli in un polimero biocompatibile, senza che gli stessi perdino la loro capacità di generare ossigeno di singoletto. Seguendo questo criterio, è stato sintetizzato e caratterizzato il primo esempio di un polimero solubile in acqua legante un complesso di Pt(II) in grado di generare ossigeno di singoletto.

Capitolo 4 - Il paradigma "theranostic": complessi di metalli di transizione e nanoparticelle. Un'altra alternativa per ottenere un fotosensibilizzante solubile in acqua con le "speciali" proprietà dei TMC è di incapsularlo all'interno di nanoparticelle (NPs), le quali stanno sempre più acquisendo una crescente importanza in ambito medico, grazie alla capacità di agire da sistema di rilascio e alla loro bassa tossicità.

Su questa base, sono state sintetizzate e caratterizzate un certo numero di NPs aventi un "core" d'oro e una "shell" di silice con intrappolati nella matrice complessi di Ir (III) e Ru (II), aventi la capacità di generare ossigeno di singoletto. Come prova preliminare, un campione di NPs contenenti un complesso di Ru (II), è stato

caratterizzato *in vitro* per valutarne la citotossicità in diverse linee di cellule tumorali, con risultati promettenti.

Inoltre, le "speciali" proprietà fotofisiche dei TMC consentono una disattivazione non radiativa degli stati eccitati (fenomeno necessario per la generazione di $^1O_2$ mediante un processo a trasferimento di energia) senza perdere la luminescenza. In virtù di questo, è stato possibile localizzare le NPs fotosensibilizzanti all'interno della cellula mediante microscopia a fluorescenza, rendendo le NPs sintetizzate un nuovo materiale per “theranostic purposes”.

BIO-MEDICINAL APPLICATIONS OF COORDINATION COMPOUNDS: A PHOTOPHYSICAL POINT OF VIEW

Chapter 1 INTRODUCTION

A glance at the Thesis: scope and limitations

The present book collects the principal results obtained during the three-year PhD course in Inorganic Chemistry Methods at the “Bernardino Telesio” Doctorate School (Cosenza, Italy). The research work, performed in the Laboratory of Inorganic and Coordination Chemistry (LaCIC) of University of Calabria under the supervision of Dr. Massimo La Deda, and partially in the Laboratoire de Physico-Chimie des Matériaux Luminescents (Université Claude Bernard, Lyon, France), lies at the interface between biomedicine, coordination chemistry and photochemistry, looking for a common denominator of these three fields. This has been identified in the light, as a carrier of energy and information. We have tried to highlight the role of coordination compounds in their dual aspect of sensors and therapeutic agents in photomedicine, where you try to use the light for healing. More modestly, the goal of our work was to develop a methodology and an experimental set-up in order to connect up the experience of LaCIC in the organometallic synthesis with the applications of coordination compounds in biomedical field.

We have choose three areas of research able to demonstrate the link between "coordination compounds", "light" and "biomedicine": the application of metal complexes entrapped in polymers or gold-silica nanoparticles in the generation of singlet oxygen in photodynamic therapy (Cancer PDT and Antimicrobial PDT, Chapters 3 and 4); the use of coordination compounds energy-transfer aptitude for the study of drug-protein interaction (sensing applications, Chapter 2); the use of the luminescence of nanoparticles encapsulating transition metal complexes in cell imaging.

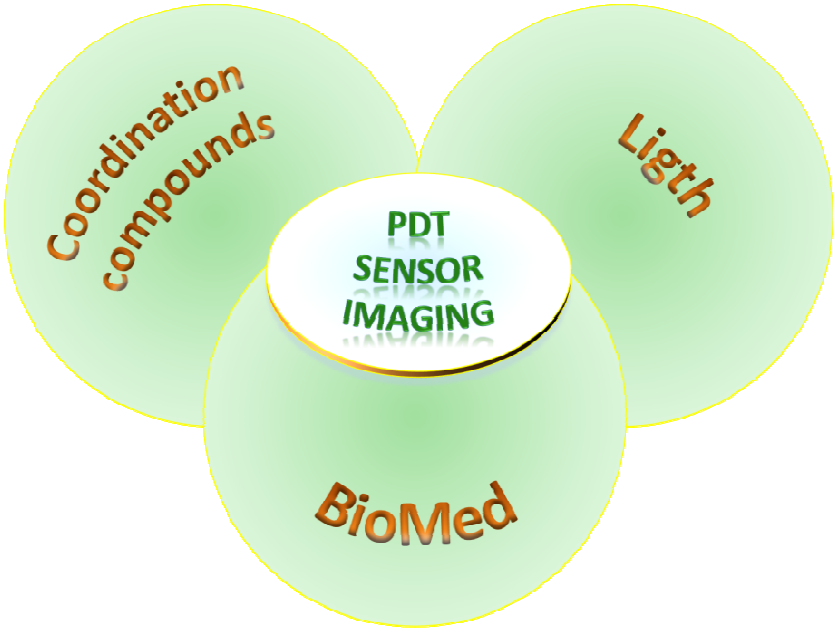

Metallopharmaceuticals: the special properties of Coordination Compounds

Metals are essential cellular components selected by nature to function in several indispensable biochemical processes for living organisms. Metals are endowed with unique characteristics that include redox activity, variable coordination modes, and reactivity towards organic substrates. Due to their reactivity, metals are tightly regulated under normal conditions and aberrant metal ion concentrations are associated with various pathological disorders, including cancer. The use of metals and their salts for medicinal purposes, from iatrochemistry to modern day, has been present throughout human history. In particular, the discovery of platinum anticancer drugs and the appearance of organ specific diagnostic-imaging agents containing technetium were prominent developments that have stimulated further interest in so-called "metallopharmaceuticals". Today, the metallopharmaceuticals industry has a global market measured in billions of euros and has well-established applications in both diagnostic and therapeutic medicine.

Metal ions or metal compounds important for our health are of both endogenous and exogenous origin. Endogenous metal compounds are required for many critical

processes such as respiration, much of metabolism, development, neural transmission, muscle contraction, signal transduction, gene expression, protection against toxic and mutagenic agents. Exogenous compound can be introduced into the organism through the diet, via interaction with the environment, or in order to induce a predetermined alteration of the system. It is notable that some organic pharmaceuticals or pollutants may be directed toward metal targets in the body or require metal binding to function.

Coordination compounds are the most suitable chemicals to use the metal special properties through chemical design, so that coordination chemistry plays a significant role in the development of metallopharmaceuticals involving metals, especially transition metals. Coordination compounds allow for the synthesis of structures with unique stereochemistry and orientation of organic ligands and structures which are not accessible through purely organic, carbon-based compounds. The kinetic inertness of the coordination/organometallic bonds make these compounds in principle similar to organic compounds. This approach immensely expands the ability to chart biologically-relevant chemical space.

A coordination compound is a sort of multifunctional agent in which, by a proper choice of metal and ligands, it is possible to conjugate a variety of properties inaccessible to single molecule. The importance of ligands in modifying the biological effects of metal-based drugs cannot be overestimated. Ligands can modify the oral/systemic bioavailability of metal ions, can assist in targeting specific tissues or enzymes; can deliver, protect, or sequester a particular metal ion, depending on the requirements, for therapy or diagnosis. Ligands can also ensure protection of tissues from toxic metal ions or, in a contrasting strategy, enhance uptake of pharmacologically beneficial metal ions. In this way, the properties of a coordination compound are something more than the simple sum of the properties of the ligand and metal. The concept of the metal as scaffold for the construction of unique, yet well-defined three-dimensional structures, rather than reactive centre, holds much promise. This highly modular approach, combined with currently available combinatorial techniques and knowledge of supramolecular chemistry, yields a very powerful method for optimizing drug interactions with carefully selected targets.

Supramolecular systems are constituted of a number of discrete molecular components with definite individual properties held together by various interactions. In natural systems the molecular components are very often assembled by intermolecular forces (hydrogen bonds, donor-acceptor interactions, van der Waals forces, etc.), whereas in artificial systems covalent or coordination bonds are used to achieve a better control of the supramolecular structure. The development of supramolecular chemistry has allowed construction of structurally organized and functionally integrated chemical systems capable of elaborating the energy and information input photons to perform complex functions. During the past decade research on transition metal supramolecular systems has experienced extraordinary progress. In terms of bonding strength, the moderate coordination bonds between transition metals and ligands are between strong covalent bonding in carbon-based systems and weak interactions in biological systems. Some advantages of employing transition metals to build supramolecular systems include the following: (i) involvement of d orbitals which offer more bonding modes and geometric symmetries than simple organic molecules; (ii) a range of electronic and steric properties which can be fine-tuned by employing various ancillary ligands; (iii) easily modified size of the desired supramolecules by utilizing various lengths of bridging ligands; and (iv) incorporation of their distinct spectral, magnetic, redox, photophysical, and photochemical properties.

The (special) photochemical properties of Coordination Compounds offered to biomed

Light can be used to alter the electronic structure of molecules, inducing changes in both physical and chemical properties. The excited state which is generated is typically short-lived; however, as the molecule returns to the ground state, the energy can be dissipated in a wide variety of ways, in the form of light or heat, a chemical modification of the structure or transfer of energy to another species.

Luminescent transition metal complexes possess many useful photophysical and photochemical properties that enable them to serve as unique biological labels and probes. First, many transition metal complexes, especially those with a charge-transfer excited state, show intense and long-lived emission in the visible region,

which is an advantage for detection and imaging studies. Although numerous organic compounds also exhibit intense emission in the visible region, their lifetimes are very short due to their singlet excited state. Thus, background interference in the samples cannot be easily removed by time-resolved detection. Förster-type resonance energy transfer (RET) quenching is commonly employed to study interactions between biological molecules because the range of usual Förster distances is similar to the dimensions of common biomolecules. Fluorescent organic labels in these studies rely essentially on steady-state emission measurements. The longer excited-state lifetimes of transition metal complexes mean that RET quenching can be readily examined by lifetime measurements as an additional monitoring method. Furthermore, metal complexes of long excited-state lifetimes are attractive candidates in the development of new anisotropic probes to study the hydrodynamics of proteins and new assays involving high-molecular antigens and antibodies. A number of transition metal complexes exhibit rich photoredox properties, which allow studies of photocleavage of DNA and photoinduced electron-transfer reactions in metalloproteins. Most importantly, the choice of various metal centres and a wide range of ligands renders it possible to fine-tune the ground-state and excited-state redox potentials of transition metal complexes, which facilitates the development of new photoredox-active biological labelling reagents and probes in specific investigations. Additionally, many transition metal complexes respond sensitively to their local environment, and can thus serve as luminescent reporters of their surroundings. In particular, complexes with a charge-transfer excited state usually show significant changes in their emission energy, intensities and lifetimes in different media. These favorable properties enable the complexes to act as luminescent molecular probes to report biomolecular recognitions that are associated with a change of hydrophobicity. Furthermore, owing to the phosphorescent nature of most luminescent transition metal complexes, their Stokes shifts are much larger than those of the organic fluorophores. Thus, biological molecules can be multiply labelled with metal complexes without reduced fluorescence intensities due to self-quenching, which often occurs in organic fluorophores.

In contrast to organic species, metals have excited states that are often easily accessible by irradiation with visible and UVA light. Transition metal complexes with d^6 and d^8 electronic configurations are particularly promising, due to the favorable photophysical properties and the relative non-lability of complexes with these configurations. In particular, d^6 transition metal complexes can be used to exemplify the diversity of excited states that can be generated by light excitation, and the chemistry that is associated with their generation. Excitation leads to electronically- and vibrationally-excited states with the same multiplicity as the ground state. The transitions to the excited electronic states are formally classified according to the character of the orbitals involved in the electronic transition:

- *Metal-centred (MC) transitions, i.e. d-d or ligand-field (LF) transitions.* These are orbitally (Laporte)-forbidden, and can also be spin-forbidden if the spin state changes. Consequently, they give rise to weak absorptions (ε ~ 1-20 x 10^3 $M^{-1}cm^{-1}$) which can be masked by stronger, formally allowed charge-transfer transitions. Since MC transitions typically populate antibonding orbitals, the excited states generated often lead to bond lengthening and favor ligand substitution. Photochemical lability is commonly a feature of complexes in which a MC excited state is lowest in energy, such as those metal complexes which photorelease a bioactive molecule (*e.g.* CO, NO).

- *Charge-transfer (CT) transitions, metal-to-ligand (MLCT), ligand-to-metal (LMCT) or to-solvent (TS).* These give rise to more intense transitions (typically ε ~ 1-100 x 10^3 $M^{-1}cm^{-1}$) and can lead to redox reactions (of both the complex and molecules in the local environment *e.g.* solvent) and also result in homolytic bond cleavage, reducing the metal centre and generating radicals. Production of radicals under biological conditions is a well established mechanism for causing damage to cellular components (*e.g.* DNA).

- *Ligand-centred (LC) transitions, or interligand (IL) transitions*. These generally involve only ligand-centered orbitals and are often seen in large delocalized systems.

Once these excited states are generated they can undergo a series of physical radiationless processes which ultimately lead to the ground-state electronic structure: intersystem crossing (ISC), internal conversion (IC) vibrational relaxation, intramolecular vibrational redistribution and solvation dynamics (reorganization of solvent shells). Radiative processes such as fluorescence (singlet–singlet) and phosphorescence (triplet–singlet) result in a return to the ground state, with emission of light of longer wavelength than was used for the excitation. Beside these monomolecular radiative or non-radiative processes, an excited state can undergo a bimolecular process involving a ground-state molecule that receives the energy content of the excited molecule. Fluorescence RET quenching is an example.

The unique properties of metal compounds, especially very rich photochemistry and photophysics of transition-metal compounds, make them suitable candidates for selected applications in photomedicine.

The Thesis in a nutshell

The use of metal compounds in bio-medicine explored in the present work concerns the properties of their excited states; as above mentioned an excited state deactives along two paths: a non radiative decay and/or a radiative decay.

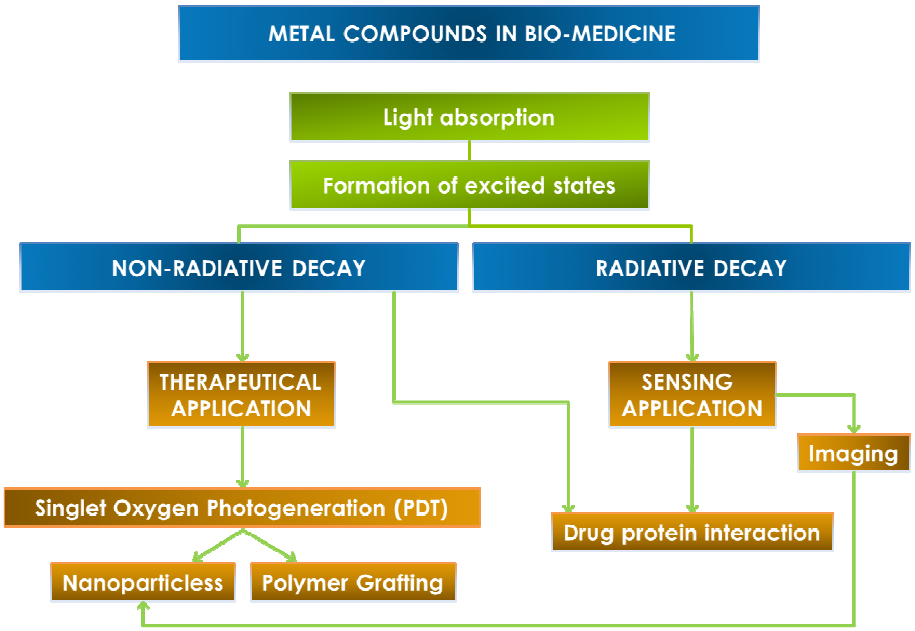

Chapter 2 - Sensoristic applications of coordination compounds: drug-protein interaction. A new zinc complex, recently synthesized in the LaCIC, showed interestingly *in vitro* cytotoxic properties versus some types of tumor cells. Nevertheless, the *in vitro* test is only the first step to propose this complex as antineoplastic drug; a successive step is to study its biodistribution. Unfortunately, this Zn complex is scarcely water soluble, so a way to reach a good bioavailability is through its interaction with Human Serum Albumin, the most abundant protein in the bloodstream that increases the solubility of hydrophobic drugs in plasma and modulates their delivery to cell *in vivo*.

Thanks to the protein fluorescence, it was possible to study its luminescence quenching correlating it to the binding interaction with the Zn complex, and to determine the bimolecular rate constant value, which account for a static quenching. But, the "special property" of the zinc coordination compound, its intrinsic luminescence, has made possible to study the binding interaction from another point of view, with interesting conclusion, that highlight the multifactorial aspect of the complex: therapeutical and sensoristic.

Chapter 3 - Light-activated processes in coordination compounds: photogeneration of singlet oxygen. Photodynamic Therapy (PDT) refers to the application of light

to obtain a therapeutical effect; more precisely it refers to the ability of photogenerate the highly reactive species $^1O_2$ (which is the "true" therapeutical agent) by a molecule called photosensitizer. Among the therapeutical effect exerted by $^1O_2$ there are an antimicrobial therapy and, above all, an anticancer therapy: both prefer water soluble photosensitizer.

Transition metal complexes (TMC), due to their "special" photophysical properties, are excellent photosensitizers, but many of them are scarcely hydrophilic. A way of making TMC water soluble can be to entrap them into a biocompatible polymer, without losing their capacity to generate singlet oxygen. Following this criterion, it was synthesized and characterized the first example of a water soluble polymer grafting a Pt(II) complex able to generate singlet oxygen.

Chapter 4 - The theranostic paradigm: transition metal complexes and nanoparticles.

Another way to obtain a water soluble photosensitizer with the "special" properties of TMCs, is to entrap them into nanoparticles (NP). Nanoparticles are having an increasing importance in the medical field, deserving a new branch of medicine, the so-called "nanomedicine". This is due to the ability of the NPs to have a little toxicity and to act as drug-delivery system. Moreover, gold NP carried out therapeutical effect thanks to the intriguing properties of the gold plasmon (photothermal therapy).

On this basis, it was synthesised and characterized a number of silica-shell/gold-core NPs entrapping Ir(III) and Ru(II) complexes, which show qualitative ability to generate singlet oxygen. As preliminary test, a sample of gold-silica NP entrapping a Ru(II) complex was characterized in vitro to measure the cytotoxicity against tumor cells, giving promising results.

Moreover, the "special" photophysical properties of TMCs allow having non-radiative deactivation of the excited states (necessary to generate $^1O_2$ by energy transfer process) without losing luminescence. By virtue of this, it was possible to localize the photosensitizing NPs inside the cell by fluorescence microscope, making the synthesized NPs a new material for theranostic purposes.

Chapter 2 SENSORISTIC APPLICATIONS OF COORDINATION COMPOUNDS: DRUG-PROTEIN INTERACTION

2.1 Coordination Compounds in Cancer Therapy

Medicinal inorganic chemistry (Hambley 2007; Orvig 1999; Guo 1999) is a field of increasing prominence as metal-based compounds offer possibilities for the design of therapeutic agents not readily available to organic compounds. The wide range of coordination numbers and geometries, accessible redox states, thermodynamic and kinetic characteristics, and the intrinsic properties of the cationic metal ion and ligand itself offer the medicinal chemist a wide spectrum of reactivities that can be exploited. Although metals have long been used for medicinal purposes in a more or less empirical fashion (Thompson 2006), the potential of metal-based anticancer agents has only been fully realized and explored since the landmark discovery of the biological activity of cisplatin, *cis*-$(NH_3)_2Pt(Cl)_2$. To date, this prototypical anticancer drug remains one of the most effective chemotherapeutic agents in clinical use.

Early investigations on the action mechanism of cisplatin suggested a formation of an adduct with nuclear DNA by a covalent bond of the metal complex with two adjacent guanines on the same DNA strand (Fig. 1) that, causing a distortions in the DNA structure, interfere with replication, triggering cellular events that lead to the death of cancer cell (Wang 2005).

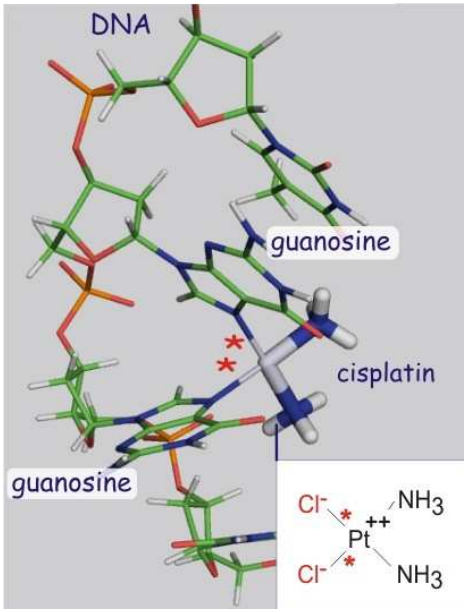

Figure 1. DNA and cisplatin form an adduct leaving two amino groups coordinated to the platinum atom.

Cisplatin is particularly active against testicular cancer and, if tumours are discovered early, an impressive cure rate of nearly 100% is achieved. Besides cisplatin, several other platinum complexes (carboplatin, oxaliplatin and more recently, picoplatin and satraplatin) have been screened as potential antitumor agents (Kelland 2007); however, it must be noted that only a limited number of tumours can be treated with platinum-based anti-cancer drugs. Moreover they produce several side effects including bone marrow suppression, neurotoxicity and above all nephrotoxicity (Jung 2007). In fact, platinum complexes are known to react not only with DNA but also with many other cell components such as glutathione and other sulphur-containing biomolecules, present in relatively high doses inside the cell, and recent studies have shown that the inactivation of the thiol-containing enzymes causes serious side effects in the kidney. In addition to the high systemic toxicity, inherent or acquired resistance is a second problem often associated with platinum-based drugs, with further limits their clinical use (Galanski 2005). Much effort has been devoted to the development of new platinum drugs and the elucidation of cellular responses to them to alleviate these limitations (van Zutphen 2005; Bruijnincx 2008).

These unresolved disadvantages stimulate research on the development of novel non-platinum metal complexes as anticancer agents, with mechanisms of action different

from cisplatin, *i.e.* based on non-covalent interactions with DNA, such as groove binding, insertion or intercalation. Ruthenium compounds, for example, are considered to be promising candidates for anticancer drug design, with two Ru(III) complexes already entered in clinical trials, NAMI-A and KP1019 (Fig. 2); these new octahedral complexes differ structurally from the square planar platinum (II) drugs, offering a more elaborate interaction with double-helical DNA, not only forming coordination bonds, but also H-bonds and intercalation between DNA base pairs (Peacock 2008). Despite modest cytotoxic activity, these complexes have attracted significant interest because of their ability to prevent the formation of metastases and inhibit their growth.

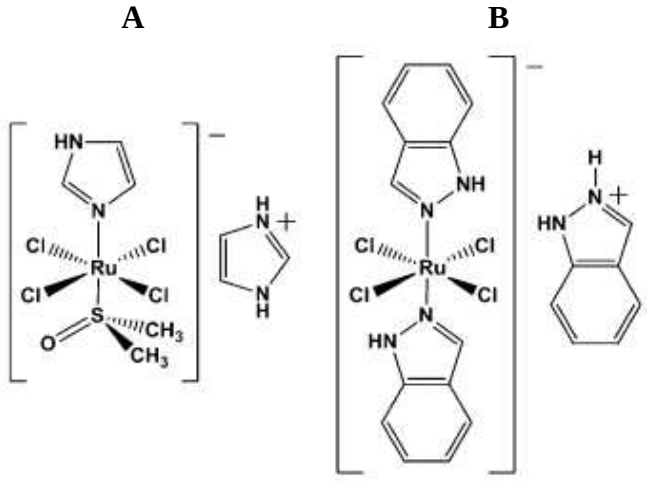

Figure 2. Structure formula of NAMI-A (**A**) and KP1019 (**B**).

Homoleptic complexes of Cu(II) and Zn(II) (Wang 2009) have proved to be great examples of intercalating metal compounds and, in addition, the presence of intrinsic fluorescence allows in a single molecule combination of anticancer properties with an excellent tool for investigating their mechanism of action through optical methods. Moreover, in the chemically diverse environment within an organism, issues of metal release can be very important as a complex will subject to a wide variety of enzymatic degradation processes. In this light, the use of zinc, for example, compared to other metals such as platinum, leads to a reduction of the correlated side-effects. In fact, as well known, zinc is an essential nutrient for all organisms, because it serves as a catalytic or structural cofactor for several proteins and is involved in the regulation of mitochondrial apoptosis of many mammalian cells (Franklin 2007; Franklin 2009).

Recently, it has been reported the synthesis, characterization, biological evaluation and mode of interaction with DNA of a heteroleptic pentacoordinated Zn(II) complex, (Bpy_9)Zn(Cur)(Cl), which bears a bipyridine functionalized in *para* position with an aliphatic 9-members chain as N,N'-donor ligand, and a curcumin (1,7-bis-(4-hydroxy-3-methoxyphenyl)-1,6-heptadienes-3,5-dione) as O,O chelating ligand (Fig. 3) showing promising anticancer properties (Pucci 2012). This complex exhibits an antiproliferative activity, observed *in vitro* against prostatic tumor cells, with an IC_{50} value of ~12 μM, very interesting compared to that of cisplatin (IC_{50}= 33). Moreover, the complex shows a significant green luminescence, and this property was useful to demonstrate some form of intercalation with the DNA helices. Unfortunately, (Bpy_9)Zn(Cur)(Cl) is insoluble in water, so the *in vitro* test was carried out in ethanol/water mixture; this can be a serious problem for any *in vivo* tests.

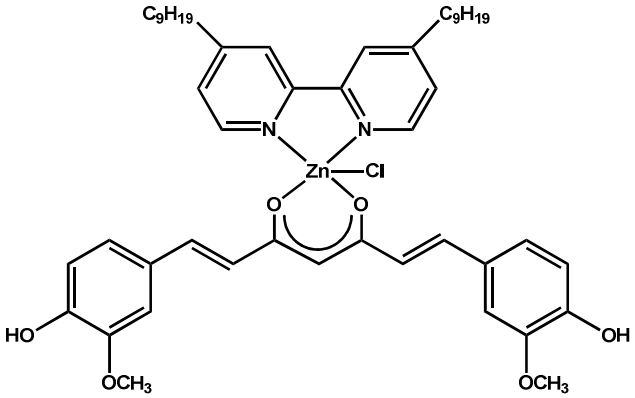

Figure 3. Structure formula of **(Bpy_9)Zn(Cur)(Cl)** complex.

The IC_{50} determination is only the first step to propose a drug for a clinical trial; very interesting is the study of the biochemical behaviour of a drug, including its interaction with blood plasma proteins, which would be the primary target molecules, when it is administered intravenously. In fact the determination of drug binding to plasma proteins (in particular serum albumins) is considered another important factor in pre-clinical drug studies (Zhou 2007; Sulkowska 2002; Yang 2007): this type of interaction can influence the drug stability and toxicity during the chemotherapeutic process; moreover, the adduct drug-plasma protein can overcome problem linked to a scarce water solubility of the drug (Kratz 2008).

2.2 The serum albumin proteins: a capital role in drug bioavailability

Human serum albumin (HSA) is the most abundant protein in the bloodstream, which constitutes up to 60% of the total protein and contributes for 80% to the colloid osmotic blood pressure maintenance (Carter 1994). One of its most extraordinary properties is the ability to bind reversibly a large variety of endogenous and exogenous ligands, such as nutrients, hormones, fatty acids, a great number of therapeutic drugs such as penicillins, sulfonamides, indole compounds, and benzodiazepines to name just a few (Peters 1996). In particular, it increases the solubility of hydrophobic drugs in plasma and modulates their delivery to cell *in vivo* and *in vitro* (Yue 2009). Consequently, binding to this protein controls the free, active concentration of a drug, provides a reservoir for a long duration of action, and strongly affects its absorption, metabolism, distribution and excretion.

HSA is a globular protein consisting of a single peptide chain of 585 amino acids (He 1992; Dugaiczyk 1982), with three structurally similar α-helical domains I-III, each containing two subdomains A and B. The crystal structure analyses indicate that the main regions of ligand binding sites in albumin are located in hydrophobic pockets in IIA and IIIA subdomains (Fig. 4A). These binding sites are known as Sudlow I and Sudlow II, respectively (Sudlow 1975; Sudlow 1976). HSA contains a single tryptophan residue (W214) within the hydrophobic binding pocket of subdomain IIA (Fig. 4B), which significantly contributes to the intrinsic fluorescence of the protein.

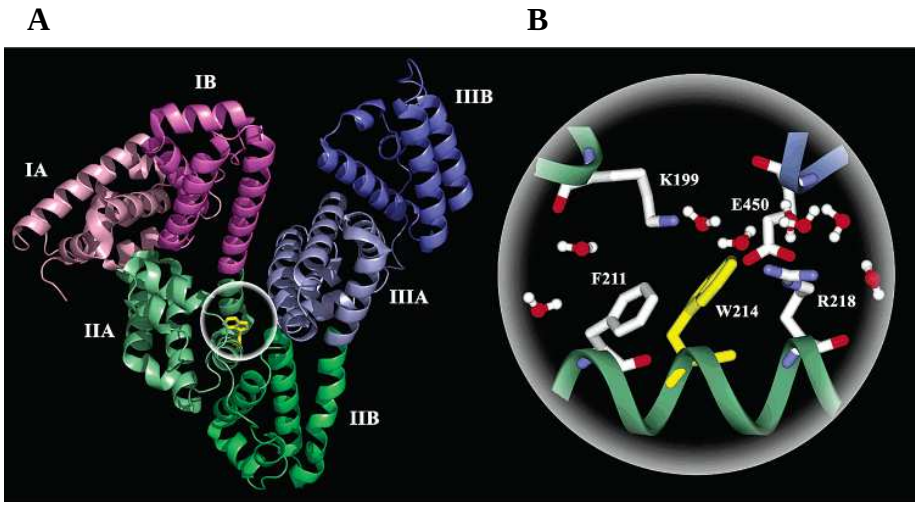

Figure 4. X-ray crystallographic structure of human serum albumin (**A**), and local configuration around the only one tryptophan residue (W214) of the protein (**B**) (Qiu 2006).

2.2.1 Protein fluorescence

Among biopolymers, proteins are unique in displaying useful intrinsic fluorescence. They contain three aromatic amino acids residues that contribute to their ultraviolet luminescence, phenylalanine, tyrosine and tryptophan, used as fluorescent probes for the investigation of protein conformation, structure and function (Lakowicz 2003). These chromophores have different absorption and emission spectra because of their structure (Fig. 5).

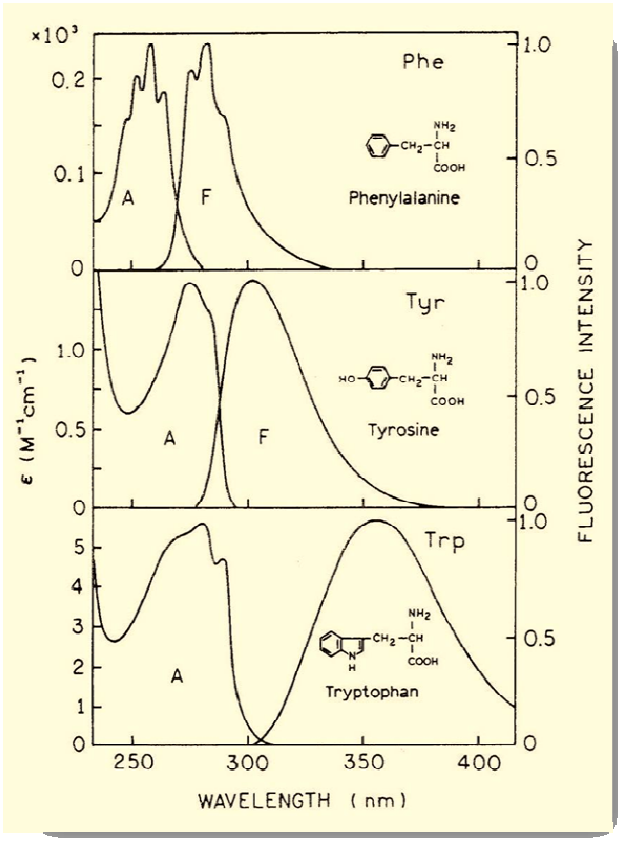

Figure 5. Absorption (A) and emission spectra (F) of the aromatic amino acids in pH 7 aqueous solution (Lakowicz 2003).

Due to tryptophan's largest extinction coefficient, highest quantum yield, and absorption at the longest wavelength, the fluorescence spectrum of a protein, containing the three amino acids, strongly resembles that of tryptophan. Indeed, because of their spectral properties, resonance energy transfer can occur from phenylalanine to tyrosine to tryptophan resulting in a reduced contribution of phenylalanine and tyrosine to the emission of proteins, dominated by the tryptophan residues.

The emission maximum of tryptophan in aqueous solution occurs around 350 nm (Fig. 5). This fluorescence signal, mainly due to the excitation and transition processes of π electrons in the benzene ring, is highly sensitive to the microenvironment with changes in response to protein conformational transitions, subunit association, substrate binding or denaturation.

In particular, as previously mentioned, the Human Serum Albumin has the advantage to have only one tryptophan residue, located in position 214 along the chain in the binding pocket of the subdomain IIA, which significantly contributes to the strong fluorescence of the protein (§ 2.4.1). Therefore, the fluorescence spectroscopy can easily reveal changes in the surrounding environment of tryptophan and be used for determining the binding affinities (Lakowicz 2003).

2.3 Drug-albumin interaction: the protein's fluorescence quenching as method of investigation

Many types of analytical methods can be applied to determine the binding constant of the drug-HSA interaction, but fluorescence spectroscopy offers many advantages (high sensitivity, rapidity and ease of implementation) over conventional techniques such as affinity and size exclusion chromatography, dialysis and ultrafiltration (Zhang 2008; Mandeville 2009; Yue 2009; Nanda 2007; Faridbod 2011; Qi 2008). It offers a simple method without needing to separate the bound and unbound molecule and this reduces the time required for the experiment and eliminates the need for a size selective membrane. In addition, dialysis and ultrafiltration cannot be used when the drugs bind extensively to the membrane, a frequent and serious problem with highly hydrophobic drugs. By measuring the intrinsic fluorescence quenching of HSA, the accessibility of quenchers to the fluorophore groups of HSA can be estimated. This information can help to predict the binding mechanisms of drug to human serum albumin.

Fluorescence quenching is a decrease in the quantum yield of fluorescence from a fluorophore induced by a variety of molecular interactions with quencher molecules. The different mechanisms of fluorescence quenching are usually classified as either **dynamic** or **static quenching**, the first resulting from collisional encounters between the fluorophore in the excited state and the quencher, the second resulting from the formation of a ground-state complex between the fluorophore and the quencher (Lakowicz 2003). In both cases, molecular contact is required between the fluorophore and the quencher for fluorescence quenching to occur. The application of fluorescence quenching as a technique can also reveal the accessibility of the

quenchers to the fluorophores.

Generally, the mechanism accepted to be responsible in fluorescence quenching of protein is the fluorescence resonance energy transfer (FRET). This process occurs whenever the emission spectrum of a fluorophore, called the donor (D), overlaps with the absorption spectrum of another molecule, called the acceptor (A). The extent of energy transfer is determined by the distance between the donor and the acceptor, and the extent of spectral overlap.

FRET usually occurs over distances comparable to the dimensions of most biological macromolecules, that is, about 10 to 100 Å. The following equations consider energy transfer between a single linked D/A pair separated by a fixed distance r and originate from the theoretical treatment of Forster (Lakowicz 2003). The energy transfer rate $k_T(r)$ between a single D/A pair is dependent on the distance r between D and A and can be expressed in terms of the Forster distance R_0.

$$k_T(r) = (1/\tau_D)\,(R_0/r)^6$$

τ_D is the lifetime of the donor in absence of energy transfer; R_0 is the distance between D and A at which 50% of the excited D molecules decay by energy transfer, while the other half decay through other radiative or non-radiative channels. R_0 can be calculated from the spectral properties of the D and A species:

$$R_0 = 9.78 \times 10^3\,[\kappa^2\, n^{-4}\, \Phi_D\, J(\lambda)]^{1/6} \quad \text{(in Å)}$$

The factor κ^2 describes the D/A transition dipole orientation and can range in value from 0 (perpendicular) to 4 (collinear/parallel). There has been much debate about which dipole orientation value to assign for particular FRET formats. Only in few cases the crystal structure of the D/A molecules can be determined; there is no other reliable experimental method to measure absolute or fixed κ^2 values, which leads to potential uncertainties in subsequent calculations (Lakowicz 2003). Fortunately, the accumulated evidence has shown that the mobility and statistical dynamics of the dye linker lead to a κ^2 value of approximately 2/3 in almost all biological formats. The refractive index *n* of the medium is ascribed a value of 1.4 for biomolecules in aqueous solution. Φ_D is the quantum yield of the donor in the absence of the acceptor

and J(λ) is the overlap integral, which represents the degree of spectral overlap between the donor emission and the acceptor absorption. The values for J(λ) and R_0 increase with higher acceptor extinction coefficients and greater overlap between the donor emission spectrum and the acceptor absorption spectrum.

There have already been several studies on the fluorescence quenching of HSA induced by the interaction with drugs (Faridbod 2011; Liu, X., 2009; Qi 2008; Trynda-Lemiesz 2010; Katrahalli 2010), small molecules (Zhang 2008; Mandeville 2009; Wu 2009; Nanda 2007; Trnková 2011) or metal complexes (Yue 2009; Wu 2010; Tarushi 2010; Divsalar 2009; Wu 2008). All experiments are performed by studying the decrease of the HSA fluorescence intensity by adding increasing amount of drugs that act as quencher. The fluorescence quenching data are analyzed using the Stern-Volmer equation:

$$F_D / F_{DA} = 1 + k_q \tau_D [Q]$$

where F_D and F_{DA} are the fluorescence intensities before and after the addition of the quencher Q, k_q is the bimolecular quenching rate constant and τ_D is the lifetime of the fluorophore in the absence of the quencher.

Just to remind some example, Faridbod et al. (2011) reported an interaction study of *pioglitazone* (a drug with hypoglycemic action) with albumin using fluorescence emission and UV-Vis absorption spectra. Experimental results revealed that this drug have an ability to quench the intrinsic fluorescence of HSA tryptophan residue through a static quenching mechanism. Fluorescence quenching data, analyzed by Stern-Volmer equation, give a binding constant value of 4.45×10^5 M^{-1} (at 300 K).

Most non steroidal anti-inflammatory drugs (NSAID) show a high degree of binding to albumin, which is a primary determinant of their pharmacokinetic properties (Trynda-Lemiesz 2010). The interaction of *meloxicam*, an NSAID, with HSA at physiological conditions (pH 7.4) was evaluated by measuring the intrinsic fluorescence intensity of protein before and after its addition. The strong quenching of the fluorescence clearly indicated that the binding of the drug to HSA changed the microenvironment of tryptophan residue and the tertiary structure of the protein.

The interaction between human serum albumin and *fluoxetine hydrochloride* (a psychotropic drug) have been studied by using different spectroscopic technique

(fluorescence, UV-vis absorption, circular dichroism) under simulated physiological conditions, and the fluorescence quenching analyses support a static mechanism (Katrahalli 2010). The study showed that the drug binds the protein most likely at the hydrophobic pocket located in subdomain IIA of site I. Fluorescence data give a binding constant value of 1.64×10^3 M^{-1} (at 300 K).

The HSA fluorescence quenching study (Mandeville 2009) was determinant to determine the binding constants K of *curcumin* and *genistein*, two molecules present in turmeric and in soybean, respectively, having a wide spectrum of physiological and pharmacological functions. Based on the spectroscopic results curcumin and genistein bind human serum albumin via both hydrophilic and hydrophobic interactions with stronger affinity for curcumin ($K_{curcumin} = 5.5 \times 10^4$ M^{-1}) than genistein ($K_{genistein} = 2.4 \times 10^4$ M^{-1}).

An accurate HSA-binding study of eight *catechins*, including the epigallocathechin gallate, contained in green tea, has been performed (Trnková 2011) by fluorescence quenching; a static mechanism was clarified, and the Stern-Volmer analyses give a series of binding constant values ranging from 0.34×10^4 to 10.57×10^4 M^{-1}, that were correlated to the chemical structures of the catachins: a balance between their hydrophilic hydroxyl groups and the aromatic moieties resulted determinant to give a good arrangement within the hydrophobic pocked of the albumin.

Instead, examples of HSA binding investigations with metal complexes are rare. Platinum complex oxaliplatin, an antineoplastic drug, show a binding constant of 3.3×10^3 M^{-1}, determined by Ster-Volmer analysis of the HSA fluorescence quenching , and a static mechanism was reported (Yue 2009). A study involving an antibacterial drug based on a zinc complex (Tarushi 2010) accounted for a static quenching mechanism with a binding constant of 6.9×10^4 M^{-1}.

2.4 Photophysical studies of a cytotoxic Zn(II) complex and Human Serum Albumin

The interaction of the (Bpy_9)Zn(Cur)(Cl) complex (Fig. 3) with Human Serum Albumin has been investigated by fluorescence spectroscopy. The emissive properties of the zinc complex allow possible to study the binding from a dual perspective: *(i)* the HSA fluorescence quenching, and *(ii)* the change of (Bpy_9)Zn(Cur)(Cl) intrinsic luminescence.

2.4.1 Photophysical characterization of Human Serum Albumin

The basic photophysics of HSA was studied by preparing a 4.4 x 10^{-6} M buffer solution (pH = 7.4) of the protein, purchased from Sigma-Aldrich (purity 96-99%). The buffer solution was prepared by dissolving phosphate buffer saline tablet (Sigma-Aldrich) in 200 mL of water. The applied general methods are reported on § Appendix.

The absorption spectrum of the buffer solution showed a maximum at 278 nm, and a strong fluorescence emission band at 345 nm was recorded by fixing the excitation wavelength at 280 nm, due to the HSA single tryptophan residue de-excitation (Fig. 6).

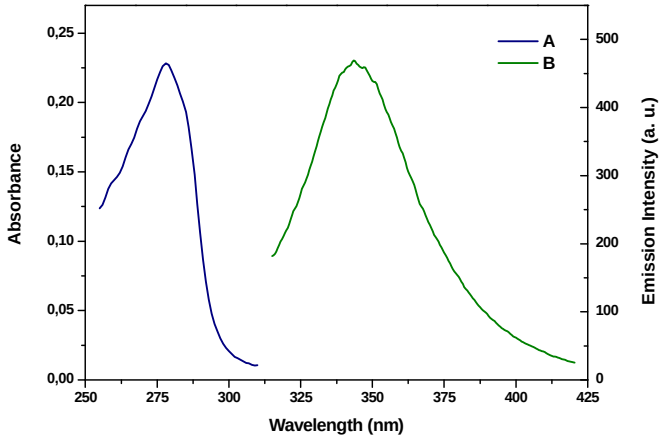

Figure 6. Absorption (**A**) and emission (**B**) spectra of HSA in buffer solution (pH = 7.4) at room temperature.

The emission quantum yield measurement, performed by optically-diluted method by using 2-aminopyridine in ethanol as standard (§ Appendix), gave $\Phi = 0.20$, while the excited-state decay profile (Fig. 7) was fitted by a biexponential function, giving an average lifetime of 5.71 ns (reduced $\chi^2 = 0.98$; § Appendix). A quick rise is noted in the first part of the time profile, which is due to rapid energy transfer occurring from phenylalanine to tyrosine to tryptophan (§ 2.2.1).

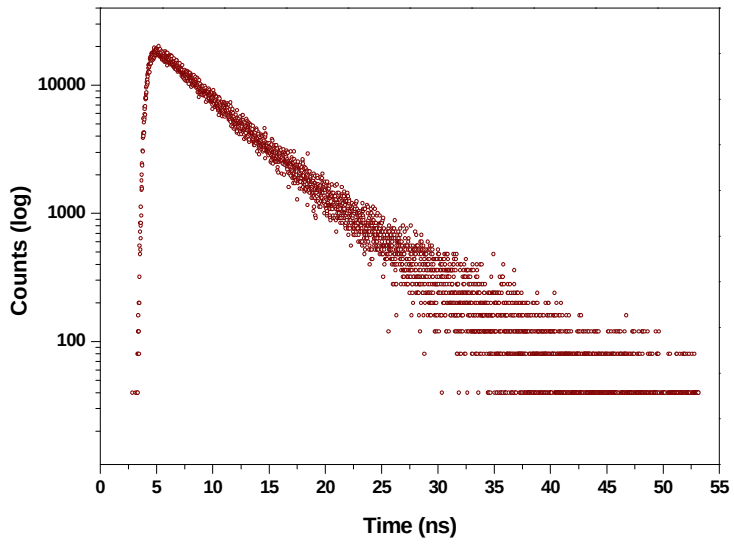

Figure 7. HSA in buffer solution (pH = 7.4): time-resolved fluorescence decay recorded at 345 nm upon irradiation by a 265 nm Nanoled (§ Appendix).

2.4.2 Photophysical characterization of $(Bpy_9)Zn(Cur)(Cl)$

The Zn(II) complex $(Bpy_9)Zn(Cur)(Cl)$, synthesized in the Laboratory of Inorganic and Coordination Chemistry (University of Calabria) by using the method reported in Scheme 1, was available from previous study (Pucci 2012).

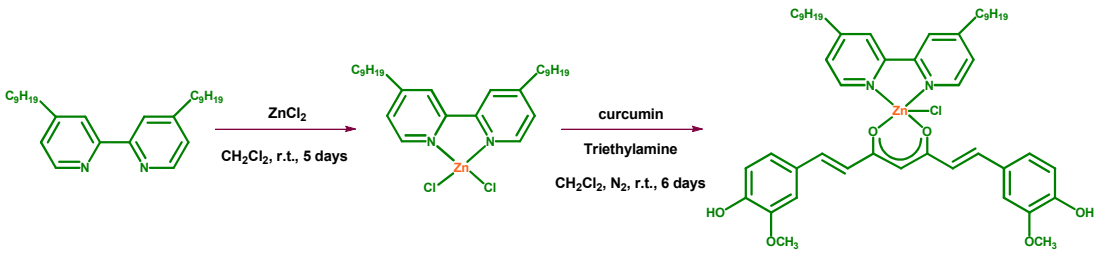

Scheme 1. Synthesis of $(Bpy_9)Zn(Cur)(Cl)$ complex.

The photophysical characterization of the complex shows a green luminescence with a fluorescence emission band centered 540 nm in EtOH solution, confirmed by the excitation (Fig. 8); the emission quantum yield measurement, performed by optically-diluted method by using $Ru(bipy)_3Cl_2$ (bipy = 2,2'-bipyridine) in water as standard (§ Appendix), gives a value $\Phi = 0.20$; the lifetime value (τ = 1.2 ns) is typical of a fluorescence decay.

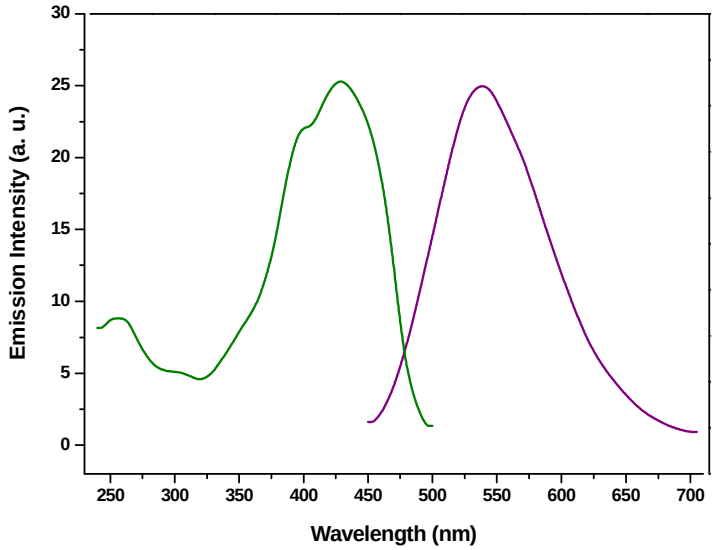

Figure 8. Excitation (λ_{em} = 540 nm) and emission (λ_{ex} = 430 nm) spectra of $(Bpy_9)Zn(Cur)(Cl)$ in EtOH solution.

2.4.3 Study on the interaction between Zn(II) complex and Human Serum Albumin by fluorescence spectroscopy

The interaction between the Zn(II) complex and the HSA was achieved by adding, to a buffer solution 4.4 x 10^{-6} M of albumin (§ 2.4.1), an increasing amount of Zn(II) complex dissolved in ethanol to a final concentration not exceeding 10%. Higher concentrations of organic solvent, as reported in literature (Lin 2004), may denature the protein by a great exposition of its hydrophobic areas, and reducing its solubility. Five solutions (Table 1) having an increasing $[(Bpy_9)Zn(Cur)(Cl)]/[HSA]$ ratio ranging from 0 to 5 were prepared, and fluorescence emission of HSA at 345 nm were observed by exciting at 295 nm.

Sample	Added volume of $(Bpy_9)Zn(Cur)(Cl)$ ethanol solution to HSA buffer solution	Mol of $(Bpy_9)Zn(Cur)(Cl)$ contained in the HSA solution
1	0	0
2	50 µL	1.14×10^{-8}
3	150 µL	3.42×10^{-8}
4	200 µL	4.56×10^{-8}
5	250 µL	5.70×10^{-8}

Table 1. Composition of five examined samples of HSA in buffer solution (2.5 mL, 1.12 E-8 mol) obtained by adding different aliquots of a $(Bpy_9)Zn(Cur)(Cl)$ 1.14×10^{-4} M ethanol solution.

The gradual addition of Zn(II) complex to the protein solution caused a gradual decrease in the HSA fluorescence intensity (Fig. 9); due to the comparative low volume of the added Zn complex solutions, the HSA absorption intensity of the five samples remained unvaried, so excluding any dilution effect on the fluorescence intensity. The HSA fluorescence intensity decreases until the ratio $[(Bpy_9)Zn(Cur)(Cl)]/[HSA] = 5$; successive additions of the zinc complex solution do not cause further reduction of the fluorescence intensity. Furthermore, there was a slight blue-shift at the maximum wavelength of HSA fluorescence emission when the solution of $(Bpy_9)Zn(Cur)(Cl)$ was added. This suggests that the chromophore of protein was placed in a more hydrophobic environment after addition of the zinc complex (Zhang 2008).

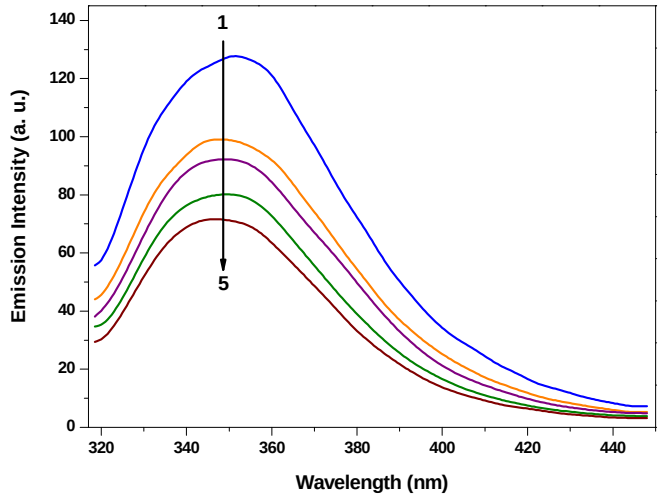

Figure 9. Fluorescence emission spectra of HSA (λ_{ex} = 295 nm) in buffer solution (pH 7.4) in the presence of increasing concentrations of the Zn(II) complex. [(Bpy_9)Zn(Cur)(Cl)]/[HSA] in samples **1**-**5**: 0, 1, 3, 4, 5.

Quenching of the HSA intrinsic fluorescence is attributed to an interaction with the Zn(II) complex. In fact, the spectral overlap of the absorption spectrum of the complex with the emission spectrum of the protein (Fig. 10) suggests that a FRET from the protein donor (Trp residue, specifically) to the complex acceptor occurs, that is responsible of the albumin fluorescence quenching.

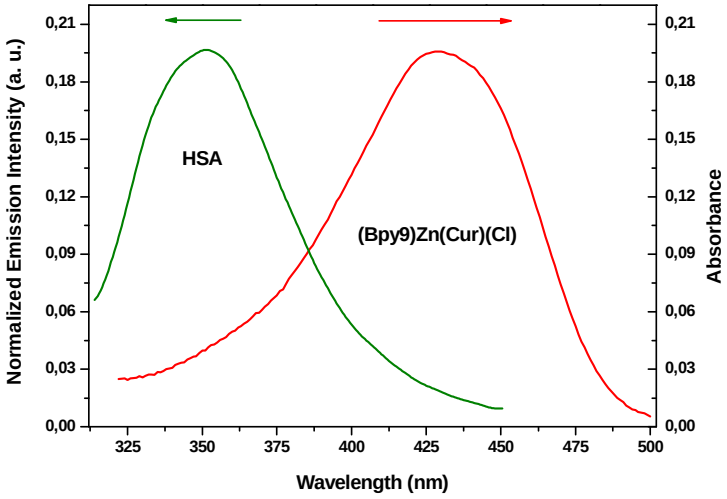

Figure 10. Spectral overlap of the emission spectrum of HSA with the absorption spectrum of Zn(II) complex in a buffer solution (pH = 7.4) : EtOH (10:1) mix.

As already mentioned (§ 2.3), the FRET Forster's model (Lakowicz 2003) predicts that the energy can be reliably transferred whenever the fluorescence emission spectrum of the donor (in our case, the HSA) and the absorption spectrum of the acceptor (the Zn(II) complex) have enough overlap, and the distance between donor and acceptor is not longer than 10 nm. These distances are comparable to the diameter of many proteins, *e.g*. HSA 5.9-6.2 nm at pH 7.4 (Lakowicz 2003).
Energy Transfer efficiency (η) is typically measured using the relative fluorescence intensity of the donor, in the absence and presence of acceptor, according to the formula

$$\eta = 1 - F_{DA} / F_{D.}$$

Using fluorescence intensities (that, taking into account the practically unvaried volume of the HSA samples, correspond to the areas under the emission spectral curves) of the HSA in the absence (F_D) and in presence (F_{DA}) of Zn(II) complex, the η was calculated, obtaining a value of 48%. Moreover, when increasing concentration of the Zn(II) complex was added to the protein, the lifetime of HSA varies within experimental error remaining almost identical to the value of the unquenched one (τ_D = 5.71 ns). The decrease of the emission intensity by adding the quencher with a constancy of the lifetimes values, account for a static quenching.

The Stern-Volmer equation (§ 2.3) was applied to determine the bimolecular quenching rate constant by plotting F_D / F_{DA} versus quencher concentration (Fig. 11); the linearity of this plot, proposes a single type of quenching process (Lakowicz 2003). The obtained value of k_q is 8.5 x 10^{12} L $mol^{-1}s^{-1}$ is typical of a binding interaction, and it indicated that the quenching was not initiated from dynamic collision but from an adduct formation, *i.e.* it is a static quenching (Lakowicz 2003). The binding constant, obtained from k_q taking into account τ_D = 5.71 ns, results 4.8 x 10^4 M^{-1}, in agreement with values reported for several other ligand-protein complexes.

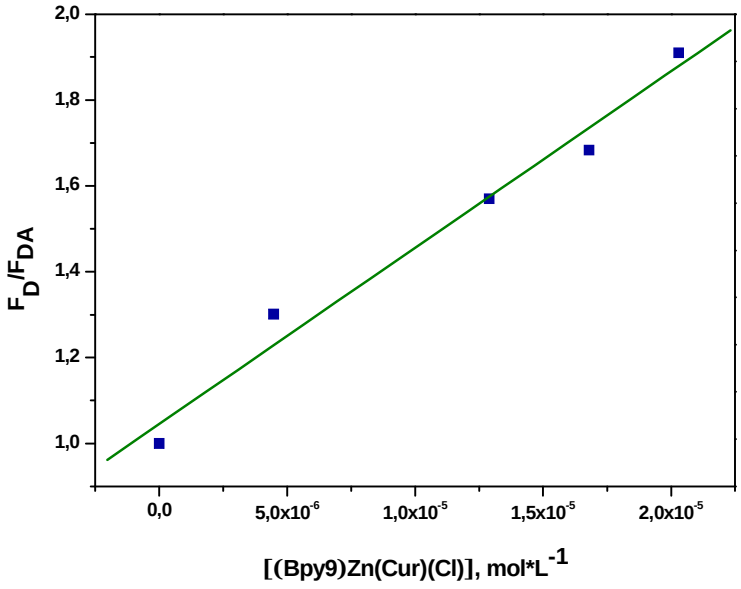

Figure 11. Stern-Volmer plot for the (Bpy_9)Zn(Cur)(Cl) quenching of the HSA fluorescence.

As above mentioned (§ 2.2.1), the intrinsic fluorescence of HSA is very sensitive to its microenvironment: it would be quenched obviously even if there is a slight change of the local surroundings of the protein, such as molecular binding, protein conformation variation and denaturation. To better confirm that the fluorescence quenching is due to a binding interaction of the protein with the complex, which penetrates into the hydrophobic binding site, and not to a simple interaction which modifies the protein conformation, a new set of measures was conducted that take advantage from the Zn complex fluorescence.

Emission spectra from solutions 2-5 (Table 1) containing HSA and (Bpy_9)Zn(Cur)(Cl) were recorded exciting at 430 nm (*i.e.* on the Zn complex absorption band, although it should be considered a solvatochromic shift, see below), and they report a 627 and a 510 nm bands (Fig. 12A). At the same time, four solutions of (Bpy_9)Zn(Cur)(Cl) in buffer were prepared, by dissolving in 2.5 mL of buffer solution, 50, 150, 200, 250 µL of (Bpy_9)Zn(Cur)(Cl) 1.14 x 10^{-4} M ethanol solution; in this way a new set of solutions (2'-5') with the same concentration of the Zn complex of sample 2-5, but without HSA, was prepared: these solutions showed, upon excitation at 430 nm, a unique band at 627 nm (Fig. 12B).

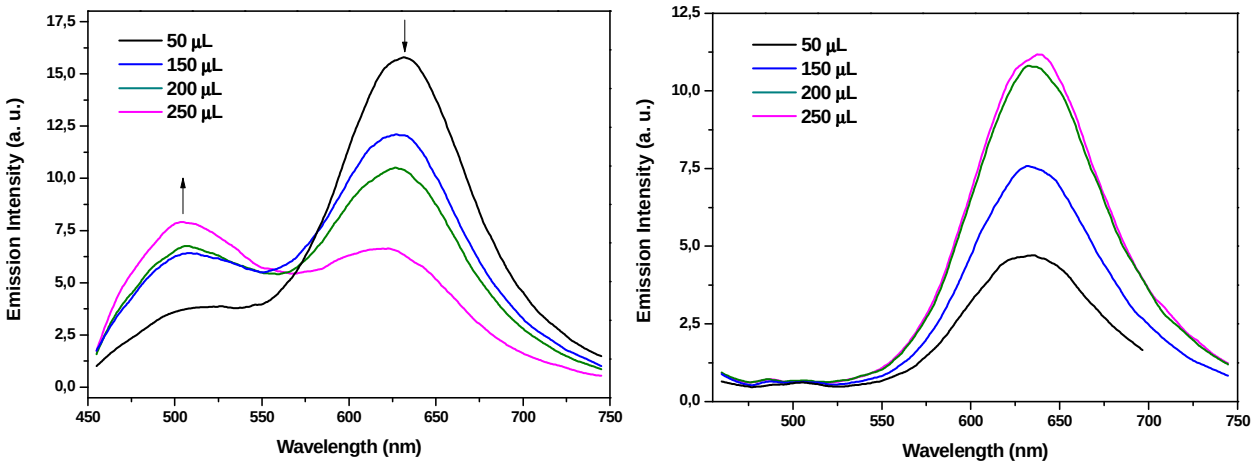

Figure 12. Emission spectra obtained by 430 nm excitation light of samples 2-5 (HSA + (Bpy_9)Zn(Cur)(Cl)), **A**, and of samples 2'-5' ((Bpy_9)Zn(Cur)(Cl)), **B**.

The obtained results, summarized in a simplified manner in Figure 13, account for the formation of an adduct between HSA and the Zn(II) complex: in fact, the emission spectrum of the (Bpy_9)Zn(Cur)(Cl)+HSA solution has been interpreted by attributing the band at 627 nm to the free complex in the hydrophilic buffer solution, and the band at 510 nm to the complex bound to the hydrophobic pockets of HSA.

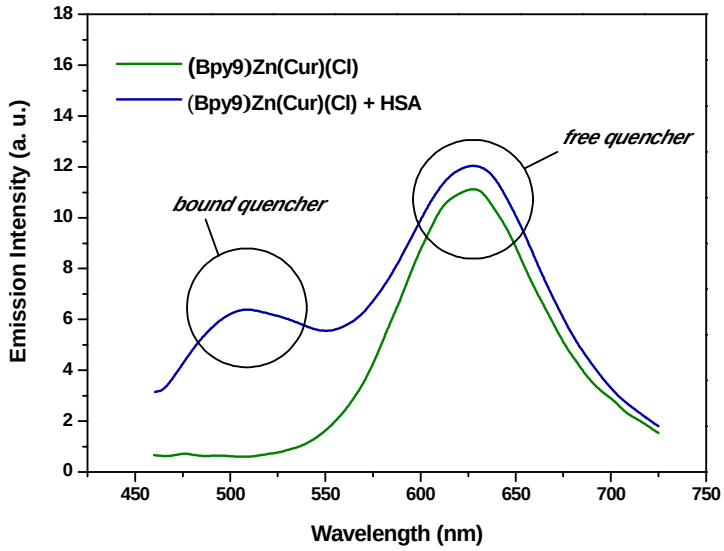

Figure 13. Comparison between the emission spectra of Zn(II) complex (λ_{ex} = 430 nm) with or without HSA in the mix buffer solution: EtOH (10:1). The two spectra are not in scale.

The blue-shift of the emission is due to a solvatochromic behavior of the Zn(II) complex, already evidenced by comparing the maximum band in ethanol (λ_{em} = 540 nm, Fig. 8) with that in buffer (λ_{em} = 627 nm, Fig. 12B). To confirm the solvatochromic properties of (Bpy_9)Zn(Cur)(Cl), emission spectra of the complex were recorded dissolving it in different solvents; actually, solvatochromic band shifts are observed: in particular a red shift of the maximum emission by increasing the solvent polarity was observed (Fig. 14).

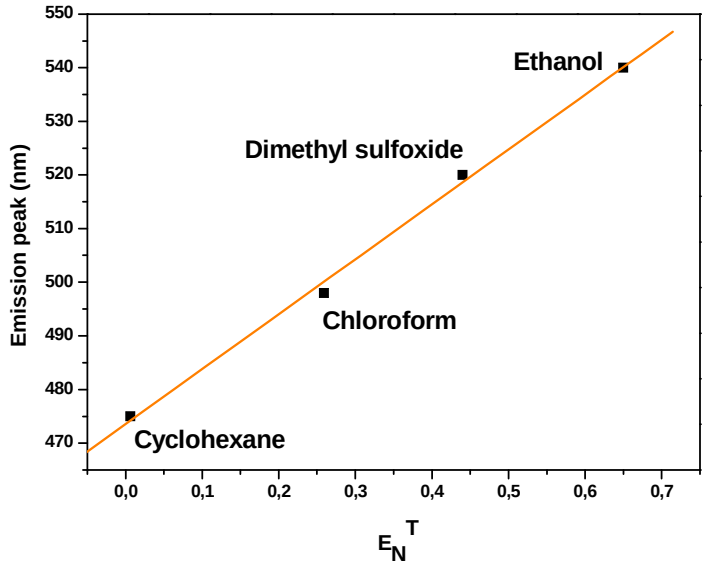

Figure 14. Linear plot of wavelength maximum of (Bpy_9)Zn(Cur)(Cl) emission versus the Reichard's parameter E_T^N values of some organic solvents where the complex was dissolved.

Finally, to explore a further effect of the FRET from HSA to Zn complex, it was recorded the emission of the acceptor Zn complex by exciting the donor HSA, *i.e.* by recording the emission of 2-5 samples reported in Table 1 by exciting at 280 nm. The obtained results showed the emission maximum of the free complex at 627, instead of the maximum of the bound complex at 510 nm. Taking into account that the free complex has an absorption band at about 280 nm (due to the bipyridine-localized levels), it can be concluded that the amount of the free complex in solution show an emission more intense that those deriving from the energy transfer from HSA to the bound complex.

2.5 Conclusion

Since the discovery of cisplatin, many metal complexes are used as chemotherapic agents against cancer diseases. The different metal coordination geometry exploitable by organometallic compounds is the key factor that allows these drugs to be effective: in fact, traditional anticancer drugs target DNA preventing cell reproduction. Besides direct coordinative binding of metallo-agents to DNA bases, other potential DNA binding modes, non-covalent in nature, include intercalation and groove binding, in which metal role is prevalently structural, like a scaffold for a variety of ligands. But the coordination compounds versatility can be exploited by inserting another function, *i.e.* to add a fluorescent ligand to the drug, so coupling the therapeutical to the sensoristic action in a unique compound. In fact, to have a simple and economical method for monitoring the biodistribution of a drug is a great advantage. In this light, fluorescence spectroscopy offers a direct connection between the spectral evidences and the molecular features of a sample.

The cytotoxic properties of many coordination complexes are test in vitro; nevertheless, this test is only the first step to propose a complex as antineoplastic drug; a successive step is to study its biodistribution. Moreover, a few of coordination compound is scarcely water soluble, so a way to reach a good bioavailability is through its interaction with Human Serum Albumin (HSA), the most abundant protein in the bloodstream that increases the solubility of hydrophobic drugs in plasma and modulates their delivery to cell *in vivo*. The protein fluorescence has opened the way to numerous studies that correlate the luminescence quenching to the binding interaction with a complex.

Unfortunately, the intrinsic fluorescence of HSA is very sensitive to its microenvironment: it would be quenched even if there is a slight change of the local surroundings of the protein, such as molecular binding, protein conformation variation and denaturation. To overcome this drawback, we have studied the interaction between HSA and a new Zn(II) complex, with twofold function: an excellent antitumor activity and an intense fluorescence. So, we have been able to look at the binding interaction from a dual perspective: the luminescence quenching of the protein and the fluorescence variation of the complex.

The fluorescence-resonance energy-transfer from protein to complex was observed by monitoring the decreases of luminescence by increasing the complex concentration; the Stern-Volmer equation was applied to determine the bimolecular quenching rate constant, obtaining a value of $k_q = 8.5 \times 10^{12}$ L $mol^{-1}s^{-1}$ is typical of a binding interaction, and it indicated that the quenching was not initiated from dynamic collision but from an adduct formation, *i.e.* it is a static quenching. While it was impossible to evidence an increase of the complex fluorescence intensity−as result of the energy-transfer−because the acceptor absorbs at the same exciting wavelength of the donor, it has been evidenced a solvatochromic shift of the emission complex as result of the hydrophobic environment experienced by the Zn compound inside the protein binding site.

The investigated Zinc compound represents an example of the multitude of applications that metal complexes can successfully offer, and the obtained results concerning the Zn(II) complex–HSA interaction can contribute to the current knowledge in the area of protein-ligand binding and confirm the capital role of the fluorescence spectroscopy in biomedical research.

Chapter 3 LIGHT-ACTIVATED PROCESSES IN COORDINATION COMPOUNDS: PHOTOGENERATION OF SINGLET OXYGEN

3.1 Singlet oxygen: a guest ghost in everyday life

3.1.1 Electronic structure and the lifetime of singlet oxygen

Despite its apparent simplicity, molecular oxygen (O_2) exhibits a number of rather unusual properties due to its unique electronic structure. Unlike many molecules, oxygen has an open-shell triplet ground state ($^3\Sigma_g^-$) with two unpaired p-electrons distributed in the highest occupied π-antibonding orbitals (Fig. 1A). Rearrangement of the electron spins within these two degenerate orbitals results in two possible singlet excited states, the $^1\Delta_g$ and the $^1\Sigma_g^+$ states, which lie 22.5 Kcal and 31.5 Kcal mol^{-1} respectively, above the ground state (Fig. 1B). In the first excited state ($^1\Delta_g$), both electrons are paired in a single orbital, leaving the other empty while the higher singlet state ($^1\Sigma_g^+$) comes from the spin pairing electrons in different orbitals (Ogilby 2010). In both forms of $^1O_2$, the spin restriction is removed so that the oxidizing ability is greatly increased (Halliwell 2007).

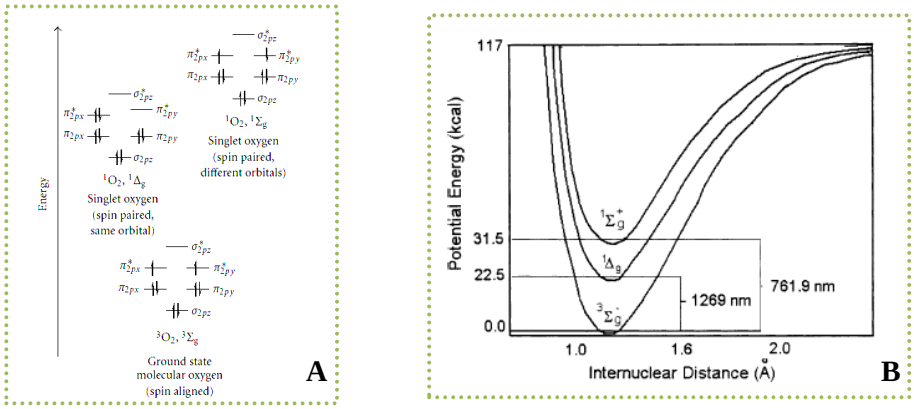

Figure 1. (**A**) Molecular orbital diagram showing the electron distribution in $^3\Sigma_g$, $^1\Delta_g$ and $^1\Sigma_g$ (Josefsen 2008); (**B**) potential energy curves of molecular oxygen (De Rosa 2002).

The higher-energy singlet oxygen state ($^1\Sigma_g^+$) is very short lived and due to a spin-allowed transition rapidly relaxes to the lower-energy $^1\Delta_g$ state with unit efficiency, before chemical reactions can occur (Wilkinson 1993). Conversely, the transition from the $^1\Delta_g$ state to the ground state is spin forbidden, thus the $^1\Delta_g$ oxygen is a relatively long-lived species with a lifetime strongly dependent on the nature of the solvent (Table 1).

Solvent	**τ/μs**	**Solvent**	**τ/μs**
H_2O	4	D_2O	68
CH_3OH	10	CH_3CN	75
C_4H_8O	23	$CHCl_3$	244
C_6H_6	31	C_6F_6	3900
C_6H_5Cl	45	CS_2	34000
CH_3COCH_3	54	CCl_4	87000

Table 1. Lifetime of singlet oxygen in several solvents (Gorman 1989; Schmidt 1989; Wilkinson 1995; Montalti 2006).

In fact, in most solvents, singlet oxygen's lifetime is reduced because the electronic excitation energy of $^1O_2$ is dissipated as heat by coupling with the vibrational frequencies of the solvent molecules. The most probable energy-accepting oscillator of a solvent molecule is its terminal atom pairs with the highest vibrational energy (*e.g.*, O-H, C-H); molecules with low energy oscillators, as C-F and C-Cl, act as poor quenchers (Fujii 2004; Schmidt 1989).

The $^1\Delta_g$ state decays to the triplet ground state through a radiative deactivation and the spectral profile of its phosphorescence is unique, with a distinct and narrow band centered at ~1275 nm (Fig. 2).

$$O_2\,(^1\Delta_g) \rightarrow O_2\,(^3\Sigma_g^-) + h\nu\ (1275\ nm)$$

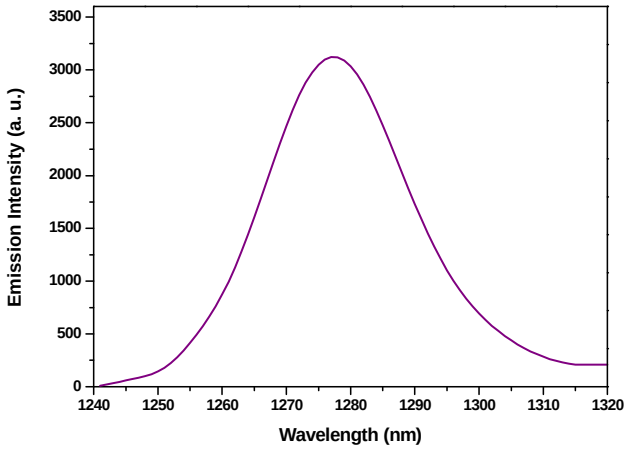

Figure 2. Singlet oxygen phosphorescence.

3.1.2 The photosensitized production of singlet oxygen

Although singlet oxygen can be produced in a variety of ways (Rosenthal 1985), a simple and controllable method involves electronic energy transfer to O_2 from an excited state of a given molecule - the photosensitizer - that acts as light absorber. The photochemical processes that generate singlet oxygen from ground-state oxygen are represented by the Jablonski diagram in Figure 3. With the irradiation of light of appropriate wavelength, the photosensitizer in its S_0 state is excited to the S_1 state. The lifetimes of the S_1 state are in the nanosecond time range which is too short to allow for significant interactions with the surrounding molecules. The photosensitizer can relax back to the ground state by emitting a fluorescence photon or it can populate the triplet state via intersystem crossing (ISC). From triplet excited state the photosensitizer can return to the ground state by emitting a phosphorescence photon or transferring energy to another molecule via a radiationless transition. In particular radiative triplet to singlet transitions are quantum mechanically ‘forbidden’ since a change of electron spins is required, thus the lifetimes of the T_1 state are in the micro- to milli- second time range, long enough for a variety of quenching processes to compete favorably with phosphorescence. In oxygenated environments a process of triplet quenching involves dioxygen, and an energy transfer from the excited triplet

state of the photosensitizer (PS) to the ground state of molecular oxygen takes place, generating singlet oxygen according to the equation:

$$^3PS + {}^3O_2 \rightarrow {}^1PS + {}^1O_2$$

Being the oxygen photosensitation a bimolecular process, its efficiency is diffusion-controlled (Schimidt 2006).

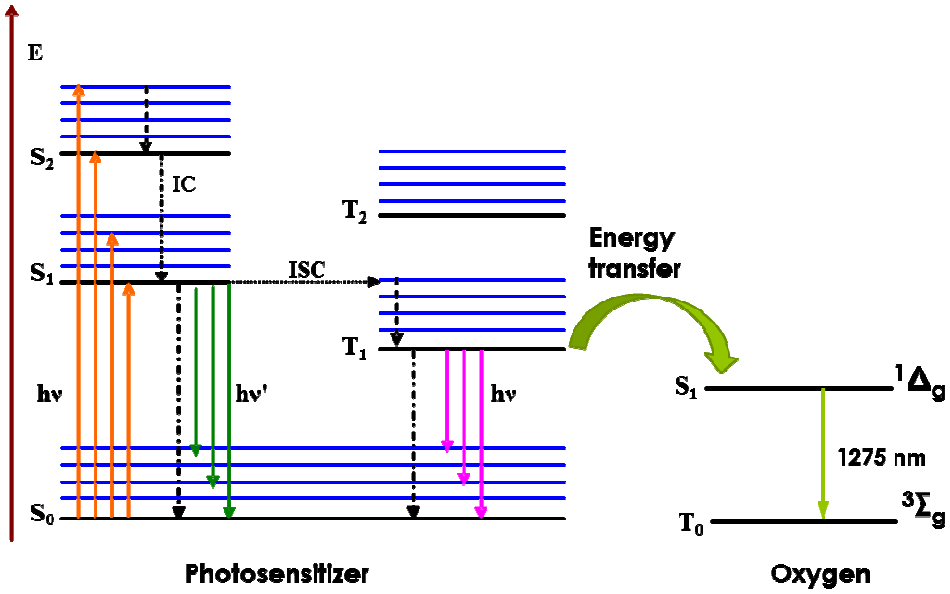

Figure 3. Jablonski diagram illustrating the photosensitized production of singlet oxygen ($^1\Delta_g$). The letter S denotes discrete states of the sensitizer with singlet spin multiplicity, and T denotes states with triplet spin multiplicity. IC and ISC denote internal conversion and intersystem crossing, respectively.

3.1.3 Singlet oxygen reactions and applications

The singlet excited state of dioxygen can be deactivated by a radiative path (showing the emission at 1275 nm) or by bimolecular interaction with another species (A), that acts as quencher; in the last case, two major ways can be followed (Bellus 1978; De Rosa 2002):

1) physical quenching: $^1O_2 + A \rightarrow {}^3O_2 + A$, in which interaction leads only to deactivation of singlet oxygen with no O_2 consumption or product formation;

2) chemical quenching: $^1O_2 + A \rightarrow P$, where the quencher reacts with singlet oxygen to give a new product (P).

Early works (Davies 2003) found that singlet oxygen could oxidize substrates that were unaffected by oxygen in its normal energy state; indeed, oxygen is ca. 1 V more oxidizing in its singlet excited state and is therefore significantly more electrophilic, reacting rapidly with unsaturated carbon-carbon bonds, neutral nucleophiles such as sulfides and amines, and as well as with anions.

Some common reactions of singlet oxygen are shown in Figure 4.

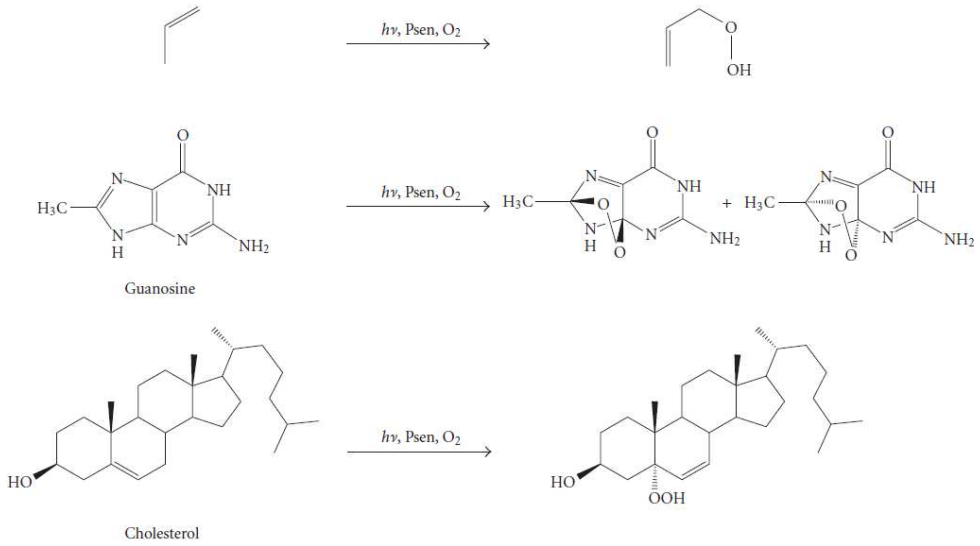

Figure 4. Typical singlet oxygen reactions (De Rosa 2002).

The rapid reactivity of $^1O_2$ with several substrates including steroids, fatty acids, amino acids residues, nucleic acid bases (Macdonald 2001), deserves to it a key role in different fields of application such as the wastewater treatment and photodynamic processes. Singlet oxygen, in fact, has a tremendous impact on the living matter: cellular membrane damage and enzyme deactivation, induced by its attack on the lipid or protein moieties, can be highly deleterious for tumoral cells, bacteria and viruses. Lipid peroxidation mediated by $^1O_2$ can be represented as:

$$LH + {}^1O_2 \rightarrow LOOH$$

where LH is an unsaturated lipid and LOOH is a lipid hydroperoxide. The chemical alterations may be localized at a single site or in the form of lipid-lipid, lipid-protein, and protein-protein cross-links.

The use of solar energy in the treatment of wastewater could be an economical solution to a difficult environmental problem. Research into photosensitized detoxification and treatment of industrial and urban wastewaters using light directly from the sun is currently underway at the Plataforma Solar de Almeria (PSA, Spain) (Oppenländer 2003).

Singlet oxygen is understood to play the major role in photodynamic effect with application in blood sterilization and Photodynamic Cancer Therapy (PDT). The photodynamic effect describes the damage of living tissue by the combination of a photosensitizer, visible light, and oxygen.

Blood sterilization: The Swiss and German Red Cross use methylene blue as a photosensitizer for the decontamination of freshly frozen plasma units (Sharman 1999): known for its lack of toxicity to humans, the dye is effective in destroying extracellulary-enveloped viruses; moreover, Silicon-based phthalocyanines are also being studied as photosensitizers for the sterilization of blood components by V. I. Technologies at the New York Blood Center (Olenick 1993).

Photodynamic cancer therapy (PDT): The healing power of light has been appreciated for several thousand years. Historically, the use of light in combination with a chemical agent for disease treatment has ancient beginnings (Edelson 1988), but it has only recently become a clinical reality as cancer treatment. Photodynamic therapy is a minimally invasive technique highly promising in treating of neoplastic diseases and of other non-malignant conditions, including age related macular degeneration and psoriasis (Brown 2004); its basic principle is a non-thermal photochemical reaction that takes place directly on the diseased tissue, and that requires the simultaneous presence of a photosensitizing agent (PS), visible light of an appropriate wavelength and dioxygen. In clinical settings the PS is administered systemically by intravenous injection or topically in the treatment of skin cancer (Fig. 5).

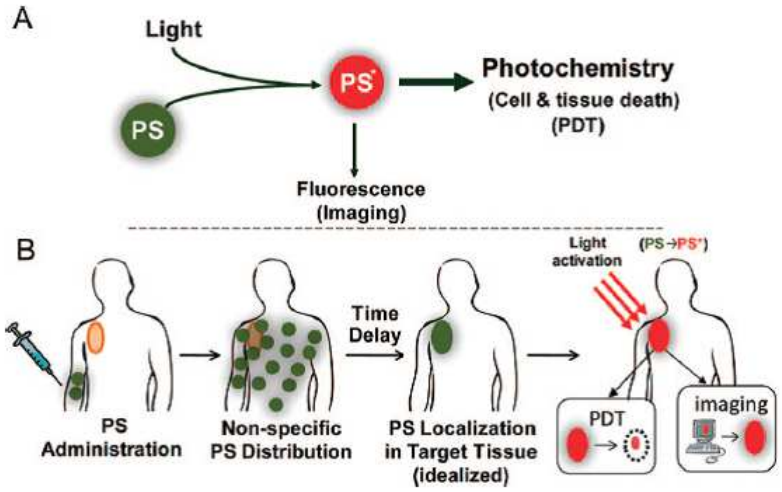

Figure 5. Schematic representation of PDT, where PS is a photoactivatable multifunctional agent, which upon light activation can serve as both an imaging agent and a therapeutic agent (**A**), and schematic representation of the sequence of administration, localization, and light activation of the PS for PDT or fluorescence imaging (**B**) (Celli 2010).

After a time interval, during which the PS accumulates preferentially in the target lesion, low-power light of a specific wavelength is directed onto the tumor, leading the activation of the sensitizer molecule. Most of the molecules used as sensitizer are luminescent species, partially quenched by oxygen. So, light activation will lead to its emission, which can be implemented for imaging applications (§ 4.2.1), as well as to the generation of singlet oxygen, which interact with cellular components inducing cell death and neoplastic tissue destruction.

Typically, the useful range of wavelengths for therapeutic activation of the PS is 600-850 nm, so-called "phototherapeutic window", the region of maximum light depth penetration into mammalian tissue. However, it is important to note that, because the PS can also serve as fluorescence imaging agent, light activation in the 400-480 nm range has been extremely useful in diagnostic imaging applications.

An ideal sensitizer for PDT application (over the basics requirements illustrated in the § 3.2) should adhere to the following criteria, envisaged by its use as a drug:

- negligible cytotoxicity in the absence of light;
- strong absorption with a high excitation coefficient in the red/near infrared region of the electromagnetic spectrum (600-850 nm)-allows deeper tissue penetration by light (Sharman 1999; Dougherty 1998);

- great retention in diseased/target tissue over healthy tissue;
- rapid clearance from the body;
- soluble in biological media, allowing direct intravenous administration and transport to the intended target; otherwise, a hydrophilic delivery system should be sought enabling efficient transportation of the photosensitizer to the target site via the bloodstream.

3.2 Photosensitizers

In order to a molecule can act as an efficient oxygen photosensitizer, it should be noted that sensitation process is a nearly diffusion-controlled bimolecular reaction between an electronic excited species and O_2. The $^1O_2$ photogeneration takes place by means of a combination of energy (eqn. a) and electron transfer (eqns. b1-b2) processes, starting from the triplet-excited state of the photosensitizer (PS*):

a) $PS^* + {}^3O_2 \rightarrow PS + {}^1O_2$

b1) $PS^* + {}^3O_2 \rightarrow PS^+ + O_2^-$

b2) $PS^+ + O_2^- \rightarrow PS + {}^1O_2$

The quantum yield of singlet oxygen formation Φ_Δ depends on the quantum yield of the PS triplet state formation Φ_T according to a simplified equation (Lang 2004):

$$\Phi_\Delta = \Phi_T \, S_\Delta$$

where S_Δ is the fraction of PS triplet molecules quenched by oxygen and yielding $^1O_2$, and is given by

$$S_\Delta = k_{et} / k_q$$

where k_q is the rate constant of the PS luminescence quenching by oxygen, and is expressed as the sum of the rate constants of the processes that involve singlet oxygen, namely energy transfer and electron transfer; its value, which is diffusion controlled, is of the order of 10^9-10^{10} $M^{-1}s^{-1}$; k_{et} is the rate constant of the energy transfer leading to the formation of $^1O_2$.

A molecule candidate to be an efficient PS should possess some basic requirements:

1. a relevant absorption cross section in the UV or Vis spectral window;
2. an excited-state lifetime to allow a mean free path enough to get oxygen collision;

3. in consequence of the previous point, having triplet excited state the lifetime long enough, an efficient intersystem crossing rate from the singlet excited state, which is initially populated upon light absorption, is required;
4. because the $^1O_2$ generation from dioxygen ground state requires 22.5 kcal/mol (Fig. 1), the potential energy of the PS excited state must be equal to or greater;
5. a better interaction between PS and dioxygen is reached if PS is a sterically undemanding molecule;
6. high photostability.

Most of the studies on singlet oxygen photogeneration involve organic dyes with extensively conjugated structures that impart to them a high absorption coefficient from the green to the red spectral region.

Well-known dyes such as Methylene Blue, Fluorescein, Rose Bengal, and Eosin Blue, all sharing the xanthene skeleton, have been studied from their photosensitizing ability point-of-view. Fluorescein (Fig. 6A), for example, exhibits intense absorption bands in the yellow-green part of the visible spectrum and produces singlet oxygen with a yield Φ_Δ= 0.1 in methanol (De Rosa 2002). The introduction of heavy halogen substituents on Fluorescein increases the yield of intersystem crossing toward the triplet state of the dye, so Rose Bengal (Fig. 6B) produces singlet oxygen with high yield (Φ_Δ= 0.76) (Redmond 1999).

Porphyrins and phthalocyanine derivatives are among the most commonly used photosensitizers (Allison 2004); their presence in natural systems makes them ideal candidates for use in biological singlet oxygen generation due to the lack of cytotoxicity in the absence of light (Sternberg 1998; Nyman 2004). Porphyrins, planar-aromatic molecules composed of four pyrrolic rings linked by methane bridges, absorb in the red portion of the electromagnetic spectrum, the region of maximum light penetration in the skin, so their derivatives have been extensively used in PDT. Moreover, porphyrins are suitable to be metalated, and the presence of a heavy metal ion coordinated at centre, promotes the ISC process, strongly reflected in the quantum yield of $^1O_2$ generation (Guldi 2000). As example, the palladium tetraphenylporphine (PdTTP) (Fig. 6C) has shown the excellent Φ_Δ = 0.88 in C_6H_6, while the metal-free analogous exhibited a Φ_Δ = 0.63 in the same solvent (De Rosa 2002).

Tuning of photophysical behaviour can be achieved also though the selection of macrocycle substituents and by inserting ligands to the axial positions of the metal ion. Phthalocyanines differ from porphyrins by having nitrogen atoms link the individual pyrrolic units and a more extended conjugation due to the peripheral benzene rings (Fig. 6D). The additional conjugation shifts their absorption at longer wavelengths than the porphyrins, and, although Φ_{Δ} values are lowers than those measured in porphyrins, the bathochromic shift of their absorption bands into the "phototherapeutic window", makes phthalocyanines ideal candidates for PDT (Leznoff 1996).

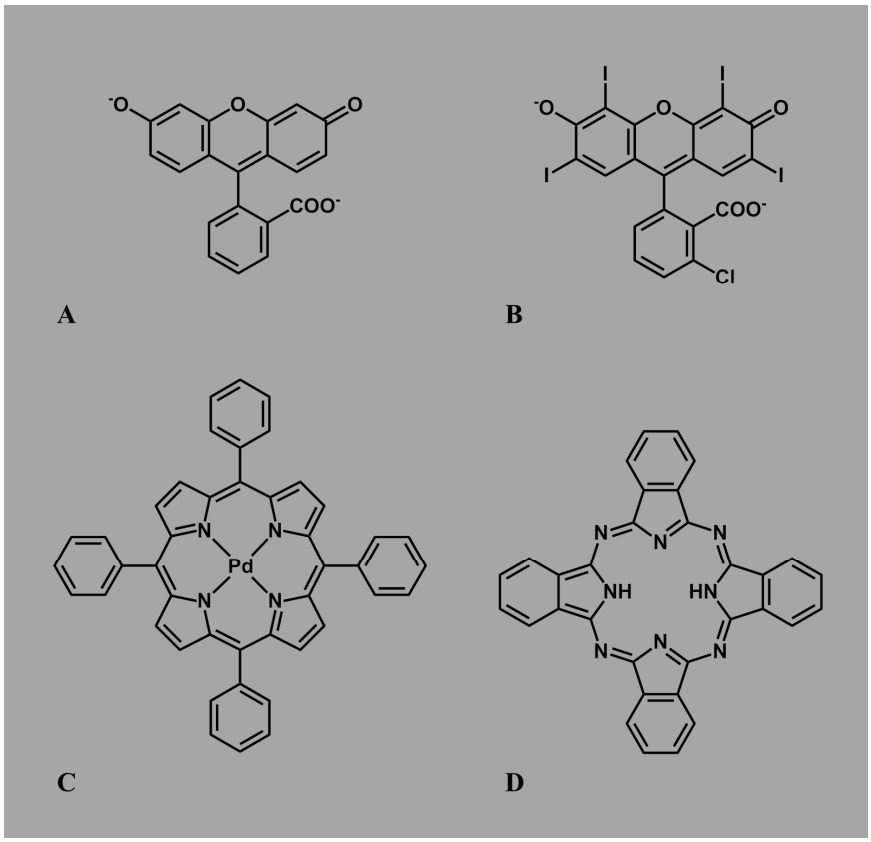

Figure 6. Molecular structures of Fluorescein (**A**), Rose Bengal (**B**), palladium tetraphenylporphine (**C**) and of a generic phthalocyanine (**D**).

3.3 Coordination compounds as photosensitizers: a viable route in singlet oxygen generation

As mentioned previously, oxygen photosensitization goes through an energy transfer from an excited state of the PS; therefore, an effective PS should possess a high quantum yield of triplet formation, long triplet lifetime and a triplet state energy greater than the energy gap between singlet and triplet dioxygen. In addition, it should be resistant to attack by singlet oxygen so as to prevent degradation and loss of sensitizing ability.

Transition metal complexes (TMCs) have been shown to be efficient PS and several examples are reported in literature (Djurovich 2007; Shavaleev 2006). These complexes show excited states with a pronounced triplet character due to the high spin-orbit coupling constant usually observed for heavy metals, that accelerates the rate of intersystem crossing (ISC) from the singlet electronic excited state. Their excited triplet states, with a concomitant longer luminescence lifetimes compared to organic dyes, have a higher probability to interact with the molecular oxygen ground state, resulting in a remarkable luminescence quenching and, on the other hand, in the generation of highly reactive singlet oxygen. TMCs geometry requirements can be accordingly tuned, depending on the metal choice, and generally they are strongly coloured. Most of the PS based on TMCs involves Cr(III), Ru(II), Pd(II), Os(II), Ir(III) and Pt(II); but the best results were achieved using Ruthenium, Iridium and Platinum as metal centre.

TMCs of Ru(II) have relatively strong absorption in the UV-Vis regions of the spectrum; the archetypical is the $[Ru(bpy)_3]^{2+}$ (bpy = 2,2'-bipyridine) (Fig. 7).

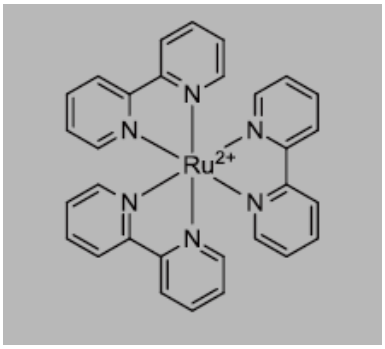

λ_{em}(nm)	Φ	Φ_{air}	τ(ns)	τ_{air}(ns)
620	0.042	0.028	650	390

Figure 7. Molecular structure and some photophysical properties of $[Ru(bpy)_3]^{2+}$ in H_2O.

The excitation of Ru(II) trisbipyridine leads to the metal-to-ligand charge transfer ^{1}MLCT state, which undergoes an efficient (quantum yield Φ close to unity) intersystem crossing to ^{3}MLCT. Long emission lifetime of ^{3}MLCT state allow oxygen quenching to be an efficient process in aerated solutions and the deactivation occurs by an energy transfer mechanism (§ 3.2, eqn. a). In recent studies (Garcia-Fresnadillo 1996) it was examined the photosensitizing ability of a series of homoleptic $[RuL_3]^{2+}$ complexes where L is bpy, 1,10-phenathroline (phen), 2,2'-bipyrazine (bpz), 4,7-diphenyl-1,10-phenanthroline (dip), diphenyl-1,10-phenanthroline-4,7-disulfonate (dpds), and 1,10-phenanthroline-5-octadecanamide (poda) in deuterated water and methanol. In this series of complexes, a wide range of quantum yields of singlet oxygen formation (Φ_Δ) were found, from 0.19 for $[Ru(bpz)_3]^{2+}$ in D_2O to 1.0 for $[Ru(dpds)_3]^2$ in CD_3OD (Table 2).

	Φ_Δ (in CD_3OD)	Φ_Δ (in D_2O)
$Ru(bpy)_3^{2+}$	0.73	0.22
$Ru(phen)_3^{2+}$	0.54	0.24
$Ru(bpz)_3^{2+}$	0.28	0.19
$Ru(dip)_3^{2+}$	0.97	0.42
$Ru(dpds)_3^{4-}$	1.0	0.43
$Ru(poda)_3^{2+}$	0.54	Insoluble

Table 2. Quantum yields of singlet oxygen generation of several homoleptic Ru(II) complexes.

Cyclometallated Ir(III) complexes, having long lived triplet excited states and excellent photoluminescence efficiencies, have been reported (Djurovich, 2007). The complexes have the formula $(C\hat{}N)_2Ir(O\hat{}O)$ where C^N is a monoanionic cyclometalating ligand such as 2-(phenyl)pyridyl or 2-(phenyl)quinolyl, and O^O is the ancillary ligand, acetylcetonate (acac) or dipivaloylmethane (dpm) (Fig. 8).

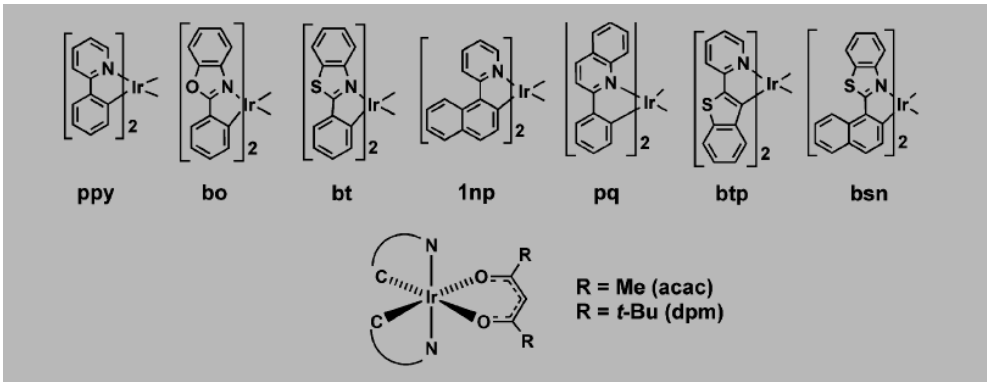

Figure 8. Cyclometalated (C^N), diketonate (O^O) ligands and coordination geometry for $(C\hat{}N)_2Ir(O\hat{}O)$ complexes.

Measured quantum yields of singlet oxygen generation, for the cyclometalated complexes, are summarized in Table 3. As reported the cyclometalated Ir(III) complexes undergo luminescent quenching by dioxygen, *via* an electron transfer mechanism, that leads to formation of superoxide anion (§ 3.2, eqn. b1). Therefore, a rapid back-electron transfer from superoxide to the oxidized Ir(III) complexes leads to singlet oxygen generation (§ 3.2, eqn. b2).

	Φ_Δ (CD_3OD)
$(ppy)_2Ir(acac)$	0.90
$(bo)_2Ir(acac)$	0.76
$(bt)_2Ir(acac)$	0.86
$(pq)_2Ir(acac)$	0.62
$(1np)_2Ir(acac)$	0.76
$(btp)_2Ir(acac)$	0.72
$(bsn)_2Ir(dpm)$	0.59

Table 3. Quantum yields of singlet oxygen generation of several Ir(III) complexes.

Photosensitization by Pt(II) complexes has also been investigated. Pt(II) differs from the other elements Ru (II) and Ir (III) in that it is a d^8 metal ion, and hence normally adopts a 4 coordinated square planar geometry as opposed to the distorted octahedral complexes of the d^6 metal ions. The relationship between the coordination geometry and the photosensitization has been examined by Djurovich (2007) by comparing octahedral Ir(III) (Fig. 8) and square planar Pt(II) complexes (Fig. 9) with identical cyclometalating ligands.

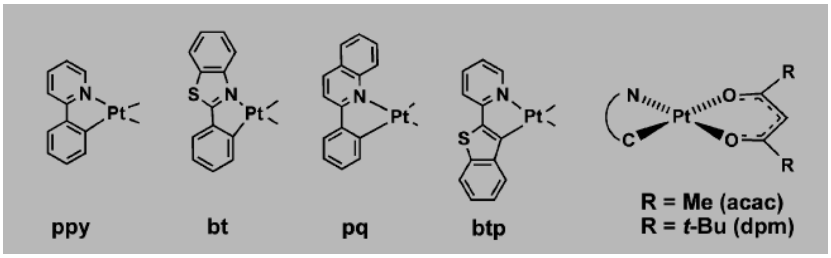

Figure 9. Cyclometalated (C^N), diketonate (O^O) ligands, coordination geometry for (C^N)Pt(O^O) complexes.

The quantum yields for $^1O_2$ formation for the Pt(II) complexes are near unity (Table 3), whereas the values found for the Ir(III) derivatives with the corresponding cyclometalating ligands are significantly lower. According the authors, this occurs because the percentage of productive collisions between $^3O_2$ and the excited photosensitizer, that result in the formation of $^1O_2$, is higher for Pt(II) complexes than the corresponding Ir(III) derivatives.

	Φ_Δ (CD_3OD)
(ppy)Pt(acac)	0.98
(ppy)Pt(dpm)	0.95
(bt)Pt(dpm)	1.0
(pq)Pt(dpm)	0.96
(btp)Pt(acac)	1.0
(btp)Pt(dpm)	1.0

Table 4. Quantum yields of singlet oxygen generation of Pt(II) complexes compiled in Fig. 9.

Early work by Shavaleev (2006) studied the oxygen quenching of (C^N)PtQ complexes, where C^N is a bidentate cyclometalating ligand, and Q is 8-hydroxyquinoline or quinolone-8-thiol (Fig. 10). These chromophores absorb intensely in the visible region and are efficient photosensitizers of singlet oxygen in air-saturated solutions, with yields in the range from 0.50 to 0.90 (Table 5).

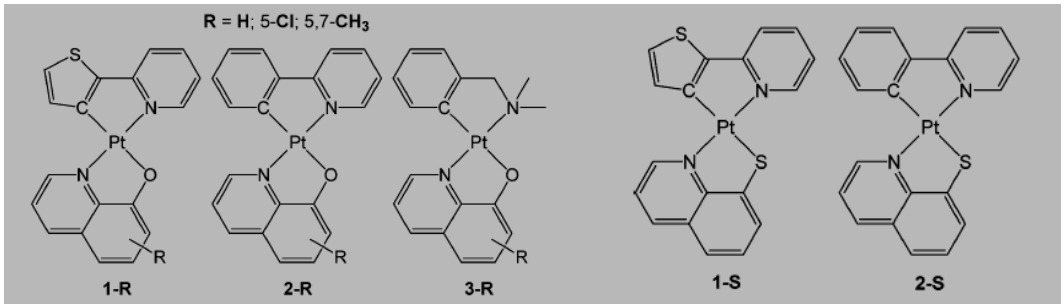

Figure 10. Structures of Pt(C^N) complexes with 8-hydroxyquinolines or quinoline-8-thiol.

	Φ_Δ (in $PhCH_3$)
1-H	0.82
2-H	0.90
3-H	0.84
1-Cl	0.85
1-CH_3	0.67
2-CH3	0.65
3-CH3	0.54
1-S	0.86
2-S	0.69

Table 5. Quantum yields of singlet oxygen generation of Pt(II) complexes compiled in Fig. 10.

3.4 Photophysical characterization of Pt (II), Ir(III) and Ru(II) complexes as photosensitizers

The photophysics of a series of transition metal complexes (TMCs), newly synthesised in the Laboratory of Inorganic and Coordination Chemistry of the University of Calabria, were studied, and their capability of sensitize dioxygen was assessed (Chart 1). The TMCs choice was made taking into account the peculiarities of three transition metal ions belonging to the triad: Ruthenium(II) (second transition row), Iridium(III) and Platinum(II) (third transition row), with coordinating or cyclometalating N^N or C^N ligands to form heteroleptic complexes. A key feature, common to the third row and many second row transition metal ions, is the high spin-orbit coupling constant that promotes rapid intersystem crossing from singlet to triplet excited states.

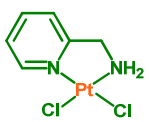

(pam)Pt(Cl)$_2$

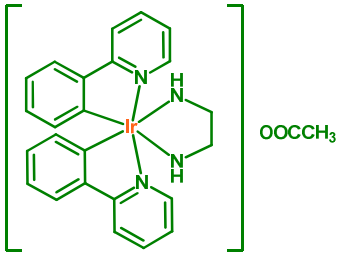

[(ppy)$_2$Ir(en)](OOCCH$_3$)

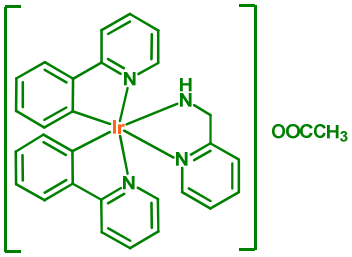

[(ppy)$_2$Ir(pam)](OOCCH$_3$)

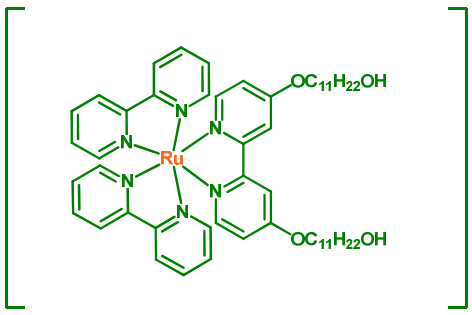

[(bipy)$_2$Ru(bipy-OH)](PF$_6$)$_2$

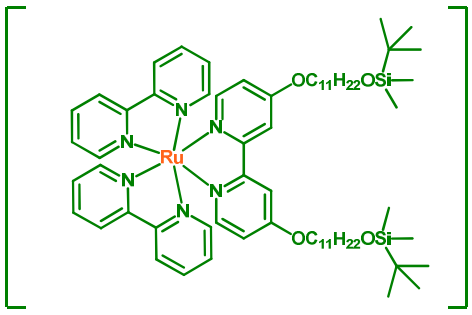

[(bipy)$_2$Ru(bipy-TBDMS)](PF$_6$)$_2$

Chart 1

Platinum(II). The most important oxidation state of Platinum is the +2, with electronic configuration d^8, that implies a thermodynamic preference to form, in the ligand field, square planar complexes. This geometry pushes a single unoccupied orbital to high energy, whilst allowing substantial stabilization of three of the occupied orbitals (Fig. 11).

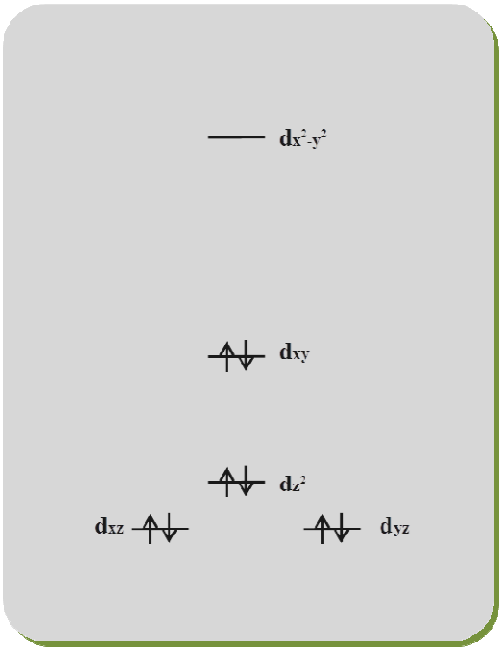

Figure 11. Simple ligand field-splitting diagram for metal d orbitals in a square planar complex.

Because the $d_{x^2-y^2}$ orbital is strongly antibonding, if it is populated, than the molecule will undergo a significant distortion upon formation of the d-d metal-centered (MC) excited state and this is unfavourable scenario for emission. In fact platinum complexes with simple inorganic ligands (*e.g.*, $Pt(NH_3)_4^{2+}$, $PtCl_4^{2+}$) are not or weakly luminescent in fluid solution; in the solid state or at low temperature, distortion of molecules is inhibited to some extent, and emission can be observed (Williams 2007). The introduction of conjugated aromatic ligands around the metal introduces ligand-centered (LC) and charge-transfer (metal-to-ligand or ligand-to-metal, MLCT or

LMCT) excited states, but, although having lower energies than the d-d states, a radiative deactivation is not always allowed because the MC levels result thermally accessible from the low-lying LC or CT excited states. The planar nature of the complexes allows, with sterically undemanding ligands, axial interactions through d_{z^2} orbitals of adjacent molecules, to form weakly bonding and antibonding $d\sigma$ and $d\sigma^*$ occupied molecular orbitals, giving rise, respect to the isolated molecule, to a lower-energy optical transition due to $d\sigma^*$-π^* excitation (metal-metal bond-to-ligand charge transfer or MMLCT). This intimate dimerization can take place in the ground state of the Pt(II)-complexes, or can involve an excited monomer and a ground-state monomer, giving rise to an excimer. This accounts for the observed spectral red-shift upon cooling crystal sample of some Pt(II)-complexes: as the temperature decreases, the lattice contracts and the Pt-Pt distance shortens (Connick 1996). Similar spectral red-shift is observed in solution for complexes with planar, conjugated aromatic ligands, due to π-π interactions between the ligands of adjacent molecules, as the concentration is increased (Kunkely 1990).

A key feature is the importance of the triplet states, a feature shared with other third row and many second row transition metal ions. The high spin-orbit coupling constant of platinum (ζ = 4481 cm^{-1}) promotes rapid ISC from singlet to triplet excited states.

Iridium(III) and Ruthenium(II). The Ir(III) trication is a $5d^6$ center, giving rise, in a ligand field, to octahedral coordination, similar to the complexes of Fe(II) ($3d^6$) and Ru(II) ($4d^6$). Because the different spatial extension for 3d, 4d and 5d orbitals, the split of the degenerate d orbitals in an octahedral ligand field (Δ) is smallest for the d orbitals with lowest quantum number. It should be noted that in all cases discussed here, light absorption is associated with electronic transitions from the ground state to singlet levels of various nature and electronic localization, ^{1}LC, ^{1}MC), and ^{1}MLCT). In addition, ^{1}LMCT can in principle be involved. On the contrary, emission is always from triplet levels, ^{3}MLCT or ^{3}LC in nature, which actually include changeable amounts of the corresponding singlets (Flamigni 2007). This is a consequence of the high spin-orbit coupling constants of the metal centers taking into account, ζ = 431, 1042, 3909 cm^{-1}, for Fe, Ru, Os, and Ir, respectively.

Unlike Fe(II), the ligand field splitting Δ for Ir(III)-polyimine complexes, is very large and the MC levels are pushed so high in energy that usually they do not affect the emission properties. These are traceable back to MLCT levels or LC levels, both of them being emissive. On the contrary, Fe(II)-polyimine complexes are not emissive. For Ru(II)-polyimine complexes, one usually observes MLCT emission at around 600 nm (Flamigni 2007). However, MC levels are thermally accessible, because Δ for the Ru(II) 4d orbitals has an intermediate value between the Fe(II) and Ir(III) cases. Thus, parasitic radiationless paths involving the MC levels contribute to deactivation of the MLCT emissive level for Ru(II)-polyimine complexes. A practical consequence is that also for this family of complexes, and apart from remarkable exceptions (Goze 2003), Φ rarely exceeds 0.1.

3.4.1 Platinum compound

The platinum spin-orbit coupling constant value makes its complexes suitable to give good photosensitiziers; in this light, a square planar coordination compound was synthesized and its phosphorescence quantum yield and lifetime were measured. To assess $^1O_2$ photogeneration, two ways were followed: (*i*) an indirect one, *i.e.* to compare the Pt-complex phosphorescence intensity of an air-equilibrated with an argon-bubbled solution, and (*ii*) a direct one, *i.e.* to detect the characteristic singlet oxygen phosphorescence at about 1270 nm.

The synthesis of dichloro(2-picolylamine)Pt(II), **(pam)Pt(Cl)$_2$**, complex was performed by adapting the method (Scheme 1) reported in literature (Munk 2003). The complex was obtained with a yield of 87%, as a yellow solid slightly soluble in the common organic solvents and it was characterized by elemental analysis, ^{1}H NMR and IR spectroscopies.

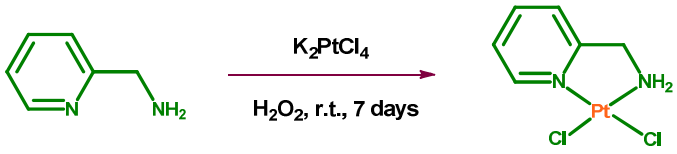

Scheme 1. Synthesis of **(pam)Pt(Cl)$_2$** complex.

The 2-picolylamine ligand is well soluble in water and in acetonitrile, and its absorption spectra in the two solvents are reported in Figure 12. In a short spectral range (255-265 nm) vibronic structure of a π-π* transition is visible, whose position is little affected by the solvent polarity; instead, a low-intensity band is present as a shoulder at about 315 and 300 nm in water or acetonitrile, respectively: the intensity and the solvatochromism account for a n-π* origin of the band. This transition gives rise to the low-energy excited state, that, symmetry-distorted respect to the ground state, does not allow a radiative de-excitation of picolylamine.

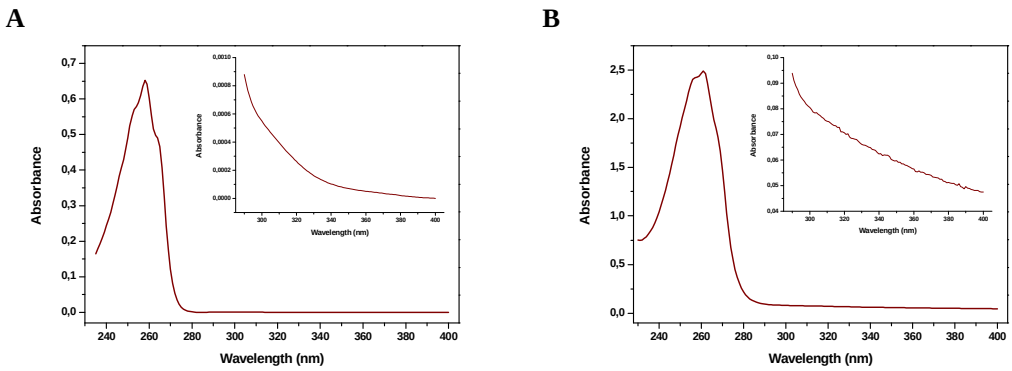

Figure 12. Absorption spectra of 2-picolylamine in water (**A**) and acetonitrile (**B**) solution.

Differently from the ligand, **(pam)Pt(Cl)$_2$** is water-insoluble, and the absorption spectrum was recorded in acetonitrile (Fig. 13), showing three bands, at 238, 265 and 300 nm. While the examined complex is already reported in literature (Munk 2003), no photophysical characterization was published until now (Ricciardi 2012). A comparison with a couple of similar Pt(II) complexes, *i.e.* $(py)_2Pt(Cl)_2$ (py = pyridine) and $(NH_3)_2Pt(Cl)_2$ (Martin 1983), it can help to propose proper bands attribution: the higher-energy bands are attributed to LC π-π* transitions, while the 300 nm band is due to the d-π* MLCT.

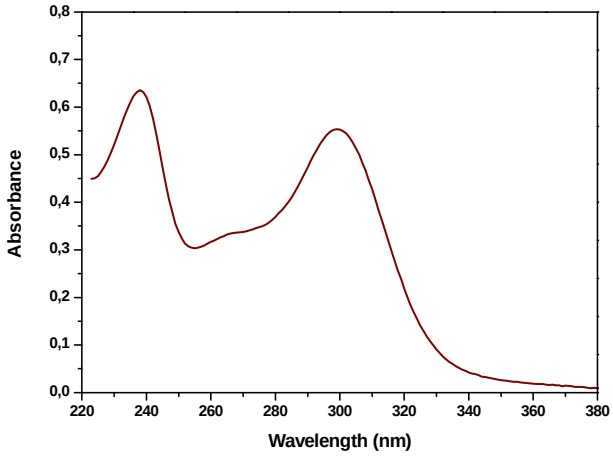

Figure 13. Absorption spectrum of **(pam)Pt(Cl)$_2$** complex in acetonitrile solution.

In air-equilibrate acetonitrile solution, no emission was detected at room temperature. Spectrum from deaerated solution, instead, shows a band at 507 nm (Fig. 14), with an

excited-state lifetime of 2.05 μs and an emission quantum yield of 7.2 10^{-3} ($Ru(bipy)_3Cl_2$ in aerated water was used as standard; see § Appendix).

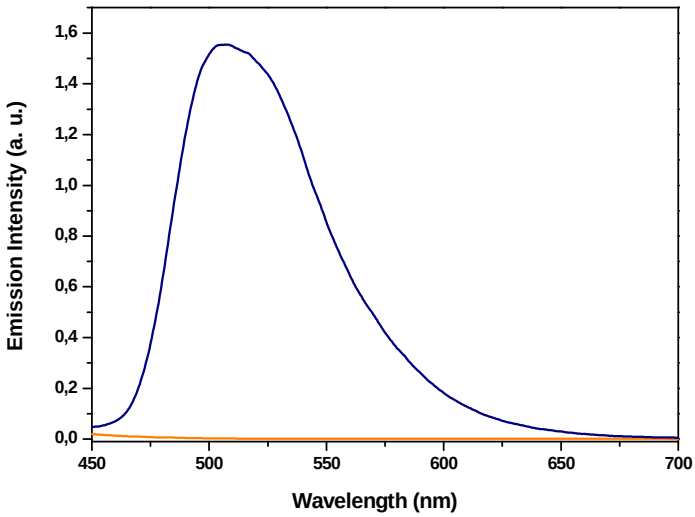

Figure 14. Emission spectra of **(pam)Pt(Cl)$_2$** complex in degassed (blue line) or air saturated (orange line) CH_3CN solution.

The emission is a phosphorescence originating from the ^{3}MLCT state deactivation. The phosphorescence band is totally quenched in presence of oxygen, and the characteristic $^1O_2$ ($^1\Delta g$) → $^3O_2$($^3\Sigma g$) emission has been monitored at 1270 nm in a CCl_4 solution of the platinum complex (Fig. 15).

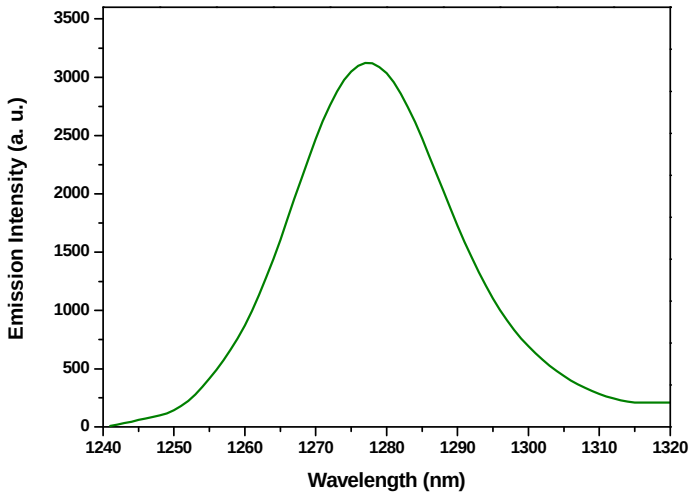

Figure 15. Singlet oxygen phosphorescence upon irradiation at 265 nm of **(pam)Pt(Cl)$_2$** in air-saturated CCl_4 solution.

In absence of quencher, the low value of the emission quantum yield of **(pam)Pt(Cl)$_2$** is ascribed to a little energy separation (ΔE) between the emitting MLCT and the deactivating MC states, that allows, particularly at room temperature (where ΔE is comparable to kT), a thermal population of the d-d excited states. The presence, in the examined complex, of weak-field ancillary ligands, such as chloride atoms, tends to favors a low ΔE value. The competitive value of the non-radiative constant rate (k_{nr}) respect to the radiative one (k_r) can be evidenced by a simple calculus.

The non-radiative constant rate is given by

(1) $$k_{nr} = \frac{1}{\tau_p}(1 - \Phi_p)$$

where τ_P and Φ_P are the observed phosphorescence lifetime and the phosphorescence quantum yield, respectively. The obtained value of k_{nr} is 4.84 10^5 s^{-1}.

The radiative rate constant is given by

(2) $$k_r = \frac{1}{\tau}$$

where τ is the radiative lifetime, and is given by $\tau = \tau_P/\Phi_P$. The obtained value of 2.85 10^{-4}, inserted in the eq. 2, gives the value of 3508 s^{-1} for k_r.

Concluding, **(pam)Pt(Cl)$_2$** complex, thanks to the high platinum spin-orbit coupling constant, shows a near-unitary Φ_{ISC} from ^{1}MLCT to ^{3}MLCT excited state, that deactives principally by non-radiative path, due the presence of thermally-accessible MC states. In presence of dioxygen, ^{3}MLCT state is effectively quenched by energy transfer process towards O_2 (Fig. 14); the formation of the singlet excited state of O_2 origins the characteristic phosphorescence band at 1270 nm (Fig. 15).

3.4.2 Cationic Iridium and Ruthenium compounds

The study of Ir(III) and Ru(II) complexes as photosensitizer agents is widely diffused in literature. Actually, an inspection of the current literature (Flamigni 2007) reveals that Ir(III) cyclometalated species are highly luminescent in oxygen-free solvent, with luminescence quantum yields as high as $\Phi \sim 0.5$ and more, and lifetimes in the range of a few μs. In air-equilibrated solvent, a remarkable quenching effect is registered, leading to a strong reduction in luminescence features with respect to degassed solutions-quenched Φ_q and τ_q values that can be as much as 60 times smaller than unquenched Φ and τ ones.

Regarding Ru(II) complexes, it has to be considered that $[Ru(bpy)_3]^{2+}$ is the first of a large family of ruthenium complexes photosensitizing oxygen (see Table 2).

To assess $^1O_2$ photogeneration, two ways were followed: (*i*) an indirect one, *i.e.* to compare the complex phosphorescence intensity of an air-equilibrated with an argon-bubbled solution, and (*ii*) a direct one, *i.e.* to detect the characteristic singlet oxygen phosphorescence at about 1270 nm in suitable solvent.

3.4.2.1 Synthesis

The synthesis of $[(ppy)_2Ir(en)](OOCCH_3)$ (**1**, ppy=phenylpyridine, en=ethylendiamine), $[(ppy)_2Ir(pam)](OOCCH_3)$ (**2**), $[(bipy)_2Ru(bipy\text{-}OH)](PF_6)_2$ (**3**, bipy=2,2'-bipyridine, bipy-OH=2,2'-bipyrimide(4,4'-bis(oxyundecan1-ole), $[(bipy)_2Ru(bipy\text{-}TBDMS)](PF_6)_2$ (**4**, bipy= 2,2'-bipyridine, bipy-TBDMS=2,2'-bipyrimide(4,4'-bis((tert-butyldimethylsilyl)oxy)undecyl) was performed in the Laboratory of Inorganic and Coordination Chemistry (University of Calabria) by using the method reported (Scheme 2). All complexes were characterized by elemental analysis, ^1H NMR and IR spectroscopies.

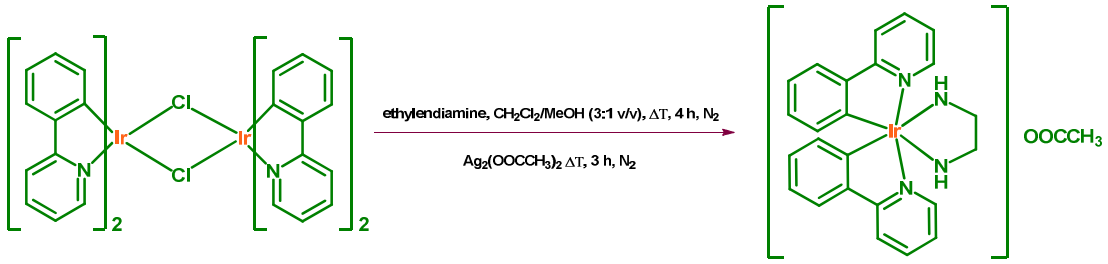

1 (81%)

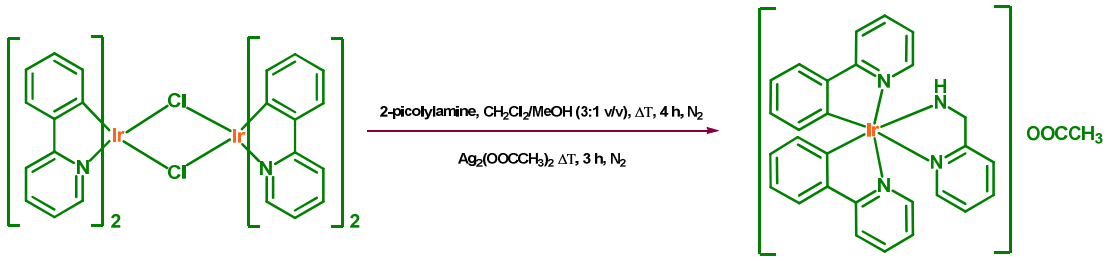

2 (83.8%)

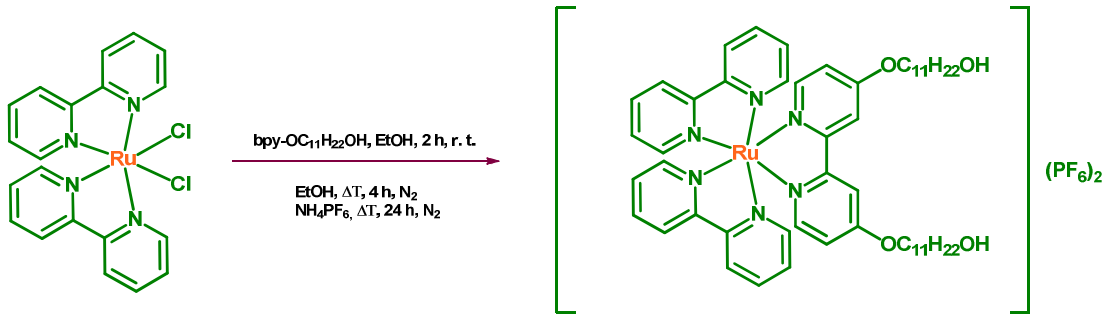

3 (65%)

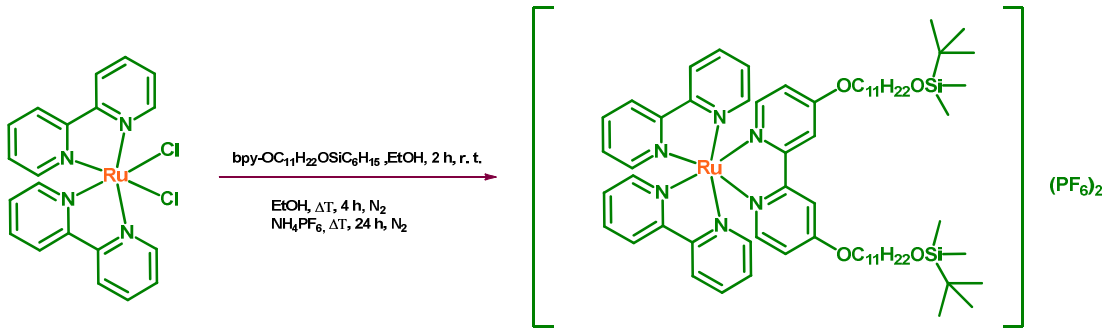

4 (72%)

Scheme 2. Synthesis of **1**, **2**, **3**, **4** complexes. In brackets, the reaction yield is reported.

3.4.2.2 Photophysical characterization in solution

All complexes were characterized in solution at room temperature, in presence or absence of oxygen. For the emission quantum yield measurements, $Ru(bipy)_3Cl_2$ in aerated water was used as standard (§ Appendix). Table 6 and 7 report the obtained photophysical data.

Table 6. Absorption data for complexes **1-4** in solution at room temperature.

	solvent	Abs, λ_{max}/nm (10^{-3} ε/M^{-1} cm^{-1})
1	H_2O	425(1.87), 392(2.5), 345(3.12), 300(sh), 270(sh), 256(24.37)
2	H_2O	420(2.42), 385(3.57), 342(5.35), 300(sh), 256(35)
3	CH_2Cl_2	465(14.102), 435(12.107), 362(7.172), 327(12.483), 289(75.053)
4	CH_2Cl_2	465(14.003), 435(12.027), 362(7.560), 327(12.027), 289(75.601)

Table 7. Photophysical data for complexes **1-4** in solution at room temperature. The phosphorescence of singlet oxygen was recorded at 1273 nm in air-equilibrated solution. Average lifetimes are reported (§ Appendix A.1).

	Em, λ_{max}/nm	Φ	τ/μs	Φ_{deox}	τ_{deox}/μs	k_r/s^{-1}	k_{isc}/s^{-1}	$k_q[O_2]/ s^{-1}$	Em 1273 nm
1[a]	515	0.10	0.395	0.58	2.182	2.56×10^5	1.93×10^5	2.11×10^6	Yes[c]
2[a]	490, 515	0.08	0.422	0.36	1.813	1.90×10^5	3.54×10^5	1.83×10^6	Yes[c]
3[b]	630	0.04	0.391	0.08	0.884	1.03×10^5	1.03×10^6	1.43×10^6	Yes[d]
4[b]	630	0.04	0.370	0.08	0.874	1.08×10^5	1.05×10^6	$1,55 \times 10^6$	Yes[d]

[a]H_2O solution; [b]CH_2Cl_2 solution; [c]D_2O solution; [d]THF solution.

Iridium complexes. The absorption spectra of complexes **1** and **2** were recorded at room temperature in water solution (Table 6; Fig. 16). The UV region is dominated by intense spin-allowed $^1\pi$-π^* (^{1}LC) transitions involving the aromatic ligands. At lower wavelength (350-450 nm), less-intense ^{1}MLCT bands are present. Because absorption spectrum of **2** is superimposable to that of **1**, where ligand-to-ligand charge transfer (LLCT) band are absent (due to the absence of aromatic ancillary ligands), it can be concluded that also in **2** picolylamine ancillary ligand is not involved in low-energy transitions. Additionally, the weak tails observed above 450 nm are due to direct spin-forbidden population of the triplet excited states (^{3}MLCT

and ^{3}LC ($^3\pi$–π^*) transitions), enabled by the high spin-orbit coupling of the iridium metal core that allows the mixing of triplet states with the higher-lying ^{1}MLCT levels (Costa 2012).

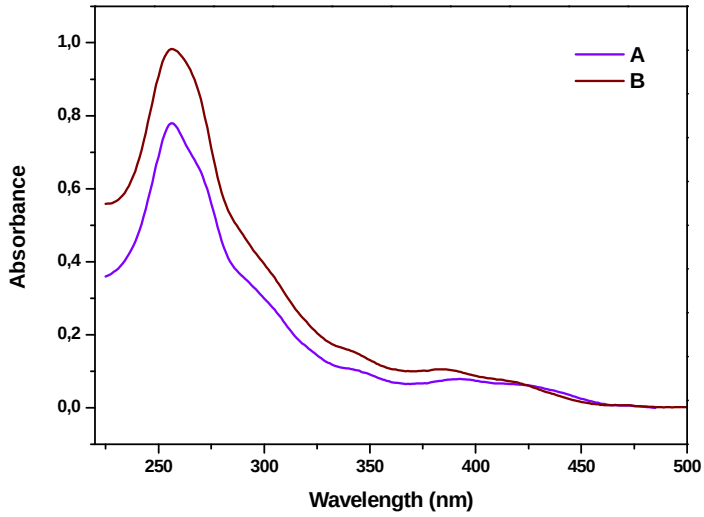

Figure 16. Absorption spectrum of **1** (**A**) and **2** (**B**) in water at room temperature.

The high spin-orbit coupling of Ir(III) yields almost unitary intersystem crossing efficiency from singlet to triplet excited states, therefore iridium(III) complexes always exhibit efficient spin-forbidden phosphorescence emissions. The emitting state is the lowest-energy triplet which normally arises from "mixed" triplet levels, due to the contributions of ^{3}MLCT and ^{3}LC states. Depending on the extent of contribution of the CT states, the emission profile is substantially affected: the presence of vibrational features suggests a low CT character, whereas broader and less structured shapes are indicative of a high charge-transfer character. Complexes **1** (Fig. 17) and **2** (Fig. 18) show a good luminescence at about 515 nm, slightly structured in **2**, probably due to a major ^{3}LC contribution respect to **1**; as expected, the emission is highly sensitive to the oxygen.

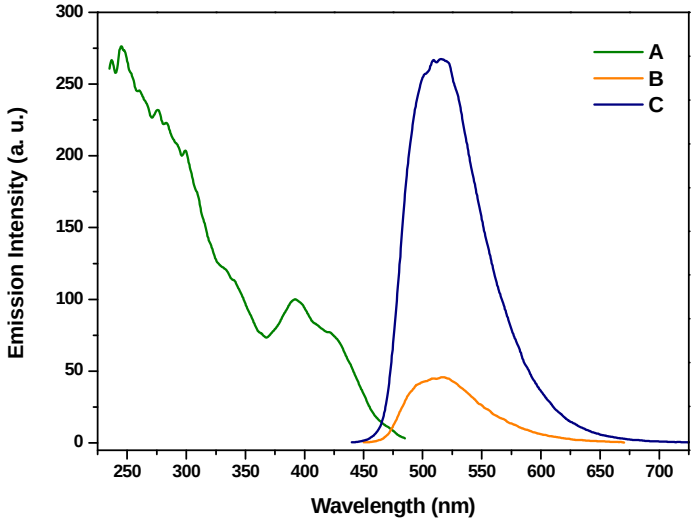

Figure 17. Excitation spectrum (**A**) in degassed water (λ_{em}= 515 nm) and emission spectra of **1** at room temperature in air-saturated (**B**) or in degassed (**C**) water (λ_{ex}= 260 nm).

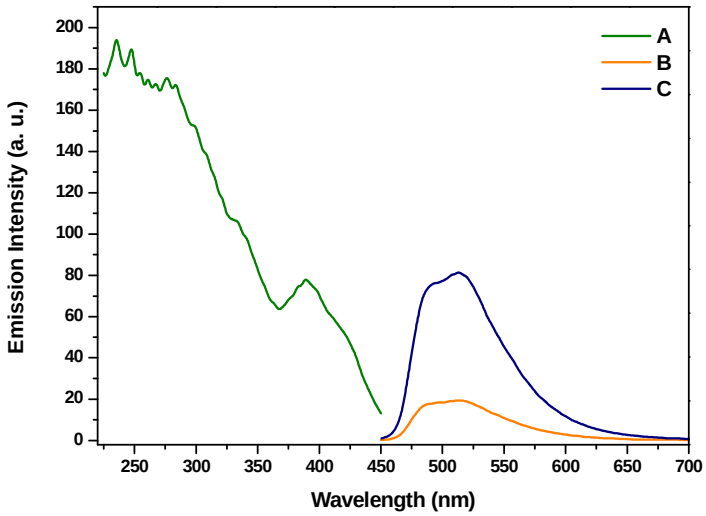

Figure 18. Excitation spectrum (**A**) in degassed water (λ_{em}= 510 nm) and emission spectra of **2** at room temperature in air-saturated (**B**) or in degassed (**C**) water (λ_{ex}= 382 nm).

Time-dependent emission intensities of **1** (Fig. 19) and **2** (Fig. 20) have been fitted by a mono-exponential decay. Bi-exponential function, despite give a better χ^2 value (§ Appendix A.3), provided a couple of lifetime values in the same temporal range with

a pre-exponential terms ratio of 9:1 in favor of the slower lifetime, which almost coincide with the average lifetime reported in Table 7. In Ar-equilibrated solutions, **1** and **2** show a lifetime of 2.18 and 1.81 μs, respectively, that are reduced to 0.39 and 0.42 μs in presence of oxygen. Similar values and behavior have been recorded for the parent compound $Ir(ppy)_3$ (Holzer 2005). Correspondingly, emission quantum yield value decreases from 0.58 and 0.36, recorded for **1** and **2**, respectively, in absence of oxygen, to 0.10 and 0.08 in air-equilibrated solution. The Φ-value of **1** in deaerated water solution appears to be among the highest values ever reported for Iridium cyclometalated complexes (a comparable value of 0.64 was reported by Barigelletti et al. (Shaffner-Haman 2004) for a tris-cyclometalated Ir complex of a substituted phenyl-pinenopyridine).

On the basis of the high-value of the Iridium spin-orbit coupling constant, is reasonably to consider near unitary the Φ_{isc} value of the intersystem crossing path towards emitting triplet state of iridium complexes; therefore the rate constant for radiative de-exciting process (k_r) of the energy-lowest excited state is given by:

(3) $$k_r = \Phi/\tau$$

In the absence of any quencher, non-radiative path of the lower-energy triplet state coincides with the intersystem crossing toward ground-state; therefore the rate constant for non-radiative process (k_{nr}) is given by:

(4) $$k_{nr} \equiv k_{isc} = (1- \Phi_{deox})/\tau_{deox}$$

In presence of oxygen, the luminescence of the complexes is quenched with a rate that can be drawn on the basis of the equation below:

(5) $$\tau_{deox} / \tau = 1 + k_q \tau_{deox} [O_2].$$

By comparing the values of k_r, k_{isc} and $k_q [O_2]$ of the iridium complexes **1** and **2** (Table 7), it can be stated that:

1) iridium complexes show an intense luminescence due to the high k_r value respect to k_{isc};

2) iridium complexes luminescence is strongly quenched by oxygen due the higher value of $k_q [O_2]$ respect to the competitive k_r and k_{isc}; taking into account the oxygen concentration in water (Montalti 2006), the k_q values for **1** and **2** are 7.80×10^9 and

6.77 x 10^9 sec^{-1}, respectively. These appear to be among the highest value ever reported for quenching of luminescence of transition metal complexes by oxygen; for comparison purposes, k_q is ca. 2 x 10^9 $M^{-1}s^{-1}$ for both $Ru(bipy)_3^{2+}$ and $Os(bipy)_3^{2+}$, and 1.1 x 10^8 M^{-1} s^{-1} for $Ir(tpy)_2^{3+}$ (tpy = terpyridine) (Shaffner-Haman 2004).

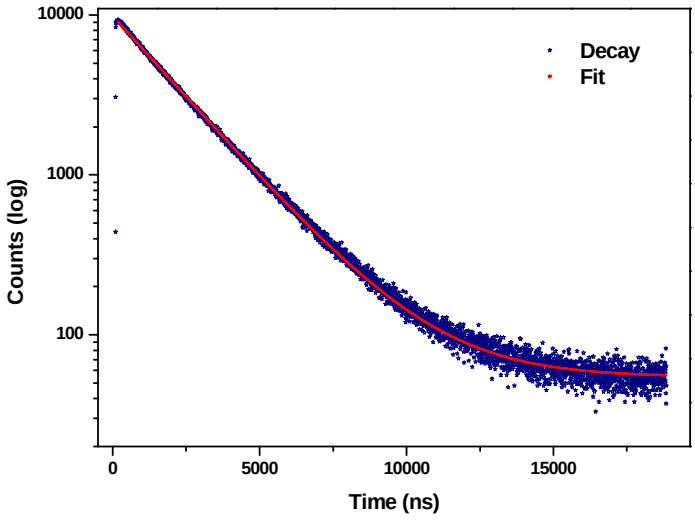

Figure 19. Time-resolved emission decay of **1** in degassed water (λ_{ex}= 379 nm, $\lambda_{monitored}$= 540 nm). Fitting results (χ^2 =1.32): τ = 2.148 x 10^{-6} s.

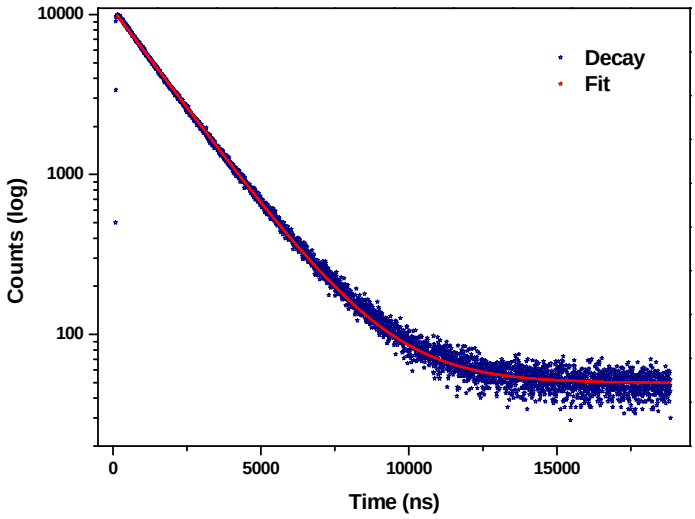

Figure 20. Time-resolved emission decay of **2** in degassed water (λ_{ex}= 379 nm, $\lambda_{monitored}$= 510 nm). Fitting results (χ^2 =1.28): τ = 1.755 x 10^{-6} s.

Concerning the fit of the intensity emission decays of **1** and **2** obtained by a bi-exponential function (§ Appendix A.3), it should be considered aggregates formation in solution. Quantitative investigations have been performed on very concentrated solutions of **1** and **2** (1.0×10^{-5} and 1.0×10^{-4}), where the formation of aggregates is predictable, according to literature (Guerrero-Martínez 2008). Nevertheless, no change in the absorption and emission spectra has been detected by varying concentration; also lifetimes remain almost unchanged. Emission quantum yield, instead, shows a variation (its value slightly increases by increasing concentration), but it has to be considered the intrinsic uncertainty of the measurement (§ Appendix A.1) and the high absorbance on the exciting wavelength of the concentrated solutions.

Ruthenium complexes. The absorption spectra of complexes **3** and **4** were recorded at room temperature in water solution (Table 6; Fig. 21), and are practically superimposable, due to the negligible effect exerted on the electronic properties by the different bipyridine substituent. The band assignment takes advantage from the several photophysical studies concerning the parent compound $Ru(bpy)_3^{2+}$ (Juris 1988), whose electronic spectrum shape and molar extinction coefficients are very similar to those of **3** and **4**. The band at 285 nm was assigned to LC π-π^* transition by comparison with the spectrum of protonated bipyridine; the band at 465 nm (with the shoulder at 435 nm) is due to a MLCT excitation, while the shoulders at 327 and 362 nm were assigned to MC transitions.

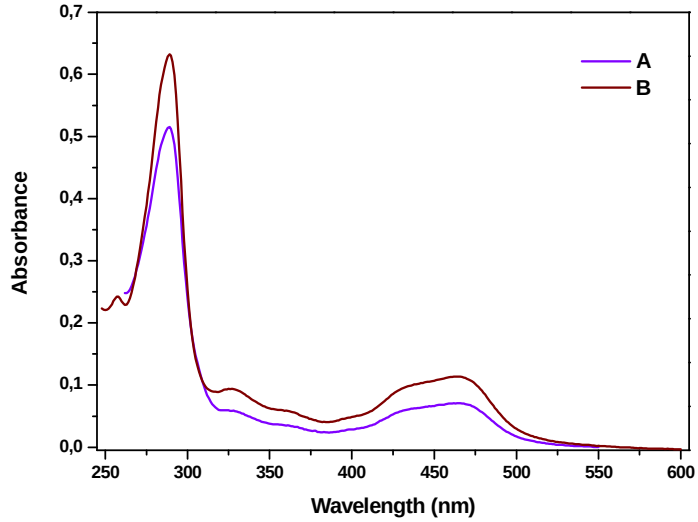

Figure 21. Absorption spectrum of **3** (**A**) and **4** (**B**) in dichloromethane at room temperature.

Like absorption, also the emission spectra of **3** (Fig. 22) and **4** (Fig. 23) in dichloromethane solution at room temperature, are superimposable and very similar to that of $Ru(bipy)_3^{2+}$. The emission origins from a ^{3}MLCT state with a maximum at 630 nm, slightly quenched by oxygen.

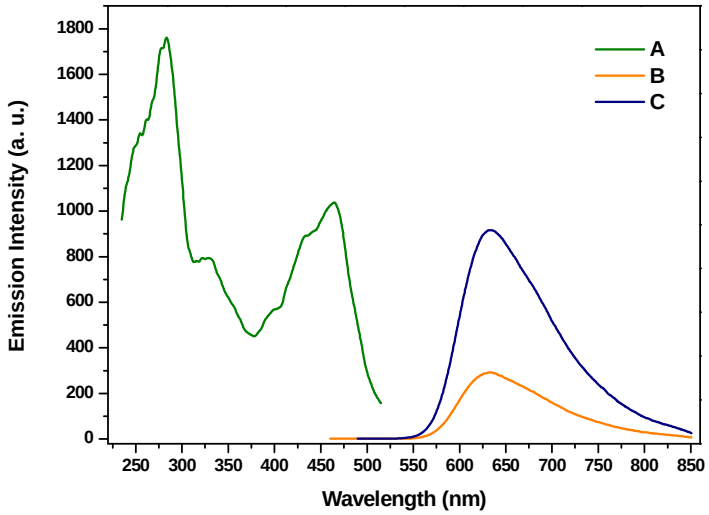

Figure 22. Excitation spectrum (**A**) in degassed dichloromethane (λ_{em}= 630 nm) and emission spectra of **3** at room temperature in air-saturated (**B**) or in degassed (**C**) dichloromethane (λex= 465 nm).

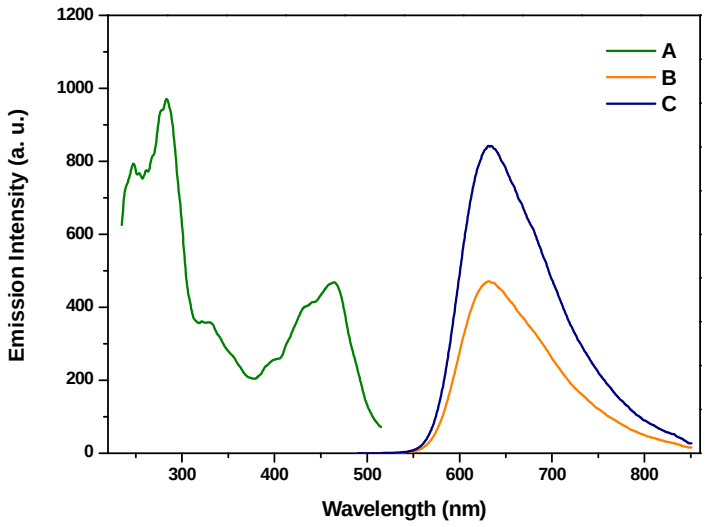

Figure 23. Excitation spectrum (**A**) in air-saturated dichloromethane (λ_{em}= 630 nm) and emission spectra of **4** at room temperature in air-saturated (**B**) or in degassed (**C**) dichloromethane (λ_{ex}= 465 nm).

The emission quantum yield of both ruthenium complexes (Table 7) is low, in absence or in presence of oxygen (ranging from 0.09 to 0.04), and similar to that of $Ru(bipy)_3^{2+}$. (Juris 1988), while lifetime decays, practically identical in **3** (Fig. 24) and **4** (Fig. 25), have been fitted with a bi-exponential function (see §Appendix A.3 for detailed values) giving an average value of 0.88 μs, in absence of oxygen, reduced to 0.39 μs in air-equilibrated solution. A mono-exponential fitting was also performed on the luminescence time decays of **3** and **4** (Fig. 24-25) giving values practically coincident with the average lifetime reported in Table 7. The scarce luminescence of ruthenium complexes is due to the thermally populated ^{3}MC states near in energy to the emissive ^{3}MLCT state, which opens efficient non-radiative path to the excite state. The rate constant k_{nr} (ca. 2.5 x 10^6 s^{-1} for both compounds) competes efficiently with k_r (1.0 x 10^5 s^{-1}) as well as with $k_q[O_2]$ (1.5 x 10^6 s^{-1}), so the ^{3}MC population is more rapid than the oxygen sensitation. Consequently, lifetimes and Φ-values are slightly affected by the oxygen presence.

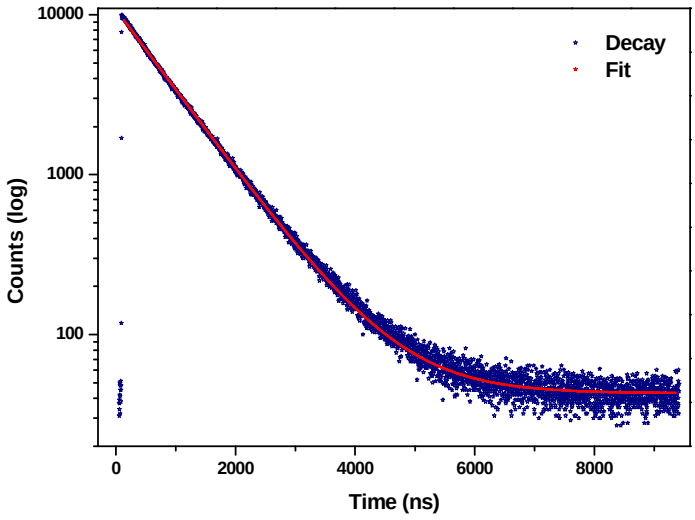

Figure 24. Time-resolved emission decay of **3** in degassed dichloromethane (λ_{ex}= 460 nm). Fitting results (χ^2 = 1.30): τ = 0.872 x 10^{-6} s.

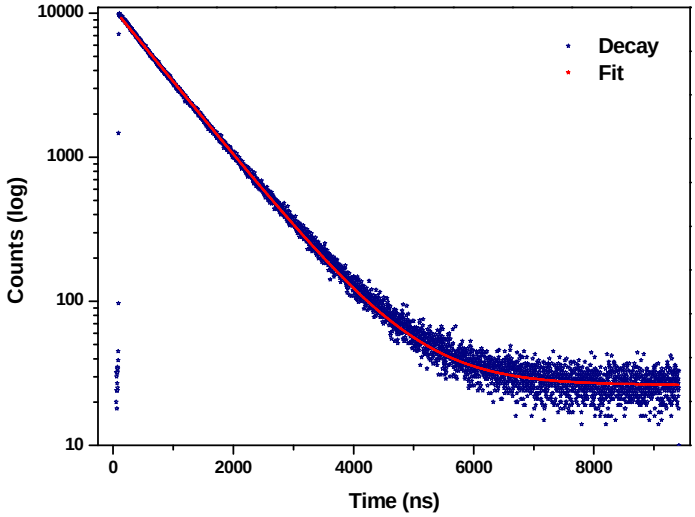

Figure 25. Time-resolved emission decay of **4** in degassed dichloromethane (λ_{ex}= 460 nm). Fitting results (χ^2 = 1.32): τ = 0.869 x 10^{-6} s.

In order to characterize the sample utilized to entrap ruthenium complexes in gold-silica nanoparticles (§ 4.3.2), a solution of **3** was prepared by adding 1 mg of complex in 0.1 mL of DMSO solution, and successively was added water to a final volume of 50 mL, obtaining a final concentration of 1.6 x 10^{-5} M. Absorption and emission spectra were identical to those recorded from dichloromethane solution, while the

emission quantum yield from air-equilibrated DMSO/water solution is $\Phi = 0.011$, a value slightly lower respect to one recorded from dichloromethane solution (Table 7). It was impossible to measure the emission quantum yield from deaerated solution because, during argon-bubbling procedure, the complex precipitated, due to its scarce water solubility. Average lifetimes $<\tau>$, obtained by a bi-exponential fitting decay, are lower respect to ones derived from the dichloromethane samples (Table 7): $<\tau>$ = 0.305 ms (τ_1 =0.25 μs, α_1 = 58.5%; τ_2=0.36 μs, α_2= 41.5%) in air-equilibrated solution; $<\tau>$ = 0.603 ms (τ_1 =0.33 μs, α_1 = 29.0%; τ_2=0.66 μs, α_2= 71.0%) in degassed solution.

3.5 Transition Metal Complexes in PDT

One of the applications of the long-lived triplet excited states of transitions metal complexes (TMCs) is the production of singlet oxygen, the key reactive species in the Photodynamic Cancer Therapy (§ 3.1.3). The high quantum yield of singlet oxygen generation is a crucial parameter that a photoactivable metal anticancer agent should have, but not the only one. Aspects such as aqueous solubility, cell uptake and stability in biological media are common considerations for any potential drug. In addition an ideal photosensitizer should have a large difference between cytotoxicity in the presence and absence of irradiation, in order to limit unwanted side-effects, and the wavelength of activation should ideally lie within the phototherapeutic window. For current clinical applications the use of red light (~630 nm) is routine although for superficial tumors shorter wavelength e.g. blue (420 nm), may be more appropriate (Radu 2003).

Traditional drugs used in PDT are based on porphyrin derivatives, *e.g.* Photofrin® (Allison 2004), with or without (transition) metal ions (§3.2). Pt(II) complexes of porphyrins with propionic acid substituents have also been reported and their photodynamic potential tested in vitro against a mammary tumor cell line and in vivo toward various murine carcinoma (Ali 1999). In particular, the diamine dicarboxylato-Pt(II) complex, reported in Figure 26, showed the highest antitumor activity, reflecting the combined effect of the cytotoxicity of the Pt complex (linked to the pincer effect of the *cis*-platinum moiety (Jamieson 1999)) and the photodynamic activity of the porphyrin moiety.

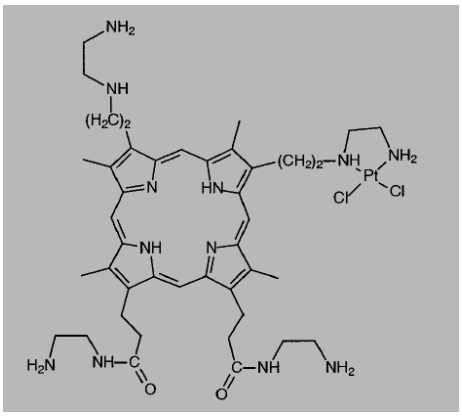

Figure 26. Molecular structure of a diamine dicarboxylato-Pt(II) complex (Ali 1999).

However, in porphyrinic systems, central metal hasn't an inductive function in $^1O_2$ photogeneration, but it enhances an intrinsic porphyrin property. Instead, in TMCs with bidentate N^N ligand or cyclometalated ones, metals are the effective inducer of the photosensitation.

TMCs of Pt(II), Ru(II) and Ir(III) able to generate $^1O_2$ with high yields, have potential as photosensitizers for PDT, but their effective phototoxicity has not yet been confirmed by cellular studies (Liu, Y., 2009; Djurovich 2007). A cyclometalated Ir(III) complex (Fig. 27), applied to the decoration of magnetic nanoparticles, has recently been reported (Wei 2008) and the resulting multimodal system used as imaging agent and PDT sensitizer. Human cervical cancer cells were chosen for cytotoxicity evaluation and the obtained results highlight an effective PDT response.

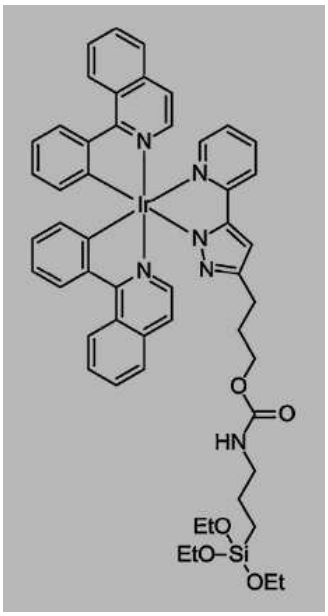

Figure 27. Molecular structure of [$(piq)_2$Ir(ppTES)] complex (Lai 2008).

In early studies (Boca 2009), a $[Ru(phen)_3]^{2+}$ complex functionalized with fluorene moieties has been reported (Fig. 28); the novel hydrosoluble complex was designed to be used *in vitro* for the first time as a Ru-photosensitizer for two-photon PDT (see below). The exposure of glioma cells to the complex in conjunction with excitation light at 740 nm, resulting in cellular damage, highlights its great potential in PDT.

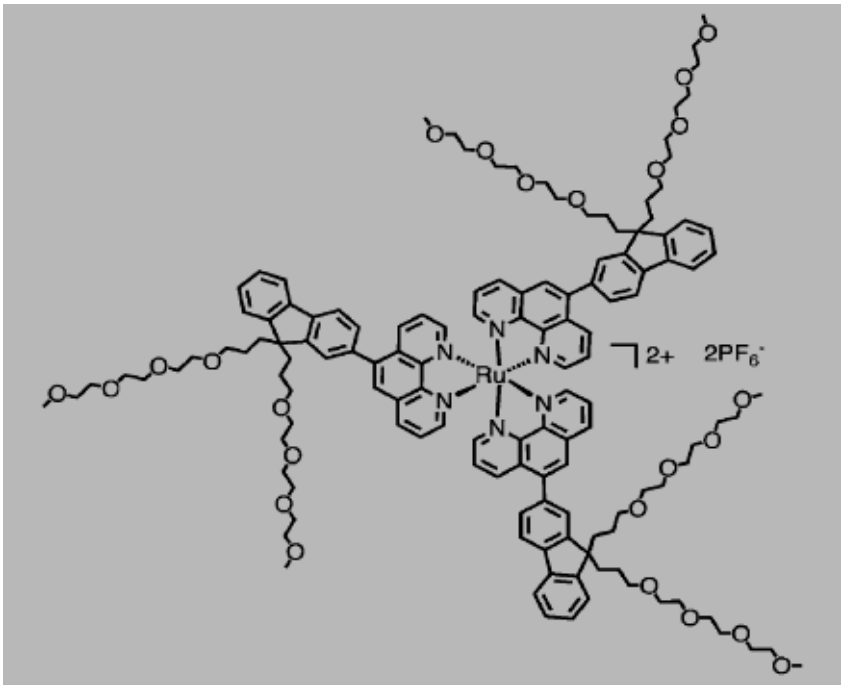

Figure 28. Molecular structure of $[Ru(phen)_3]^{2+}$ functionalized with fluorene moieties (Boca 2009).

Two-photon excitation is an effective way to extend the wavelength of excitation of a metal complex (He 2008). The advantage of the two-photon technique resides in the possibility of using higher wavelength radiations (*i.e.* in the near IR region), which are less energetic (and therefore less harmful to healthy tissues) than traditional visible-light radiations. In addition NIR light can penetrate deeper in the tissues, expanding the use of PDT to deeper lesions. It imposes constraints on the structure of the compound, and the light source needs to have a high photon density (*e.g.* a femtosecond laser).

3.6 Strategy to obtain water solubility

Despite their advantages as $^1O_2$ photogenerators, TMCs low water solubility is the most significant problem limiting their use in various application fields where an aqueous environment is involved, such as blood sterilization, wastewater treatment and photodynamic therapy. Most existing photosensitizer molecules (PS) are hydrophobic and can easily aggregate in aqueous media (Zimcik 2007; Kuimova 2009; Choi 2000; Martin 1991). This intermolecular association process promotes a non-radiative internal conversion, which is competitive with the intersystem crossing, inducing a drastic decrease of $^1O_2$ generation.

A great deal of research has been done to overcome this problem especially in the PDT context where the PS poor solubility in water also hampers the preparation of pharmaceutical formulations for parenteral administration. Therefore, many strategies have been taken into account to dissolve lipophilic compounds in a biological environment, including PS bonded to hydrophilic polymer or their incorporation in biocompatible nanocomposites, such as polymeric micelles, liposomes and polymeric nanoparticles (Konan 2002; Peng 2010; Paszko 2011; van Nostrum 2004; Allison 2008; Derycke 2004; Choi 2006; Tu 2009), which can also act as delivering agent of the PS.

Generally, there are several advantages to the use of immobilized photosensitizers in practical applications. For use in water purification, for example, the ability to recover and reuse photosensitizers makes environmental and economic sense. Moreover, because these photosensitizers are used heterogeneously, immobilized photosensitizers can be employed in a number of solvents, allowing flexibility in fine chemical synthesis. In general, immobilized photosensitizers show reduced quantum yields than their unbound counterparts, due in part to the need for oxygen to diffuse into and out of the polymer matrix in order to be sensitized and detected. Nevertheless, the ease of reuse of these systems tends to outweigh this shortcoming.

Polymer-bound PS. Polymer-bound PS are under extensive investigations and have a promising PDT applications compared to free PS due to extended intravascular

half-life, enhanced tumor selectivity and good PDT efficacy. *N*-(2-hydroxypropyl)methacrylamide (HPMA) copolymer-bound mesochlorin ethylendiamine exhibited a substantial increased cell tumour accumulation and drug efficacy compared to the free drug (Tijerina 2000; Soukos 1997). The photodynamic potential of polyethylene glycol (PEG) or poly(vinyl alcohol) (PVAL) conjugated to chloroaluminum phthalocyanine via an axial coordination bond was also evaluated *in vitro* and *in vivo* (Brasseur 1999). PEG was also bound to m-tetrahydroxyphenylchlorin (m-THPC) and this conjugate has proven to be effective in inducing tumor growth delay at m-THPC equimolar doses (Westermann 1998). However, the benefits from increased water solubility of the PS are balanced by the fact that the yield of singlet oxygen generation can undergo a decrease following the incorporation of the PS in a polymer. Work by Schaaps (1975) compared the efficiency of singlet oxygen production of free Rose Bengal to Rose Bengal immobilized on merrifield polymer (*i.e.*, a polystyrene polymer based on a copolymer of styrene and chloromethylstyrene). Results found that the free photosensitizer had a 100-fold higher production rate of singlet oxygen, due most likely to diffusion problems.

Polymeric micelles. Polymeric micelles are formed in aqueous solution from amphiphilic block or graft copolymers. In PDT, they have great potential as an effective drug delivery system for poorly soluble photosensitizers, which can be physically entrapped in and/or covalently bound to the hydrophobic core. One example, protoporphyrin IX (PpIX) encapsulated in methoxy poly(ethylene glycol)-b-poly(caprolactone) micelles: these systems show higher intracellular accumulation of the drug and higher photocytotoxicity in comparison to free PpIX (Li 2007).

Liposomes. Liposomes are lipid vehicles of one or more concentric phospholipid bilayers, containing an aqueous phase inside and between bilayers. The phospholipids typically used for preparing liposomes are comprised of a hydrophilic head group and two hydrophobic chains. This composition assures that liposomes are able to encapsulate both hydrophilic and hydrophobic drugs. Their main components (phospholipids and cholesterol) are materials also existing in the body in high amounts and may provide a good biocompatibility. Introduced to increase the solubility of hydrophobic chemotherapeutics, they have been shown to be effective in

reducing systemic side effects and toxicity, as well as in attenuating drug clearance. In PDT studies, liposomal formulations show the ability to decrease the tendency of photosensitizer to aggregate and improve the tumor-selective accumulation (Derycke 2004) are currently used as effective delivery systems in experimental studies and in clinical trials. In terms of clinical use and as a pharmaceutical success story, Visudyne® should be mentioned: it consists of a liposomal formulation of Verteporfin, a semi synthetic porphyrin approved by the FDA in 2000 for the treatment of the wet form of age-related macular degeneration (Miller 1999).

Nanoparticles. Biodegradable and non-biodegradable nanoparticles (<1 μm size) represent emerging photosensitizer carriers. In particular due to their unique characteristic, hybrid nanomaterials have recently been investigated as promising platforms for diagnosis and therapeutic applications. Nanoparticles encapsulating PS will be treated extensively in Chapter 4.

3.7 A new water-soluble polymer binding a platinum complex showing oxygen photosensitizing properties

The **(pam)Pt(Cl)$_2$** complex (§ 3.4.1), as previously illustrated, is not soluble in water, and therefore, is not applicable to biological systems to generate singlet oxygen. In order to overcome the water insolubility of the Pt(II) complex, it has adopted a new strategy by means of grafting insertion of the platinum compound into polymethacrylic acid, a well-known biocompatible compound (Fig. 29). The grafting procedure is illustrated in the Appendix.

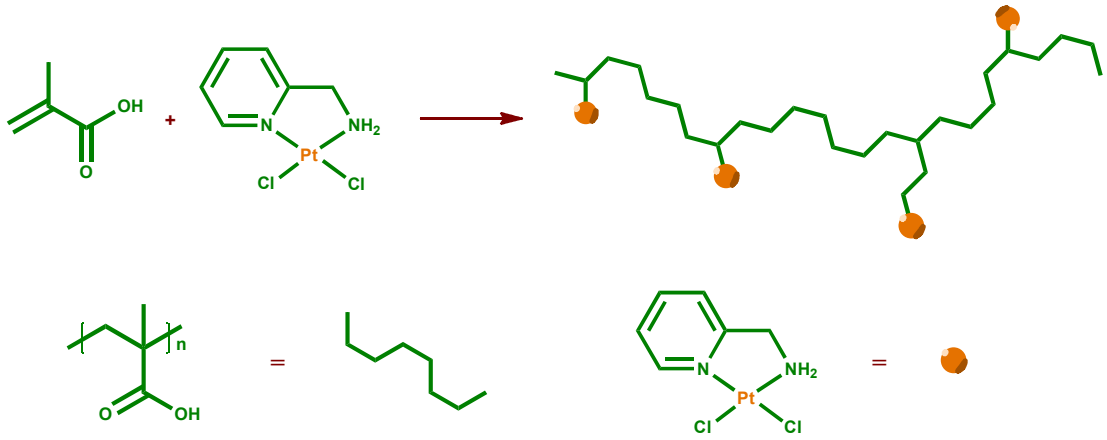

Figure 29. Grafting insertion of the **(pam)Pt(Cl)$_2$** complex into polymethacrylic acid.

The obtained grafted polymer exhibits an emission spectrum, in water solution and in air-equilibrated conditions, with a vibronic couple of bands at 483 and 516 nm (Fig. 30). Lifetime measurements gave a decay, recorded at 516 nm, that was deconvoluted obtaining a value of 0.68 μs. After the oxygen is removed, the fine structure of the phosphorescence band is lost, showing an intense band at 503 nm with a shoulder at about 515 nm (Fig. 30). The emission decay trace of the degassed water solution, recorded at 510 nm, gave a luminescence lifetime of 2.05 μs. The emission quantum yield increases from 1×10^{-3} to 9.1×10^{-3}, passing from the air-equilibrated solution to the degassed one ($Ru(bipy)_3Cl_2$ in aerated water was used as standard; see § Appendix for the Experimental Conditions).

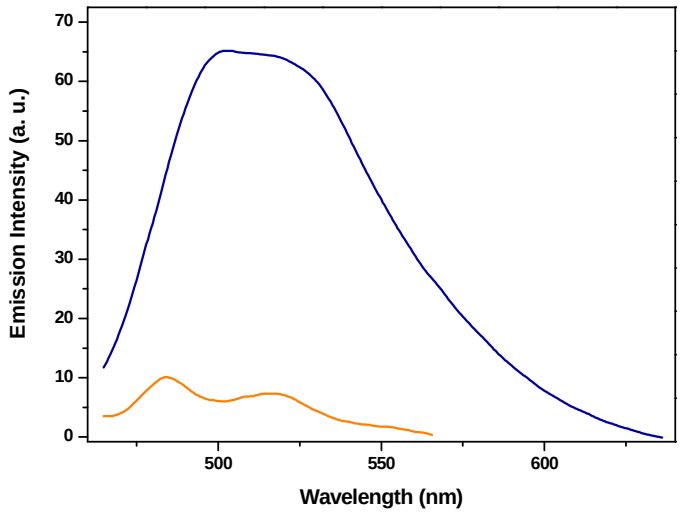

Figure 30. Emission spectra of complex grafted polymer at room temperature in air-saturated water solution (orange line) and in degassed water (blue line).

Analogously to the attribution of the luminescence of the **(pam)Pt(Cl)$_2$** free in acetonitrile solution (§3.4.1), the emission of the grafted polymer in water is attributed to a vibronic progression from the ^{3}MLCT state deactivation of the platinum complex. The spectroscopic differences between the Pt-complex grafted to the polymer and free in solution are due to the different solvent used in the two cases, and to the more rigid environment experienced by the chromophore in the polymeric matrix. In particular, while in air-equilibrated solution the free complex does not emit, **(pam)Pt(Cl)$_2$** grafted to the polymer show a weak and structured phosphorescence, which is due to the low oxygen diffusion into the polymer that reduces luminescence quenching. When oxygen is completely removed, both the intensity of phosphorescence that the lifetime increases, and the latter attains the value of 2.05 μs, which is the same value obtained from the free complex in the absence of oxygen. In degassed solution, the emission quantum yield value is higher when the Pt complex is embedded in the polymer with respect to the free complex; this behaviour is expected because in the polymer the chromophore experiences a rigid matrix that enhances phosphorescence emission.

3.8 Conclusions

Singlet oxygen is a highly-reactive species which use spans from wastewater disinfection to non-invasive treatment of cancer. A simple way to generate $^1O_2$ is to transfer excitation energy from a light-absorbing molecule, called photosensitizer, towards ubiquitous dioxygen. Since the major application field of this phototherapy concerns living matter, water solubility of singlet-oxygen photosensitizer is highly requested. Moreover, because the energy—transfer process occurs via collision between photosensitizer and O_2, the diffusion-limited rate of the process requires a long-lived excited species able to interact with ground-state oxygen.

Transition metal complexes (TMCs) excited-states show adequate lifetimes, whit a tunability of spectral properties which make them suitable to be proposed as excellent oxygen-photosensitizers. In this context, we have photophysically characterized a series of newly-synthesized complexes of second and third transition row: a neutral complex of Pt(II), two Ir(III)- and two Ru(II)-cationic complexes, starting from the assumption that the large spin-orbit coupling constant favors an excellent intersystem crossing towards the long-living triplet state.

We have used to way to demonstrate the TMCs ability to form $^1O_2$: (*i*) an indirect one, *i.e.* to compare the TMC phosphorescence intensity of an air-equilibrated with an argon-bubbled solution, and (*ii*) a direct one, *i.e.* to detect the characteristic singlet oxygen phosphorescence at about 1270 nm. In fact, the simply TMC phosphorescence quenching by oxygen does not imply a $^1O_2$ generation, because ground-state state oxygen can quench TMC triplet state via triplet-triplet annihilation or by oxygen-radical production.

The obtained results confirm singlet oxygen generation, and show different behavior of the examined complexes; Pt(II) complex is the only totally quenched by oxygen, while Ir(III) and Ru(II) show an appreciable luminescence also in presence of oxygen (Φ about 10% for iridium- and 4% for ruthenium-complexes). In absence of quencher, iridium-complexes are highly-luminescent (Φ = 58% and 36% for the two compounds), ruthenium-ones show a good luminescence intensity (Φ = 4% for both compounds), while the platinum complex shows a weak emission (Φ = 0.72%). This behavior can be rationalized by considering that, despite the spin-orbit coupling

constant of Pt(II) is the higher among the examined metals, the studied complex has a small radiative constant, so non-radiative pathways are highly-favored. On the contrary, the k_r-value of the iridium complexes effectively competes with monomolecular and bimolecular non-radiative rate constant, so giving an appreciable emission also in presence of oxygen. Ruthenium complexes behavior is intermediate between them, cause an intermediate value of k_r (but, in general, k_r in Ru(II) complexes is low for the presence of thermally-activated MC state, which depopulate the emitting state).

Because many applications of oxygen photosensitizers require their solubility in water, we have explored the possibility to insert the platinum compound into polymethacrylic acid, without losing the sensitation capability. A water-soluble polymer with photosensitizing properties was obtained, and the complex insertion is an easy, one-pot process that requires mild reaction conditions. Moreover, the covalent linking of the Pt-complex to a biocompatible polymer backbone prevents the photosensitizer aggregation in aqueous solutions, which could cause a drastic reduction of $^1O_2$ generation.

Respect to the free complex, the grafting insertion of the Pt(II) complex into the polymeric matrix causes an increases of the phosphorescence quantum yield (due to a more rigid environment respect to the solution), which favor the energy transfer towards oxygen, but, on the contrary, the reduced O_2 permeability into the polymethacrylc acid, could reduce the photosensitizing efficiency. Nevertheless, the availability of a water-soluble polymer capable of producing singlet oxygen offers the possibility of an additional functionalization of the polymethacrylic acid, which is highly required in several areas of application where the production of the singlet oxygen is the key factor. A great potential application could be the use of this water soluble grafted polymer as a photosensitizer in photodynamic therapy. Actually, a polymeric substrate is able to bind different groups: sugar as *N*-acetylglucosamine, that can induce the biocompatibility toward specific target organs, or chromophores, suitable to show two-photon-absorption (TPA) phenomena and capable of efficient Förster resonance energy transfer to the photosensitizer which is very useful to take advantage of the spectral therapeutic window.

Chapter 4 THE THERANOSTIC PARADIGM: TRANSITION METAL COMPLEXES AND NANOPARTICLES

In 2008 on Nanomedicine appeared an editorial by Sumer and Gao (Sumer 2008) that stated: "*Theranostics was coined originally as a term to describe a treatment platform that combines a diagnostic test with targeted therapy based on the test results. Here, we define theranostic nanomedicine as an integrated nanotherapeutic system, which can diagnose, deliver targeted therapy and monitor the response to therapy*". Accordingly to this definition, a theranostic system should basically made of a sensor capable of detect a diseased cell (*i.e.* to specifically localize into it and to send a signal to an operator), and of an active species able to exert a therapeutic effect on lesion.

Reliable sensors often use light as signal, *i.e.* absorbed light to be interrogated by an operator and emitted light to provide an answer. Moreover, an advisable delivering drug system should use light to be activated. Such ideal "soft" theranostic system, that combines both aspects with light, may be identified with properly functionalized nanoparticles.

4.1 Nanoparticles: a therapeutical aspect

Nanoparticles (NPs) represent a relatively new trend in drug delivery: they can improve the solubility of poorly water soluble drugs, prolong their circulation half-life in the blood, minimize enzymatic degradation of the drug after administration, decrease side effects and increase bioavailability. They show a high ability to specifically recognize and bind to target areas via surface attached specific ligand, for example monoclonal antibodies, folate etc. Moreover, nanovehicles including micelles, liposomes, and metal nanostructures, with a hydrodynamic diameter greater than the renal clearance threshold (*ca*. 6 nm) and up to 2 µm, can be expected to exhibit preferential tumour accumulation, due to the phenomenon known as "enhanced permeability and retention effect" (EPR) (Iyer 2006). In fact, in contrast to normal vessels, the angiogenic neovascolature is characterized by a highly disordered endothelium with large gaps that permit the preferential penetration of nanosized structures.

NPs the particles can be classified in two main classes: biodegradable and non-biodegradable NPs. Within the first aliphatic polyester NPs are included, while, within the latter, polyacrylamide polymers-based NPs, silica, titania or metallic NPs are comprised. More interesting are NPs having a metallic core with a silica shell. Special properties carried out by the metal can offer magnetic (iron) or plasmonic (gold) characteristics to the NP.

4.1.1 Nanoparticles developed for Photodynamic Therapy

The therapeutic efficacy of NPs is highlighted in the cancer Photodynamic Therapy (§ 3.1.3), when a photosensitizer is charged into NP. Because the efficiency of PDT can be attributed to the production of $^1O_2$, two different strategies using NPs can be followed: biodegradable nanoparticles, from which photosensitizers can be released, are irradiated to produce $^1O_2$ or, alternatively, non-biodegradable nanoparticles are used, without releasing photosensitizers from NPs carriers but the oxygen can diffuse freely in and out of the nanoparticles (Bechet 2008).

Biodegradable nanoparticles. They are made of polymers that are degraded in a biological environment, so releasing the incorporated photosensitizers. Some of the best studied systems are NPs based on *poly*(lactic acid) (PLA), *poly*(glycolic acid)(PGA), and their copolymer (PLGA). The mechanism of degradation of aliphatic polyester nanoparticles, such as PLGA, involves a hydrolytic process.

As example, the well-known photosensitizer porphyrin-derivative meso-tetra(*p*-hydroxy-phenyl)porphyrin (p-THPP) (Kreimer-Birnbaum 1989) was encapsulated into sub-150 nm biodegradable nanoparticles (50:50 PLGA:PLA, 75:25 PLGA:PLA and PLA). A follow-up study was carried out to evaluate the photodynamic activity of these p-THPP loaded nanoparticles on EMT-6 mouse mammary tumour cells and compared to free p-THPP (Konan 2003). The beneficial effect of the nanoparticle over the free drug was observed mainly at a drug concentration of 3 μg/ml. This suggests that the therapeutic index of p-THPP can be improved by nanoencapsulation since low drug concentrations could be used for satisfactory photocytotoxicity. Similar results were obtained with NPs of bacteriochlorophyll-a (BChl-a) loaded PLGA that were introduced in macrophage cell lines (Gomes 2005). In another study based on PLGA nanoparticles, Ricci-Junior et al. (2006) reported preparation, characterization and results of the phototoxicity assay of PLGA nanoparticles containing zinc(II) phthalocyanine (ZnPc), a second generation photosensitizer widely used in PDT. The phototoxicity was assessed using P388-D1 cells, and after 24h of incubation, the cellular viability was determined obtaining a value of 40%. It was concluded that ZnPc loaded PLGA nanoparticles is a promising drug delivery system for photodynamic therapy. *In vivo* studies are not described in the literature for biodegradable nanoparticles.

Non-biodegradable nanoparticles. There are many advantages of using non-biodegradable NPs: a very low size (less than 100 nm), no time for biodegradation is needed, the photosensitizer is protected from the environment, NPs can serve as multifunctional platforms. Indeed, their chemical composition can be modulated by coupling or encapsulating photoactivable units for PDT treatment; their surface can be functionalized by attaching targeting groups, which will deliver the nanoparticles to cancer cells, to vascular compartments or to cellular sites expressing appropriate receptors. The surface can also be functionalized to introduce a hydrophilic,

hydrophobic or amphiphilic character to enable dispersion in a variety of fluid media and to increase the lifetime of the nanoparticles in the plasma and finally a contrast agent can be incorporated into the core to aid the use of the nanoparticles in magnetic resonance imaging (MRI).

For the synthesis of non-biodegradable NPs, polyacrylamide polymers can be used, although most of these NPs are ceramic-based (*i.e.*, made of silica) or metallic. Particles, including silica, alumina, titania, etc., are also known for their compatibility in biological systems (Lal 2000). In addition, their surfaces can be easily modified with different functional groups (Badley 1990). Therefore, they can be attached to a variety of monoclonal antibodies or other ligands to target them to desired sites *in vivo*. The acronym ORMOSIL is a commonly used abbreviation for 'organically modified silica' and different photosensitizers, such as 2-devinyl-2-(1-hexyloxyethyl) pyropheophorbide (HPPH), methylene blue and fullerene, have been encapsulated or covalently linked to ORMOSIL particles (Table 1).

Non-biodegradable nanoparticles		Size (nm)	Photosensitizer			Photophysical properties			*In vitro* experiments	
Applications	Shell composition		Nature	Covalently linked	Encapsulated	$\lambda_{max\ absorption}$ (nm)	Φf	$\Phi\Delta$	Cell line	Phototoxicity[a]
Therapy	ORMOSIL	20	Iodobenzylpyropheophorbide	Y	N	410	-	-	Colon-26, RIF-1 (murine fibrosarcoma)	Growth inhibition 100% (RIF-1)
	ORMOSIL	30	HPPH	N	Y	420	-	-	UCI-107 (human epithelial ovarian carcinoma), HeLa (cervical carcinoma)	Growth inhibition 90% (UCI-107); 100% (HeLa)
	ORMOSIL	160	Methylene blue	N	Y	650	-	-	C6 (rat glioma)	Positive photodynamic result (confocal microscopy)
	ORMOSIL	-	Fullerene C_{60}	Y	N	-	-	-	-	-
	ORMOSIL	180	*m*-THPC	N	Y	410	-	-	-	-
	Gold based	2–4	Phthalocyanine	Y	N	695	-	0.65	HeLa	Decreasing of metabolic activity (60%) 20 min p.i.
Therapy with biphoton excitation	PAA	-	TMPyP	N	Y	-	-	-	C6	Cells death 120 min p.i.
	ORMOSIL	30	HPPH (co-encapsulated with BDSA as a donor)	N	Y	420	0.17	-	HeLa	Drastic changes in the cells morphology 15 min p.i.

Abbreviations: BDSA = 9,10-bis[40-(400-aminostyryl) styryl] anthracene; HPPH = 2-devinyl-2-(1-hexyloxyethyl) pyropheophorbide; ORMOSIL = organically modified silica; p.i. = post-irradiation; TMPyP = 5,10,15,20 tetrakis(1-methyl 4-pyridino)porphyrin tetra(p-toluenesulfonate); TOAP = tetrakis (o-aminophenyl) porphyrin; Φ_Δ = quantum yield of singlet oxygen production; Φ_f, fluorescence quantum yield. '-' = no information given. a = best values.

Table 1. Significant studies for the use of non-biodegradable polymer-based nanoparticles for PDT (Bechet 2008).

Roy and colleagues (2003) reported the first use of ceramic-based NPs as a novel drug-carrier system for PDT, using silica based spherical particles approximately 30 nm in diameter, and encapsulating HPPH. Irradiation of the photosensitizing drug entrapped into NPs by light of suitable wavelength, an efficient generation of singlet oxygen resulted, which is made possible by the inherent NPs oxygen porosity. In fact the tiny pores which are 0.50-1.00 nm in diameter are large enough to enable efficient oxygen diffusion in and out the particle. The HPPH-loaded NPs were tested on tumor cells: the irradiation at 650 nm caused significant tumor cell death, with a cell viability fewer than 10%, highlighting the potential of ceramic-based NPs as carriers of water insoluble drug in PDT.

Lai et al. (2008) described the synthesis of different multifunctional system based on silica NPs with a Fe_3O_4 core and encapsulating, in the silica shell, an iridium complex. The Ir(III) complex $[(piq)_2Ir(ppTES)]$ (§ 3.5) has a dual role both photosensitizer and phosphorescent probe. It is the only example reported in literature of a transition metal complex encapsulated in the silica shell of NPs, which have been tested for its ability to sensitize oxygen. In fact, the successful incorporation of ionic complexes $[Ru(bpy)_3]^{2+}$ and/or $[Os(bpy)_3]^{2+}$ into silica NPs has been demonstrated for applications in biological labelling and imaging (§ 4.2.1), but not yet for the $^1O_2$ sensitization experiments (Wang 2006). Instead, NPs incorporating $[(piq)_2Ir(ppTES)]$, not only act as photosensitizer, but, used in biomedical applications, it was possible to obtain MRI imaging through the Fe_3O_4 core, and optical imaging thanks to the phosphorescence of the Ir complex. The main drawback of these multifunctional NPs based on the $[(piq)_2Ir(ppTES)]$ complex was the need for irradiation at 366 nm, which has been shown to be suboptimal for light penetration into the tissue, and hence for the applications of NPs as photosensitizers in clinical PDT. Actually, the region of maximum light depth penetration into mammalian tissue is 600-850 nm, the so-called "phototherapeutic window" (§ 3.1.3).

To overcome this limit, multifunctionality of NPs is a good opportunity. In fact, the possibility to functionalise a NP with a two-photon (TP) dye opens new possibilities. TP dyes have received much attention lately because of their ability to convert absorbed low-energy radiation to higher energy emissions. Dyes which can direct transfer the higher energy to a photosensitizer for generation of singlet oxygen can be very useful in PDT because they can be activated in deep tissues. Kim et al.

(2007) described the synthesis of modified silica NPs in which HPPH and an excess of 9,10-*bis*[40-(400-aminostyryl)styryl]anthracene (BDSA), a highly two-photon-active molecule acting as an energy donor, were co-encapsulated. HPPH absorption in nanoparticles had significant overlap with the fluorescence of BDSA aggregates. It enabled an efficient energy transfer through fluorescence resonance energy transfer (FRET) mechanisms, from BDSA to HPPH, which, in turn, sensitizes dioxygen to produce $^1O_2$. The nanoparticles were taken up by tumor cells and cytotoxic effect after two-photon excitation was demonstrated. He and co-workers (2009) reported a similar approach for the synthesis of silica nanoparticles with entrapped methylene blue (MB) dyes for near-IR imaging and PDT. The therapeutic effect of this platform was demonstrated *in vitro* by using HeLa cells and both fluorescence imaging and PDT effect were observed *in vivo* in a mouse xenograft model.

Concluding, NPs are a suitable platform to obtain a multifunctional material that merge both therapeutic and diagnostic properties (Fig. 1).

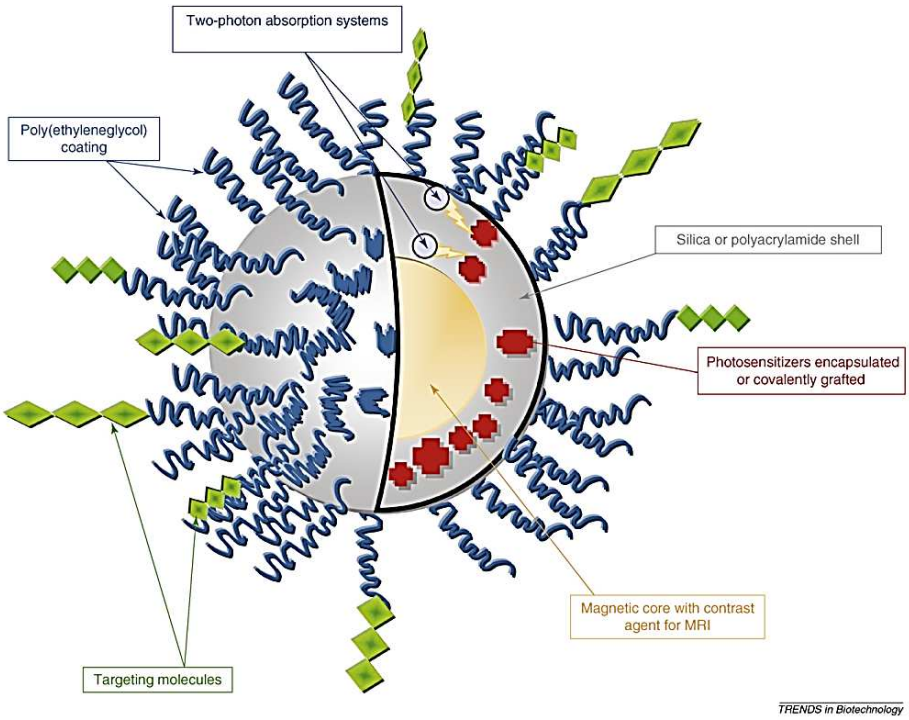

Figure 1. An ideal multifunctional nanoplatform (Bechet 2008).

4.1.2 Gold nanoparticles: a multifunctional material

Nanoparticles composed of gold (AuNPs) offer good biocompatibility, facile synthesis and conjugation to a variety of biomolecular ligands such as antibodies, proteins, nucleic acids (Cobley 2011), and other targeting moieties (Fig. 2), making them suitable for use in biochemical sensing and detection, medical diagnostics and therapeutic applications.

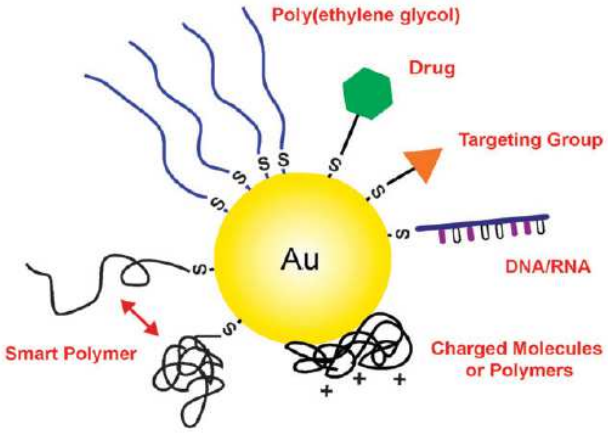

Figure 2. Gold nanoparticles can be conjugated with a wide variety of functional moieties, both through the gold–thiolate bond and by passive adsorption (from Cobley 2011).

Wieder et al. (2006) reported the development of a delivery system for PDT based on gold nanoparticles where the photosensitizer, a phthalocyanine derivative, is bound on the NP surface (Fig. 3A); the resulting drug-nanoparticle conjugates (observed by TEM) have an average diameter of 2-4 nm (Fig. 3B). When incubated with HeLa cells, the NP conjugates are taken up and, after irradiation, an improvement in PDT efficiency was observed compared to the free phthalocyanine, probably due to the 50% enhancement of singlet oxygen quantum yield observed for the phthalocyanine-nanoparticle conjugates. However, the efficacy of this system remains to be evaluated *in vivo*.

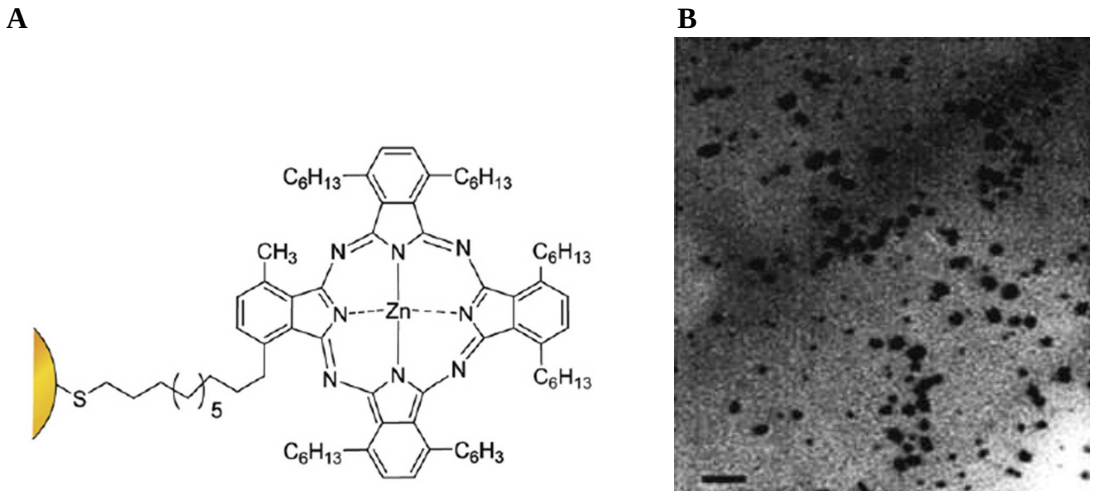

Figure 3. Phthalocyanine-functionalized gold nanoparticles for generation of singlet oxygen (**A**); TEM image of the functionalized AuNPs (scale bar represents 20 nm) (**B**).

Most recently Zhang and co-workers (Xu 2012) reported the conjugation of a precursor of the efficient photosensitizer protoporphyrin IX, the 5-aminolevulinic acid (ALA), onto AuNPs, to improve the efficacy of PDT. The ALA-AuNP conjugates showed greater cytotoxicity against K562 cells than ALA alone, and this result was attributed to the enhancement of the singlet oxygen generation yield.

Gold Plasmonics. AuNPs exhibit properties fundamentally different from the others non-biodegradable nanoparticles previously mentioned as drug delivery systems. One of the most interesting and powerful properties of gold nanostructures derive from localized surface plasmon resonance (LSPR), on which they are based many applications of these nanoscale materials. A schematic illustration of LSPR is shown in Figure 4. When a gold nanostructure encounters electromagnetic radiation of an appropriate wavelength, the conduction electrons confined to metal surface will begin to oscillate collectively relative to the lattice of positive nuclei with the frequency of the incoming light.

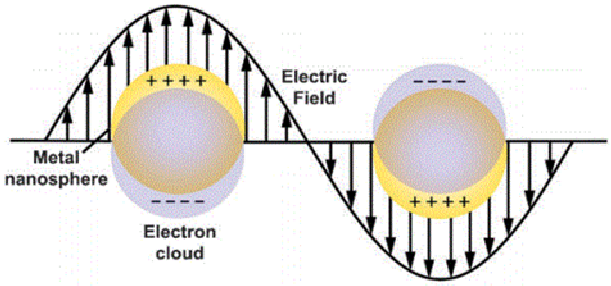

Figure 4. Localized surface plasmon resonance (LSPR) is a critical property of gold nanostructures that results from the collective oscillation of delocalized electrons in response to an external electric field.

This process can be divided into two types of interactions: scattering, in which the incoming light is re-radiated at the same wavelength in all directions, and absorption, in which the energy is transferred into vibrations of the lattice (*i.e.*, phonons), typically observed as heat. Together, these processes are referred to as extinction (extinction = scattering + absorption). In addition, LSPR generates strong electric field close to the surface of the particle. Specifics of the LSPR response of gold nanostructures depend on the size, shape, and morphology of the nanostructure, as well as the dielectric environment (Kreibig 1995). Consequently, the morphology control of gold nanostructures is a powerful route to control the LSPR response. A typical gold nanosphere has a LSPR wavelength around 520 nm. Due to the phenomenon of LSPR, the absorption and scattering cross-section of AuNPs are significantly higher than that of conventional dyes. For example, the molar adsorption coefficient (ε) of AuNPs with a diameter of 40 nm is about 7.7×10^9 $M^{-1}cm^{-1}$ (λ= 530 nm) and this value is several orders of magnitude higher than that of organic dyes (for example, rodamine-6G has ε of 1.2×10^5 $M^{-1}cm^{-1}$ at 530 nm) (Jain 2007).

The particular properties carried out by AuNPs can be harnessed for biomedical applications (Dreaden 2012), in particular heat generation (hyperthermia and photothermal applications) (Kennedy 2011). The synthesis of non-spherical AuNPs has achieved significant progress, especially anisotropic shapes such as nanorods (Perez-Juste 2005). For Au nanorods (AuNRs), two plasmon bands are observed (Fig. 5). The band around 520 nm corresponds to the transverse plasmon oscillation (oscillation along the width of AuNR), and the stronger band at longer

wavelength corresponds to the longitudinal plasmon oscillation (oscillation along the length of AuNR). The longitudinal plasmon resonance maximum can be shifted into the near-infrared (NIR) region by increasing the aspect ratio of AuNR (*i.e.*, the ratio of length along the long axis to the short axis) (Jain 2007).

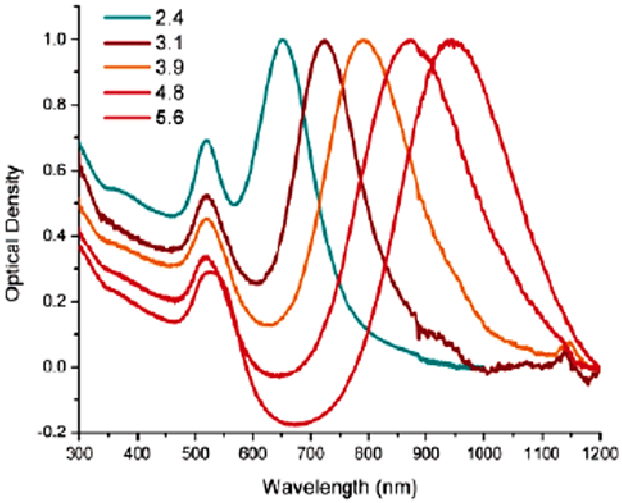

Figure 5. Surface plasmon absorption spectra of gold nanorods of different aspect ratios (Vivero-Escoto 2011).

In addition, the plasmon band in the NIR region can be tuned in silica core/Au shell structure, in which the band wavelength takes red shift with increasing core/shell ration. Red shift of plasmon band helps AuNRs to collect more NIR light, and that is beneficial for hyperthermia and photothermal imaging applications (Yi 2010).

Photothermal Therapy. Cells exposed to a temperature above 42°C for several minutes can be irreversibly damaged due to denaturation of proteins/enzymes, dysfunction of membrane transport, inhibition of nucleotide synthesis. Based on this, a harmless therapy is useful to destroy cancerous tissues based on localized heating, called Photothermal Therapy (PTT). The ability to convert absorbed light into heat makes AuNPs excellent candidates for this application. Because absorption by physiological fluids and tissues is minimal in the near-infrared region, the absorption maxima of therapeutic and diagnostic gold nanoparticles are synthetically tuned to

this “NIR window”. They have the advantage of higher absorption cross section, higher solubility and facile conjugation with targeting molecules. Huang et al. (2007) have recently reported about potential use of AuNPs in photothermal destruction of tumors. Citrate-stabilized AuNPs (core diameter = 30 nm), were coated with anti-EGFR (epidermal growth factor receptor) to target HSC3 cancer cells (human oral squamous cell carcinoma). The use of AuNPs enhanced the efficacy of photothermal therapy by 20 times. Gold core/silica nanoshells NPs have been developed by Halas and co-workers (Lal 2008) to be applied in PTT; upon NIR irradiation these nanostructures have produced highly promising results in several animal models of human tumors.

4.2 Nanoparticles: a sensoristic aspect

As described in the previous section (§ 4.1.1), silica NPs incorporating a fluorescent chromophore and/or a Fe_3O_4 core, can be used for fluorescence or magnetic resonance imaging, respectively. In particular, optical imaging based on fluorescence is a sensitive, cost-effective technology that uses light to probe molecular targets in the living subject. Because photosensitizers can generate both luminescence and singlet oxygen upon laser irradiation, they can be applied to optical imaging and PDT at the same time. Based on the intrinsic luminescence of photosensitizers, their tumor-targeted delivery can mark the location and area of the tumor tissue for optical imaging and further clinical treatment. Koo et al. (2010), for example, applied pH-responsive micelles as tumor-targeted carriers for photosensitizers, and enabled simultaneous imaging and PDT under *in vivo* conditions: the hydrophobic photosensitizer protoporphyrin IX (PpIX) was loaded to this pH-responsive micelle and applied to PDT; at the same time the intense fluorescence signal in the tumor site was observed by optical imaging.

4.2.1 Transition metal complexes in fluorescence imaging

The application of TMCs in luminescence cell imaging is a rapidly emerging area. In order to be realistic candidates for imaging in life sciences, luminescent probe molecules should ideally satisfy a number of requirements such as high extinction coefficient in the visible range, a high emission quantum yield, solubility in water, high cell permeability, low cytotoxicity, high chemical stability (maintaining its chemical integrity in the imaged object), high photostability (the compound should not undergo photobleaching when irradiated during use). Due to their photophysical properties, TMCs can offer advantages compared to common organic fluorophores on which many fluorescent probes are based (fluorescein, rhodamine, etc.):

- **Emission tuning**: The possibility of tuning the emission and the cell uptake by changing the ligands around the metal-centre, makes luminescent transition-metal complexes extremely versatile imaging agents. It is not

possible with many fluorescent organic structures, where control over color is more limited.

- **Stokes' shift**: for most organic fluorophores, the difference in energy between the lowest-energy absorption band and the emitting band is often small (usually a singlet state), with significant overlap of the absorption and emission spectra and self quenching (re-absorption of emitted light by neighboring fluorophores) can occur, as in the case of fluorophores like fluorescein. In contrast, for triplet-emitting metal complexes, the emission emanates from a different state (the triplet state) and self quenching does not occur (Fig. 6).

- **Lifetime**: the hallmark of triplet-emitting TMCs in bioimaging applications lies in the lifetimes of emission, typically two to three orders of magnitude longer than those of organic fluorophores. In bioimaging, long-lived probes can allow the elimination of autofluorescence (*i.e.*, emission from endogenous fluorophores, *e.g.* DNA, NADPH) with lifetimes $\tau < 10$ ns). Usually, a pulsed light source is used, and a delay is set between the excitation pulse and the detection of the signal or the image acquisition; using a delay of a few tens of nanoseconds, the background fluorescence decays to negligible levels

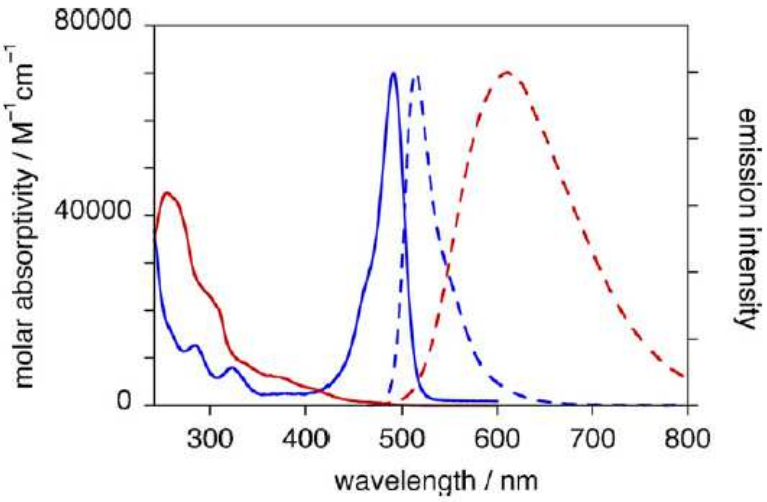

Figure 6. Absorption spectra (solid lines) and emission spectra (dashed lines) of fluorescein (blue) in aqueous solution, showing the significant overlap between them. There is not problem for triplet-emitting metal complexes such as $[Ir(ppy)_2(bpy)]^+$ (red lines) (Baggaley 2012).

The first report of the application of Ir(III) complexes in imaging came in early 2008 (Yu 2008) using a pair of cyclometallated species incorporating fluorine for lipophilicity in order to assist uptake (Fig. 7 A). The complexes 1 and 2 showed intense green (λ_{max} = 517 nm, τ = 1.1 ms) and red (λ_{max} = 623 nm, τ = 0.9 ms) luminescence, respectively. Incubation of HeLa cells with 1 and 2 resulted in intense intracellular Ir-derived luminescence at the expected wavelengths, localised in the cytoplasm rather than membrane or nucleus (Fig. 7 B). Comparison experiment with an organic dye (4',6-diamidino-2-phenylindole) demonstrated that the Ir(III) complexes show reduced photobleaching and higher photostability.

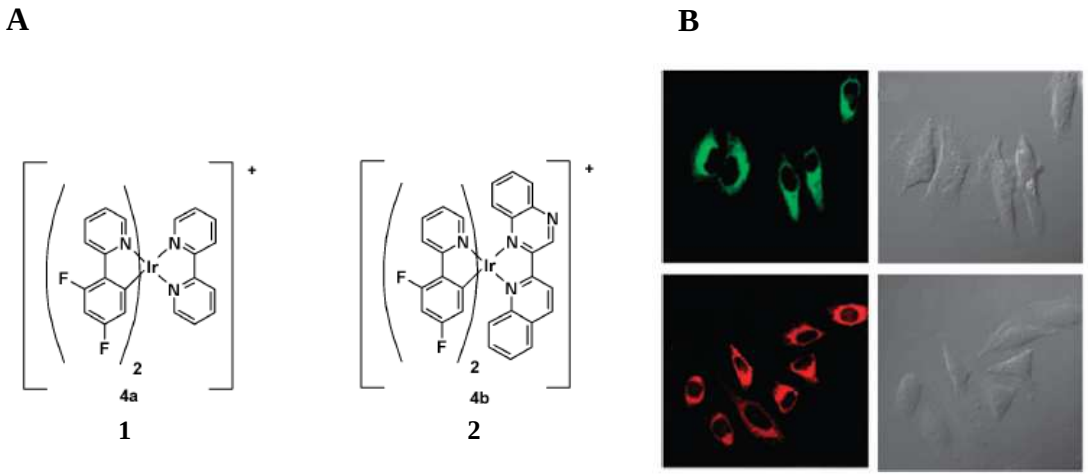

Figure 7. Cyclometallated Ir(III) complexes (**A**) and confocal luminescence and brightfield images (**B**) of HeLa cells incubated with complex **1** (top) or **2** (bottom) (Fernández-Moreira 2010).

Recently Zhang et al. (2010) reported on the application of an Ir(III) complex (Fig. 8 A) and performed hypoxia imaging in a tumor-bearing mice. For tumor imaging, five culture cell lines into the lower thigh of nude mice were transplanted: SCC-7, human glioma– derived U87, human lymphoma–derived RAMOS, human colon carcinoma–derived HT-29, and mouse lung cancer– derived LL-2. The red emission of the Ir(III) complex is clearly visible upon blue-light excitation (Fig. 8 B).

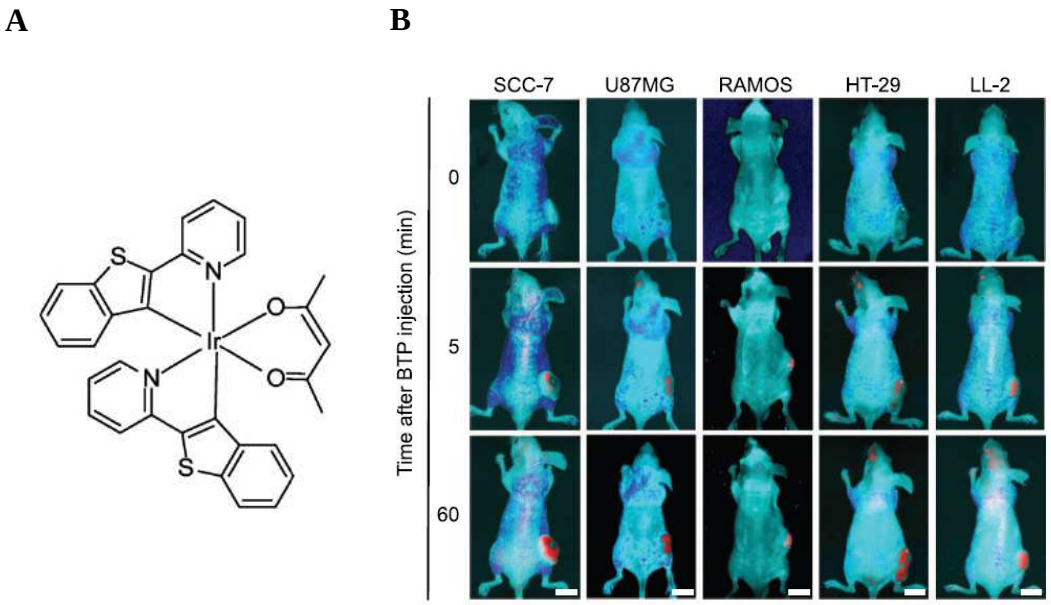

Figure 8. Ir(III) complex structure (**A**) used for in vivo imaging. Red luminescence indicating the localization of the tumor upon labeling with the complex (**B**) (Zhang 2010).

In the last few years, there have been an increasing number of reports on the design and application in cellular studies also of several Pt, Re and Ru complexes, tailor-made for imaging applications (Wu 2011; Baggaley 2012; Fernández-Moreira 2010).

4.3 Nanoparticles: a theranostic proposal

Figure 9 summarizes what has been said about the use of a potential theranostic nanoparticle for simultaneous diagnosis, therapy (PDT, PTT) and therapeutic monitoring.

Nanoparticles containing the photosensitizer/imaging agent (1) are intravenously injected and extravasate into tumor tissue (2) through the leaky vasculature by the EPR effect (enhanced permeability and retention effect; § 4.1). Photoirradiation (3) generates singlet oxygen and hyperthermia (AuNPs) within the tumor (4) leading to tumor apoptosis and necrosis (5); the intrinsic fluorescence of photosensitizers can be applied to optical imaging.

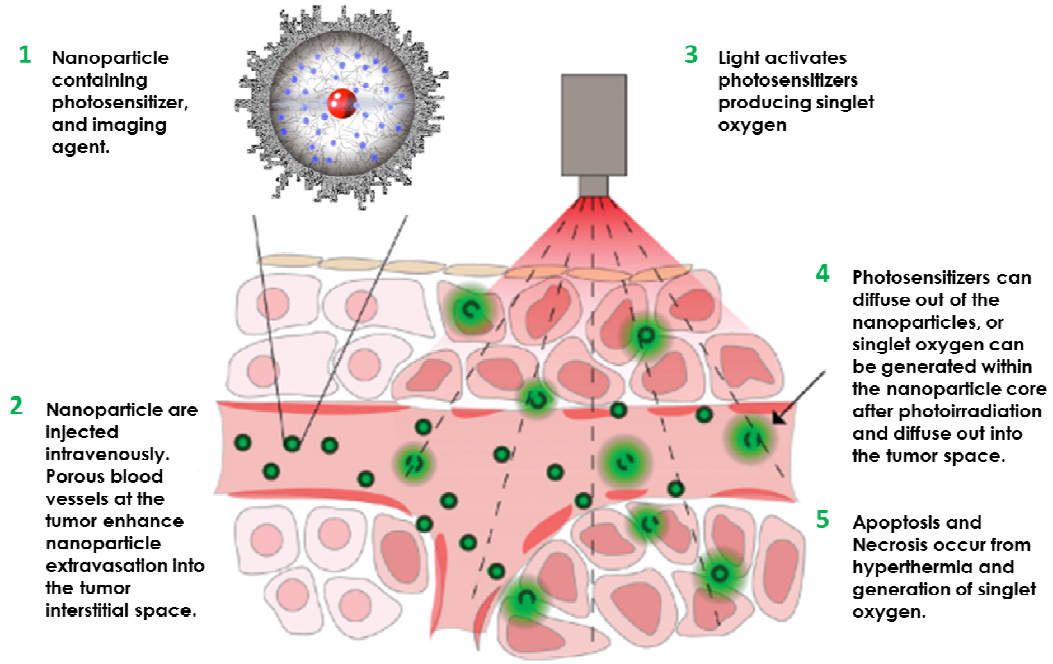

Figure 9. Illustration of theranostic nanoparticle-mediated tumor ablation.

In the following, it will be illustrated the synthesis, microscopic and photophysical characterization, *in vitro* test, and imaging records of the first examples of gold-dyes silica nanoparticles incorporating TMCs as photosensitizer and luminescent label. They will be proposed as progressive work to provide a theranostic system in cancer diseases.

4.3.1 The synthesis of Gold-Dye-Silica nanoparticles (GDS)

In the following paragraph, will be reported the used chemical method to synthesize hybrid core-shell nanoparticles with an average size of ~50 nm, with a gold core of ~5 nm and a polysiloxane shell with a thickness of ~45 nm containing a TMC entrapped via non-covalent interactions.

Usually, gold nanoparticles (AuNPs) of varying size are prepared in liquid medium by the reduction of chloroauric acid ($HAuCl_4$). This simply and generic procedure involves the addition of a reducing agent to a rapidly stirring $HAuCl_4$ water solution. This causes Au^{3+} ions to be reduced to neutral gold atoms. As more and more of these gold atoms form, the solution becomes supersaturated, and gold gradually starts to precipitate in the form of sub-nanometer particles. The rest of the gold atoms stick to the existing particles and, if the solution is stirred vigorously enough, the particles will be fairly uniform in size.

To prevent the particles aggregation, appropriate stabilizing agents that sticks to the nanoparticle surface were usually added (capping agents).

A simply way to cap AuNPs (and to prevent their coalescence) is to use long aliphatic chain thiol ligands that strongly bind gold due to the soft character of both Au and S; because these ligands are lipophilic, while chloroauric acid is hydrophilic, a phase-transfer reagent is necessary (Brust-Schriffrin method).

A more suitable method to cap AuNPs is the sol-gel procedure, typically used to prepare silica nanoparticles. The sol-gel chemistry is based on the polymerization of molecular precursors such as metal alkoxides $M(OR)_n$ by hydrolysis, and subsequent condensation at room temperature. The mild characteristics offered by the sol-gel process allow the introduction of organic molecules inside an inorganic network. Since inorganic and organic components can be mixed at the nanometric scale, hybrid nano-objects with several geometries are then possible.

The Brust-Schriffrin method for gold NPs synthesis

The Brust-Schiffrin method for AuNPs synthesis, published in 1994 (Brust 1994), has had a considerable impact on the overall field in less than a decade (Daniel 2004), because it allowed the facile synthesis of thermally stable and air-stable AuNPs of reduced dispersity and controlled size (ranging in diameter between 1.5 and 5.2 nm).

Indeed, these AuNPs can be repeatedly isolated and redissolved in common organic solvents without irreversible aggregation or decomposition, and they can be easily handled and functionalized just as stable organic and molecular compounds.

Water solution of $AuCl_4^-$ is transferred to toluene solution using tetraoctylammonium bromide as the phase-transfer reagent, and reduced by $NaBH_4$ in the presence of dodecanethiol (Fig. 10). The organic phase changes color from orange to deep brown within a few seconds upon addition of $NaBH_4$.

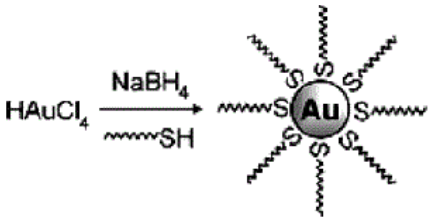

Figure 10. Formation of AuNPs coated with organic shells by reduction of Au(III) compounds in the presence of thiols (Daniel 2004).

The TEM photographs showed that the diameters were in the range 1-3 nm, with a maximum in the particle size distribution at 2.0-2.5 nm, with a preponderance of cuboctahedral and icosahedral structures. Larger thiol/gold mole ratios give smaller average core sizes, and fast reductant addition and cooled solutions produced smaller, more monodisperse particles. A higher abundance of small core sizes (≤2 nm) is obtained by quenching the reaction immediately following reduction or by using sterically bulky thiol ligands (Ingram 1997; Templeton 2000).

The sol-gel method for silica NPs synthesis

In general, the sol-gel process involves the transition of a system from a colloidal "sol" towards a gel-like network containing both a liquid phase and a solid phase. The starting materials used in the preparation of the "sol" are usually inorganic metal salts or metal organic compounds such as metal alkoxides. These precursors are subjected to a series of hydrolysis and polymerization reactions to form a colloidal suspension, or a "sol". One of the most used metal alkoxide is tetraethyl orthosilicate (TEOS) (Fig. 11) (Brinker 1988).

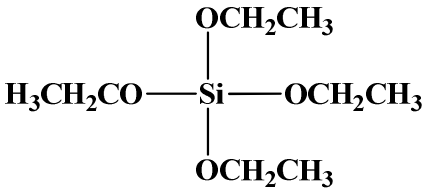

Figure 11. Structure of TEOS, the metal alkoxides starting material.

The **hydrolysis reaction**, that produces silanol groups, occurs by nucleophilic attack of water to the silicon atom. The reaction is resumed in Scheme 1:

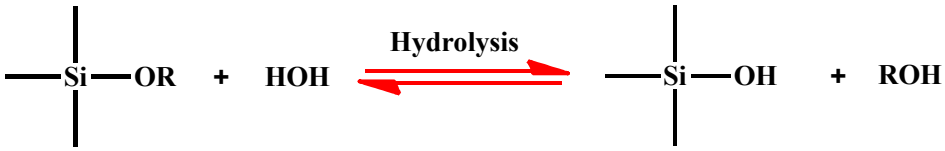

Scheme 1. The first occurring reaction: a catalyzed hydrolysis of TEOS to produce silanol moiety.

Depending on the amount of water and catalyst present (acidic or basic) hydrolysis may proceed to completion, so that all of the OR groups are replaced by OH groups. In order to form spherical nanoparticles, the base-catalyzed hydrolysis is preferred: ammonium hydroxide works as a basic catalyst and the hydrolysis reaction is probably initiated by the attacks of hydroxyl anions on TEOS molecules.

Following the hydrolysis reaction, the **condensation reaction** occurs immediately. The silanol groups reacts with either the hydroxyl group of another hydrolysis intermediate (water condensation) or the ethoxy group of other TEOS (alcohol condensation) to form Si-O-Si bridges (Scheme 2).

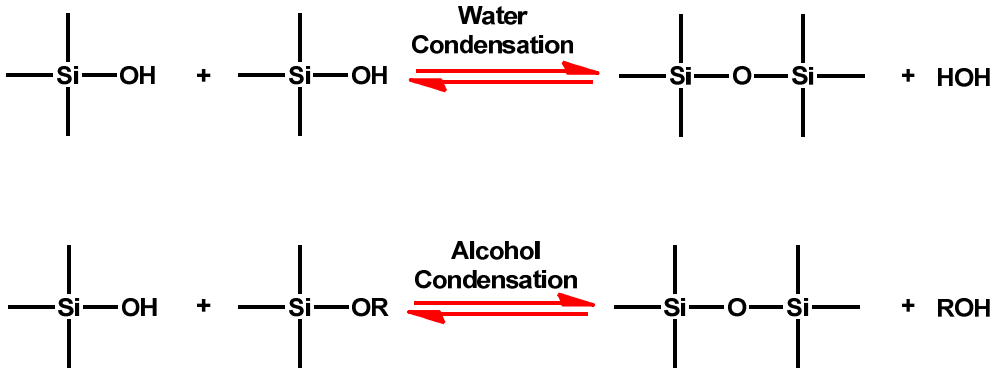

Scheme 2. The second occurring reaction: silanol condensation to produce organic/inorganic hybrid polymer.

The competition between hydrolysis and condensation conditions gives the growth and coalescence of particles for different final geometries. This competition may be controlled by the pH and the salinity of solutions, because the speed and the surface charge are modified.

In acid medium (pH > 1), the hydrolysis is fast respect to condensation, which determines the rapid formation of smaller monomers and consequently the formation of small particles whose size does not exceed the nanometre. These nanosized particles are incorporated then to form ramified polymeric clusters of weak density. This sol remains in suspension without precipitating. The sol gradually occupies an increasingly large volume fraction up to a value close to the unit. Therefore the viscosity of the medium becomes important then and the liquid starts the gelation step.

On the contrary, in neutral or moderately basic solution, the condensation of the silicon species is faster than the hydrolysis and the polymerization is then gradually supported by monomers. The stage of formation of the basic units is a monomeric aggregation. This mechanism leads to the formation of dense silica particles. The final size may reach several hundreds of nanometres and the surface is negatively charged. The electrostatic repulsion prevents the aggregation between particles which remain in suspension within the solvent. The main advantage of silica nanoparticles over polymer nanoparticles is the ease of introduction of functional groups such as amines, thiols, carboxyls, and methacrylate on the surface by modification of surface hydroxyl groups, through the use of so-called “silane

coupling agents". The characteristic of these molecules is to have the ability to form a durable bond between organic and inorganic materials.

The silica coating of gold nanoparticles: the microemulsion method

The silica-coating procedures reported in the literature generally involve surfaces with a significant chemical or electrostatic affinity for silica. However gold metal has very little affinity for silica because, unlike most other metals, it does not form a passivating oxide film in solution. Furthermore, there are usually adsorbed carboxylic acids or other organic anions present on the surface to stabilize the particles against coagulation. These stabilizers also render the gold surface vitreophobic.

The microemulsion method uses a micellar system as an ensemble of nanoreactors within the sol-gel synthesis takes place. It opens new ways towards hybrid structure synthesis since the particle growth by the micellar compartmentalisation of synthesis environment ensures a better control, and allows preparation of ultrafine metal particles within the size range 5 nm < particle diameter < 50 nm.

Microemulsions are thermodynamically stable, isotropic liquid mixtures of oil and water stabilized by a surfactant, frequently in combination with a co-surfactant. A surfactant is a molecule that possesses both polar and non-polar moieties. In a very diluted water (or oil) solutions, it dissolves and exists as monomer, but when its concentration exceeds the so-called critical micelle concentration (CMC), the surfactant molecules associate spontaneously to form aggregates-micelles (Capek 2004).

Two kinds of droplet-type microemulsions can be recognized: spherical oil droplets dispersed in a continuous medium of water (oil-in-water microemulsion, O/W) or spherical water droplets dispersed in a continuous medium of oil (water-in-oil microemulsion, W/O). Thus, in a ternary systems (oil, water, surfactant), where the immiscible phases, water and oil, coexist with a surfactant, the surfactant molecules may form a monolayer at the interface between the oil and water, with the hydrophobic tails of the surfactant molecules dissolved in the oil phase and the hydrophilic head groups in the aqueous phase. The hydrocarbon chains of surfactant tend to self-associate to minimize the contact with water molecules, resulting in the

formation of spherical aggregates, the micelles. Two types of micelles can distinguished: direct micelles, from oil-in-water emulsion, or inverse, from water-in-oil emulsion (Fig. 12).

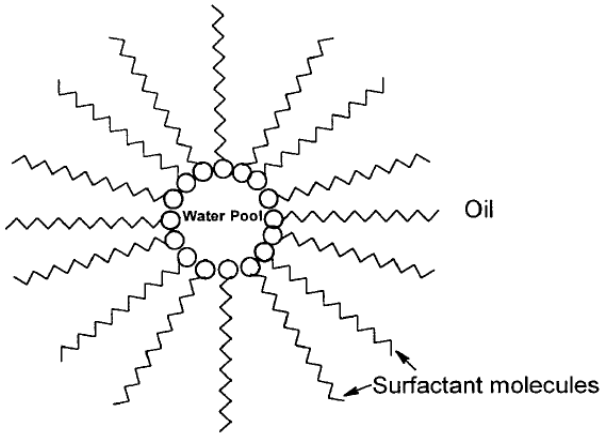

Figure 12. Water-in-oil (W/O) microemulsion.

It is known that more highly hydrolyzed TEOS species become more hydrophilic, because it is due to the presence of polar silanol groups in the molecule. Interfacial tension measurements suggest that the partially hydrolyzed species become surface active, and therefore remain associated with the reverse micelles once they are formed. Consequently, all further reactions (hydrolysis and condensation) are restricted to the local environment of the reverse micelles. It is inside this aqueous compartment that chloroauric acid and reducing agent form gold core, and, if added, a dye is encapsulated into the silica shell.

Dye-doped nanoparticles prepared in this thesis work were synthesized using a reverse microemulsion (water-in-oil) method, where water droplets are dispersed as nanosized liquid entities in a continuous domain of oil and stabilized by surfactant molecules at the water/oil interface (Martini 2009). The droplets dimension can be modulated by various parameters, in particular W (W=[water]/[surfactant]) (Zhang 2001). Moreover, recent studies indicated that with the assistance of cosurfactant, the size of nanoparticles prepared in quaternary reverse micelle system is more controllable (Curri 2000). The surfactant-covered water pools act as a nanoreactor for the confined synthesis and silica coating of nanometer-sized particles. The final size

of colloidal particles is directly influenced by the number of microemulsion droplets that host reacting species. In general, increasing the number of droplets present, will be greater the physical compartmentalization of the reactant species in solution to form nuclei (Arriagada 1999).

4.3.1.1 Materials and methods

Transition metal complexes $[(ppy)_2Ir(en)](OOCCH_3)$, $[(ppy)_2Ir(pam)](OOCCH_3)$, $[(bipy)_2Ru(bipy\text{-}OH)](PF_6)_2$, $[(bipy)_2Ru(bipy\text{-}TBDMS)](PF_6)_2$ have been synthesized in the Laboratory of Inorganic and Coordination Chemistry (University of Calabria). Triton X-100, n-hexanol, cyclohexane, $HAuCl_4 \cdot 3H_2O$, sodium 2-mercaptoethanesulfonate (MES), $NaBH_4$, tetraethoxysilane (TEOS), (3-aminopropyl)triethoxysilane (APTES) were purchased from Aldrich. NH_4OH (25% in water) was purchased from Chimie Plus. N-(3-Triethoxysilylpropyl)gluconamide (Si-12) (50% in ethanol) and N-(3-triethoxysilyl)propylsuccinic anhydride (Si-20) (94%) were purchased from ABCR (Fig. 13). Only Milli-Q water (ρ>18 MΩ) was used for the preparation of the aqueous solution.

Characterization. Transmission Electron Microscope Analysis. The size and morphology of the gold silica nanoparticles synthesized in W/O microemulsion were measured using a transmission electron microscope (JEOL 2010F). The samples for transmission electron microscopy (TEM) were prepared by depositing a drop of a diluted colloidal solution on 200 mesh carbon-coated copper grids. After evaporation of the solvent in air at room temperature, the particles were observed at an operating voltage of 200 kV.

Size Measurements. The particle size characterization was performed using Dynamic Light Scattering (DLS), a non-invasive technique for measuring the size of nanoparticles in a dispersion. All measurements reported were performed on a Zetasizer Nano S at 25° C from Malvern Instrument. The Nano S contains a 4mW He-Ne laser operating at a wavelength of 633 nm and an avalanche photodiode (APD) detector. The scattered light was detected at an angle of 173°.

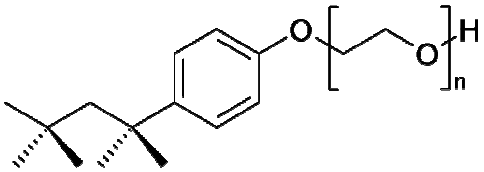

Triton X-100

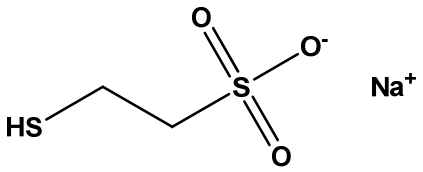

Sodium 2-mercapto-ethanesulfonate (MES)

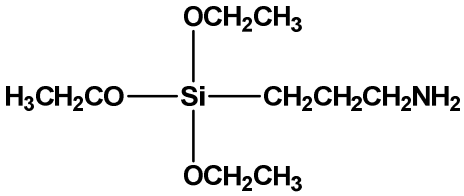

APTES (3-aminopropyl)triethoxysilane

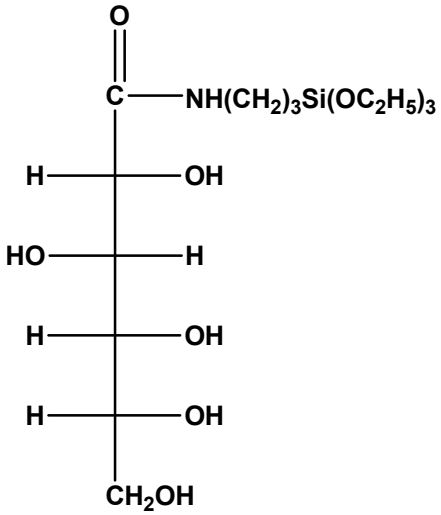

N-(3-triethoxysilylpropyl)gluconamide

(Si-12)

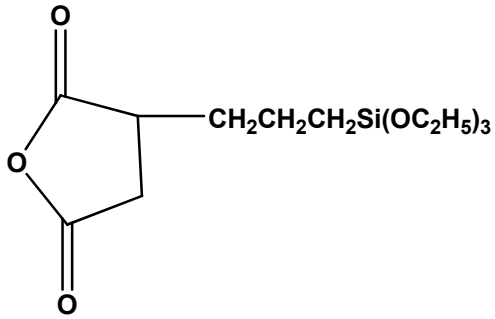

3-(triethoxysilyl)propylsuccinic anhydride

(Si-20)

Figure 13. Structures of reactants used in gold dye-doped silica nanoparticle synthesis.

4.3.1.2 Synthesis of Au core - Ru and Ir complexes doped silica shell nanoparticles

The TMCs solutions were prepared by direct dissolution of 1 mg of complex in 0.1 mL of water (Ir complexes) or DMSO (Ru complexes) under stirring at room temperature.

Quaternary W/O microemulsion was prepared by mixing 7.2 mL of Triton X-100 (surfactant), 7.2 mL of n-hexanol (co-surfactant), 30 mL of cyclohexane (oil) and a water solution consisting of mixture of 1.8 mL of 12.75 mM $HAuCl_4 \cdot 3H_2O$ water solution, 1.8 mL of 36.5 mM MES water solution and 0.6 mL of 423 mM $NaBH_4$ water solution, in order to synthesize the gold nanoparticle.

After 5 min, 0.1 mL of the TMC solution was added to the microemulsion solution, followed by addition of 0.020 mL of APTES and 0.300 mL of TEOS. After 30 min, the silica polymerization reaction was completed by adding 0.160 mL of NH_4OH (25%) water solution, and then stirred for 24 h.

Since the colloidal stability in water is required for their applications, a protective (and charged) shell was synthesized by adding 0.030 mL of Si-12 or Si-20 after 24 and after 48 h. After 24h the microemulsion was broken by the addition of an amount of isopropanol and water in a volume ratio 1:1:1 with the obtained microemulsion solution, followed by the purification steps consist of several washing using VIVAFLOW 200 system (100 KDa). Nanoparticles dispersed in water are filtered by a 200 nm filter.

Moreover, NPs without the dye have been synthesized, following the above illustrated procedure.

4.3.1.3 Incorporation of dyes and gold nanoparticles in silica beads and surface modification

The starting step is the preparation of the quaternary W/O microemulsion, constitutes by the mixture of Triton X-100 (surfactant), n-hexanol (co-surfactant) and cyclohexane (oil), following by addition of aqueous solution.

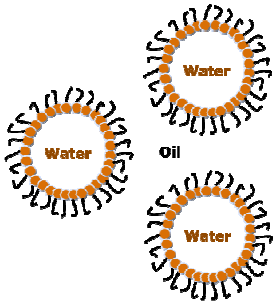

Starting step

MICELLAR TEMPLATE

(water, cyclohexane, n-hexanol, Triton X-100)

In the aforesaid microemulsion system, we will form firstly the metallic core by the direct reduction of Au salt, in the presence of sodium 2-mercaptoethansulfonate, by $NaBH_4$, according to the Brust's method. The reactant metal salts and reducing agents are soluble in water and therefore the nucleation of metal particles proceeds in the water pools of the microemulsion (Step 1).

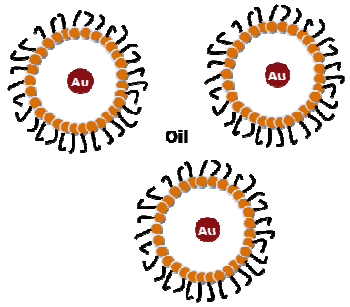

Step 1

CORE FORMATION

($HAuCl_4$, MES, $NaBH_4$)

After the reduction of the metal to the zero valence state, the dye dissolved in DMSO or water was added to the microemulsion solution, followed by APTES, TEOS and ammonia. The surface of gold is well-known for forming strong, stable gold–thiolate bonds (Au–S, ~50 kcal/mol) to molecules with thiol (–SH) or disulfide groups (S–S) (Love 2005), therefore, coalescence between gold clusters is avoided via surface

functionalization by adding sodium-2-mercaptoethanesulfonate. The ratio of thiol molecules to Au(III) controls the size of the resulting nanoparticles by adjusting the relative rates of particle nucleation and growth (higher ratios yield smaller particles); in fact methods of forming gold nanoparticles in the presence of thiols can only be used to form small (<5 nm in diameter) particles. At the same time, the sulfonate group of MES is able to fix electrostatically the amino groups of APTES molecules. As a result, the passivation of the metallic surface induces an increase of the affinity for polysiloxane precursors. The silanol groups of APTES molecules serve as grafting sites for hydrolyzed TEOS precursors and the particles grow radially.

We supposed that the metallic core is surrounded by a thin layer with a thickness of 2-3 nm composed of adsorbed thiols and APTES molecules. The kinetics of electrostatically attraction between thiols and APTES is quicker than the silanol condensation and all of gold clusters are coated before the condensation takes place. The addition of the silane precursors (APTES and TEOS) will be followed by ammonia to complete silica polymerization (Step 2).

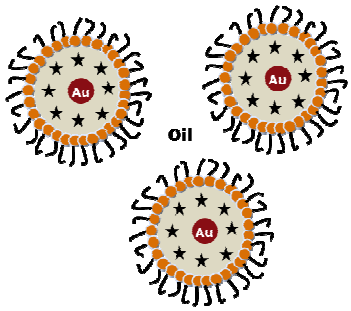

Step 2

SHELL FORMATION

(dyes, APTES, TEOS, NH_4OH)

The sol-gel reaction continues at room temperature for 24 hours. To stabilize nanoparticles and to prevent the coalescence into bigger aggregates, additional bead functionalization is necessary: first of all the use of silane precursors Si-12 or Si-20. The modified silane precursors must not be added during the core particle formation, but in a successive coating step (24 hours and 48 hours after the ammonia addition), thus as to contribute to increase the diameter of the nanoparticles and not the number

of beads. The microemulsion was finally broken (Final steps) by the addition of isopropanol and water (decantation), followed by the purification steps. The purification was performed by several washings and finally the nanoparticles dispersed in water were filtered by a 0.2 µm filter.

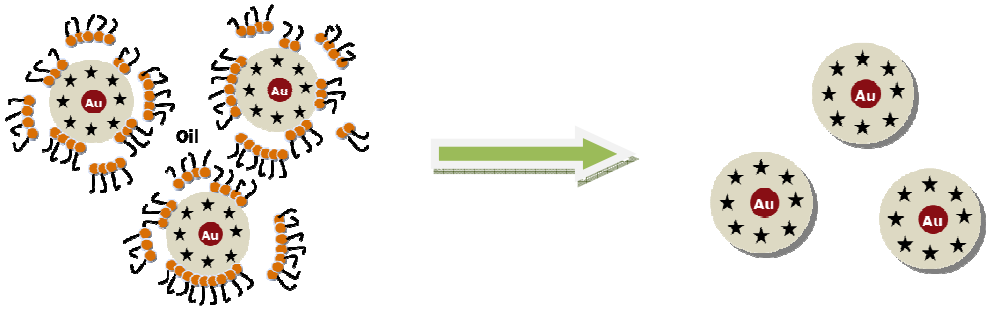

Final steps

DECANTATION

(microemulsion + water + isopropanol)

COLLOID in polar phase

(isopropanol-water)

Colloids are characterized to collect information about the morphology (size, polydispersity, stability) using TEM (JEOL 2010F) apparatus for structural and morphological information, and Dynamic Light Scattering (Zetasizer NanoS) for the hydrodynamic size and stability.

TEM images show the spherical morphology of the gold nanoparticles and a diameter of 50 nm in agreement with the DLS values. Looking at DLS data it is evident a better polydispersity for the particles functionalized with Si-20 compared to Si-12 (Fig. 14). Moreover, particles functionalized with Si-20 have proved to be stable in solution over time compared to particles functionalized with Si-12; the stability has been checked by repeated DLS measurements after weeks. Furthermore, the stability of the same has been checked by DLS measurements in biological media such as RPMI (Roswell Park Memorial Institute medium) and DPBS (Dulbecco`s Phosphate Buffered Saline).

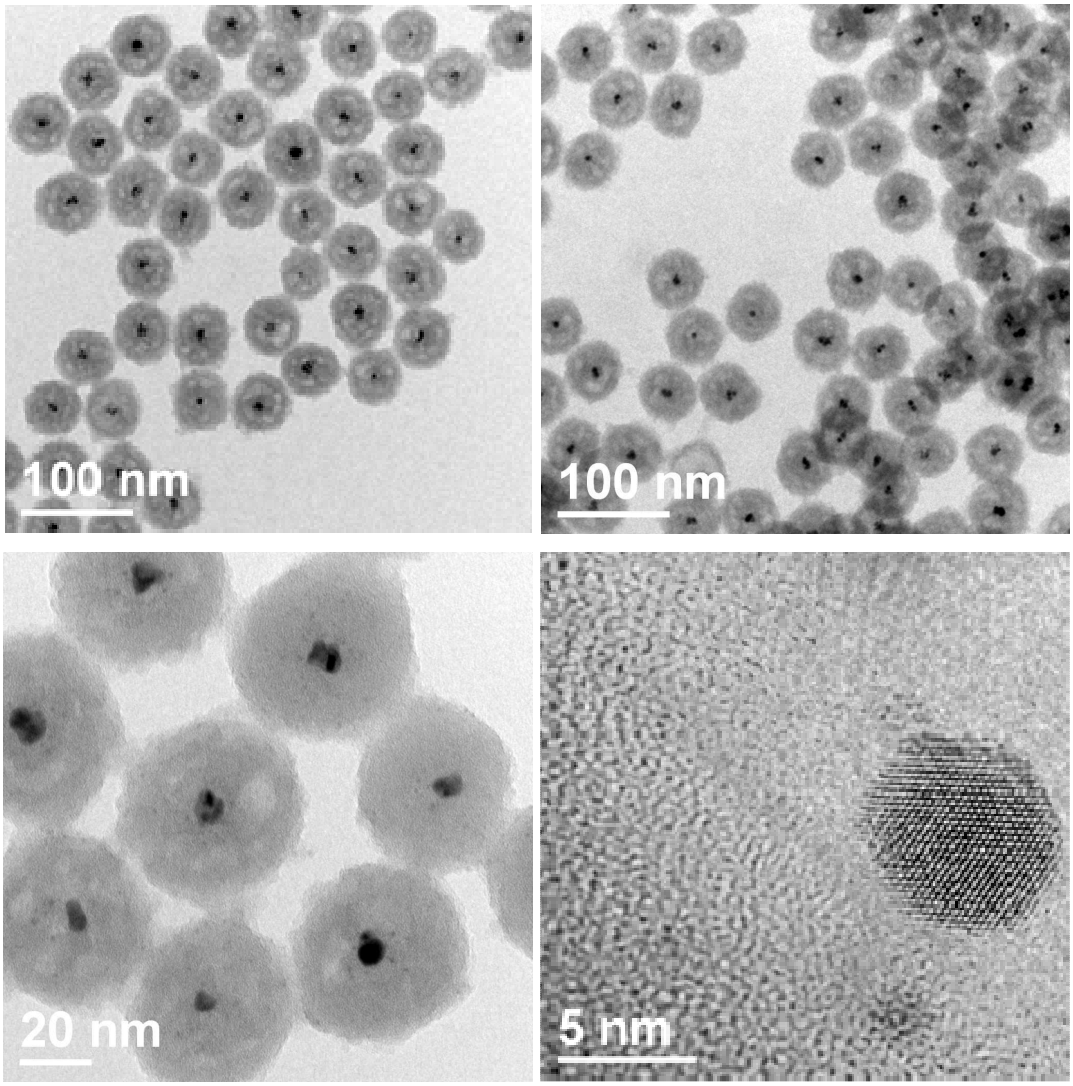

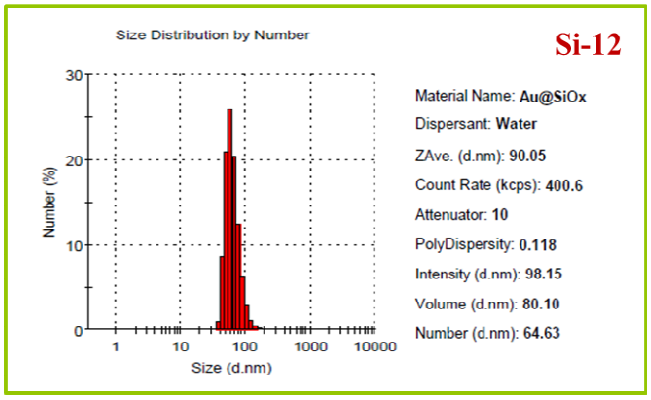

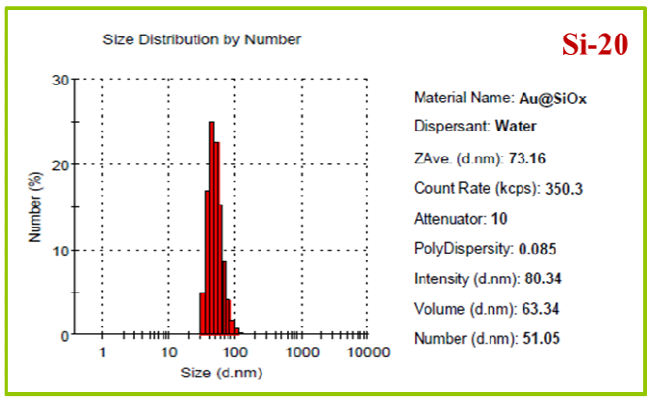

Figure 14. TEM images (Si-12) and DLS analysis of synthesized gold silica nanoparticles.

4.3.2 Photophysical characterization

Here are presented the photophysical characterization of monocore gold-silica NPs (GSNPs) entrapping the four complexes **1-4**, previously illustrated in Chapter 3 (§ 3.4.2.2): **1@GSNP**, **2@GSNP**, **3@GSNP** and **4@GSNP**, respectively. Among the various synthesized samples, were chosen GSNPs functionalized with Si-20. The spectral studies were performed in water solution, at room temperature, picking up a volume of 3 mL directly from the solution obtained by the synthesis.

4.3.2.1 Absorption spectra

It was prepared a water sample of GSNPs with Si-20 but without incorporating dye, **0@GSNP**, following the previously illustrated synthetic procedure. Figure 15 reports the absorption spectrum; but, due to the high scattering contribution of the GSNPs, an extinction (absorbed light + scattered light) intensity *vs.* wavelength plot was obtained.

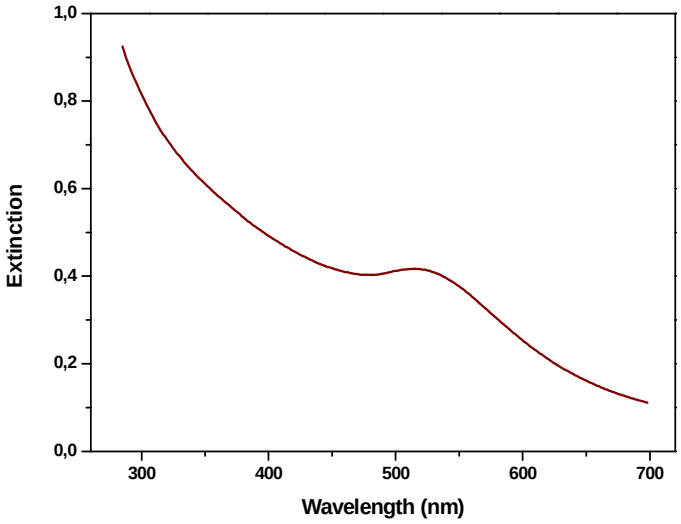

Figure 15. Extinction spectrum of **0@GSNP** in water at room temperature.

The extinction profile follows a sharp decay as the wavelength increases, discontinued at 515 nm by the band attributed to the gold plasmon (Jain 2006). At a first glance, in the extinction spectra of the four samples (Figures 16-19), no other feature than the gold plasmon is clearly observable, being the absorption bands of the

coordination compounds submerged by the scattering contributions of the nanoparticles.

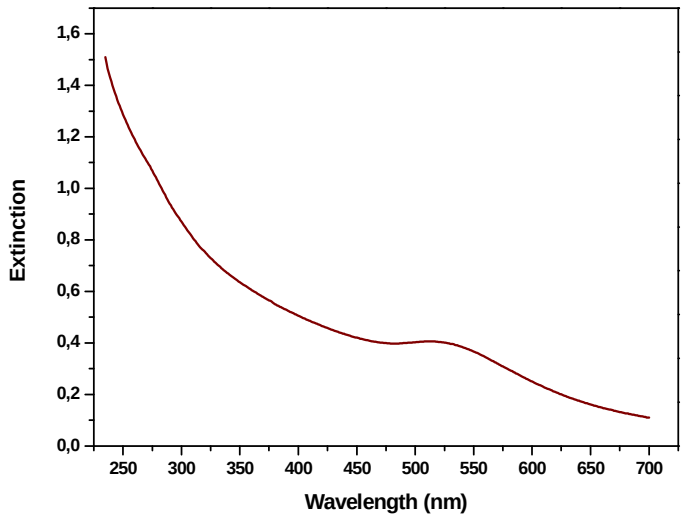

Figure 16. Extinction spectrum of **1@GSNP** in water at room temperature.

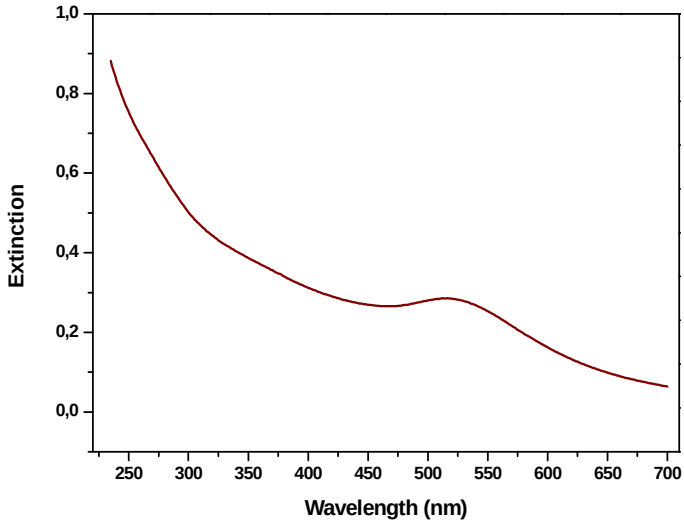

Figure 17. Extinction spectrum of **2@GSNP** in water at room temperature.

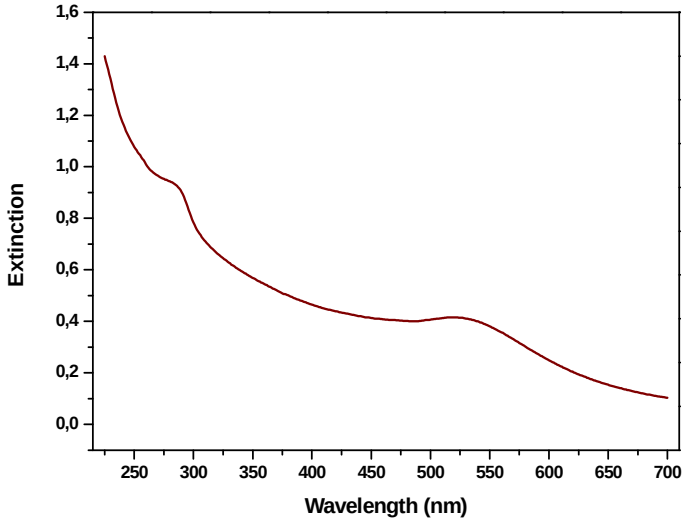

Figure 18. Extinction spectrum of **3@GSNP** in water at room temperature.

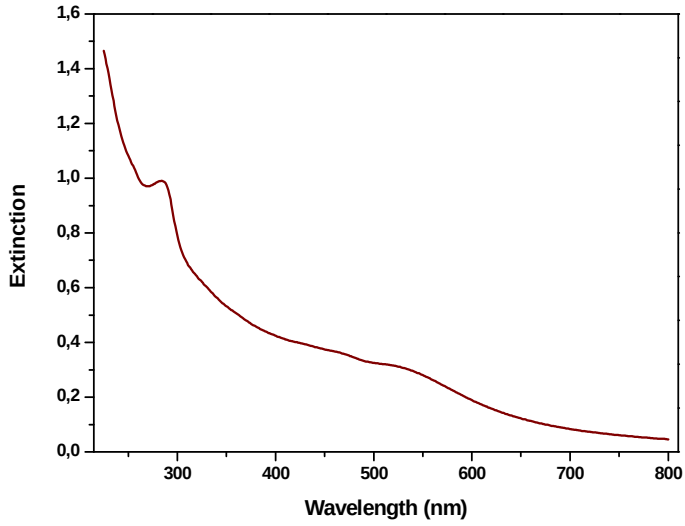

Figure 19. Extinction spectrum of **4@GSNP** in water at room temperature.

Subtracting from the extinction spectrum of each **1-4@GSNP** solutions the extinction spectrum of the **0@GSNP**, it was possible to eliminate the scattering contribution, and to obtain the absorption profile of the complex entrapped (Glomm 2005). The obtained difference spectra for **1@GSNP** and **4@GSNP** are reported in Figures 20 and 21, respectively. The spectral shapes have been compared with the absorption spectra of the complexes **1** and **4** in solution (§ 3.4.2.2), confirming the uptake of the photosensitizers into nanoparticles.

Moreover, taking into account that the NPs concentration is the same in all prepared samples (**0-4@GSNP**), assuming a similar scattering in all solution, and assuming the molar absorptivity value of each complex equal in solution and in silica matrix, the intensity of the difference spectrum should provide an estimate of the absorption of the complex into nanoparticles.

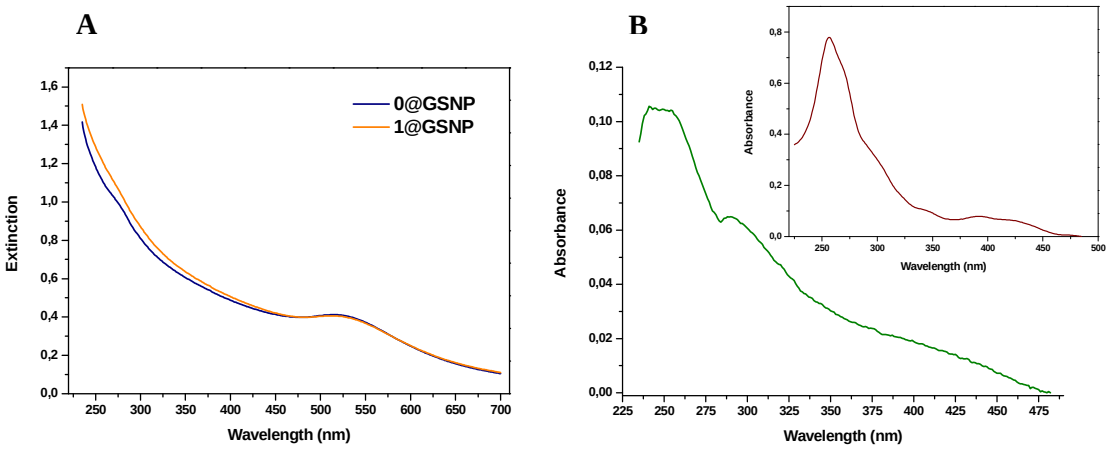

Figure 20. (**A**) Extinction spectrum of **0@GSNP** solution (blue line) and the ground state extinction spectrum of **1@GSNP** (orange line). (**B**) Spectrum (green line) obtained by subtraction of the two spectra shown in (A); in the insert is reported the absorption spectrum of **1** (purple line).

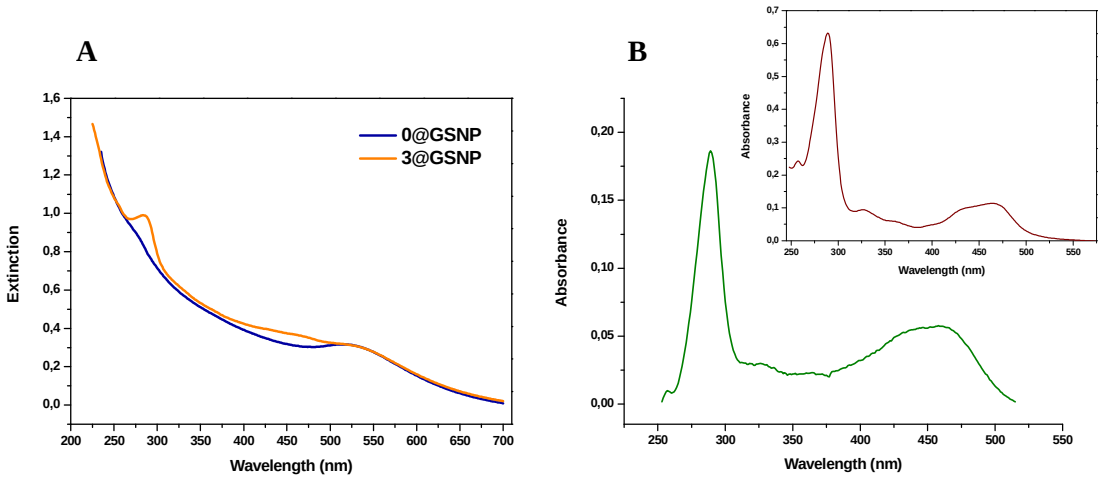

Figure 21. (**A**) Extinction spectrum of **0@GSNP** solution (blue line) and the extinction spectrum of **4@GSNP** (orange line). (**B**) Spectrum (green line) obtained by subtraction of the two spectra shown in (A); in the insert is reported the absorption spectrum of **4** (purple line).

4.3.2.2 Luminescence and photosensitizing properties

All samples were characterized in solution at room temperature, in presence or absence of oxygen. For the emission quantum yield measurements, $Ru(bipy)_3Cl_2$ in aerated water was used as standard (§ Appendix). Table 2 reports the obtained photophysical data.

Table 2. Photophysical data for complexes **1-4@GSNP** in water solution at room temperature.

	Em, λ_{max}/nm	**τ/μs (α/%)**	**τ_{deox}/μs (α/%)**	**$k_q[O_2]$/ s^{-1}**
1@GSNP	510	τ_1 = 0.408 (32.0); τ_2 = 1.210 (68.0)	τ_1 = 0.683 (9.8); τ_2 = 2.610 (90.2)	5.18×10^5
2@GSNP	490, 510	τ_1 = 0.809 (26.0); τ_2 = 2.390 (74.0)	τ_1 = 1.040 (17.1); τ_2 = 2.820 (82.9)	7.88×10^4
3@GSNP	620	τ_1 = 0.173 (17.0); τ_2 = 0.585 (83.0)	τ_1 = 0.262 (25.0); τ_2 = 0.718 (75.0)	2.86×10^5
4@GSNP	638	τ_1 = 0.269 (29.0); τ_2 = 0.634 (71.0)	τ_1 = 0.260 (30.0); τ_2 = 0.637 (70.0)	2.97×10^3

Nanoparticles entrapping Ir complexes **1** and **2**, *i.e.* **1@GSNP** and **2@GSNP**, respectively, show an emission spectrum (Fig. 22 and 23) almost superimposable to that of the corresponding complex in solution (§3.4.2.2), except a slight blue-shift attributed to the more rigid environment experienced in the silica rigid matrix. The intensity of the spectra is clearly diminished in air-equilibrated solution, due to the quenching effect of the oxygen. The O_2 sensitation is demonstrated by collecting the 1270 nm $^1O_2$ phosphorescence in D_2O solution of **1@GSNP** and **2@GSNP** (not reported for the bad signal-to-noise ratio, due to the extremely low concentration of the samples, obtained dissolving in D_2O a little amount of the H_2O solution of the nanoparticles).

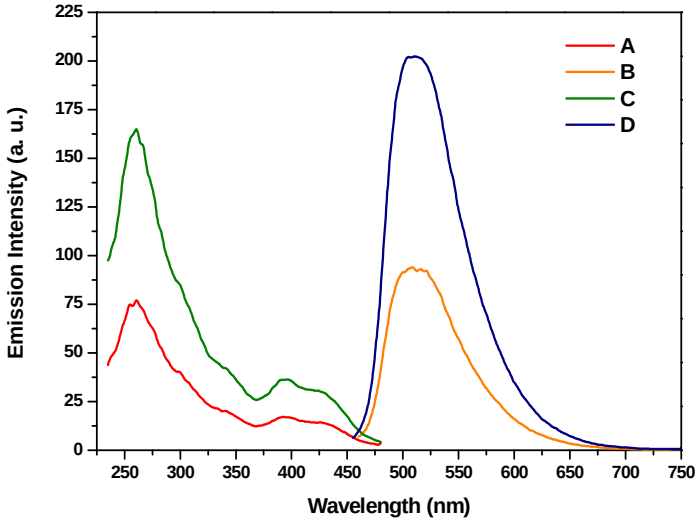

Figure 22. Excitation spectra (λ_{em}= 510 nm) and emission spectra (λ_{ex}= 260 nm) of **1@GSNP** at room temperature in air-saturated (**A**)(**B**) or in degassed (**C**)(**D**) water.

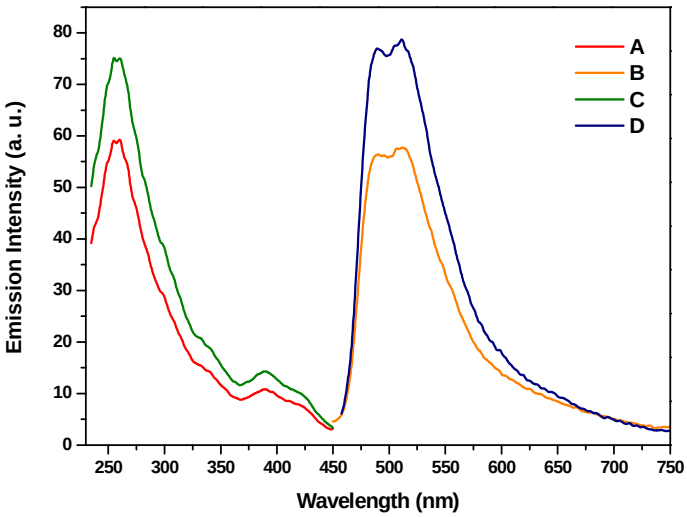

Figure 23. Excitation spectra (λ_{em}= 500 nm) and emission spectra (λ_{ex}= 260 nm) of **2@GSNP** at room temperature in air-saturated (**A**)(**B**) or in degassed (**C**)(**D**) water.

The oxygen quenching is also evidenced by observing (Table 2) how the lifetime increases when oxygen is removed. Ir complex-containing nanoparticles follow a bi-exponential lifetime decay, in presence as well as in absence of O_2 (Fig. 24 and 25; see § Appendix A.3 where the time profiles of air-equilibrated solutions emission are

reported). Likewise for the free Ir complexes (properly fitted by a mono-exponential function), also for the complexes-containing nanoparticles it was tried to fit lifetime decays by a mono-exponential function, but the obtained χ^2-value were unacceptable. By comparing lifetime values of **1@GSNP** and **2@GSNP** with the correspondent values of **1** and **2**, it can be noted a general enhance, in accordance with the more rigid environment experienced into the nanoparticles; the rigid matrix may be the cause of the double lifetime, taking into account that for such complexes the emitting state is a mixture of a ^{3}LC and ^{3}MLCT states; these two states could be not completely equilibrated resulting in a bi-exponential decay (this behavior has been observed in Ir complexes at 77 K (Ramachandra 2011). In Table 2 have been reported the rate constants of the bimolecular quenching $k_q[O_2]$ of GSNP samples obtained by means of the eq. 5 § 3.4.2.2 using the average lifetimes; the values are considerably lower than the corresponding ones of free complexes (Table 7 § 3.4.2.2): this is attributed to a lower oxygen diffusion inside the nanoparticles respect to the solution.

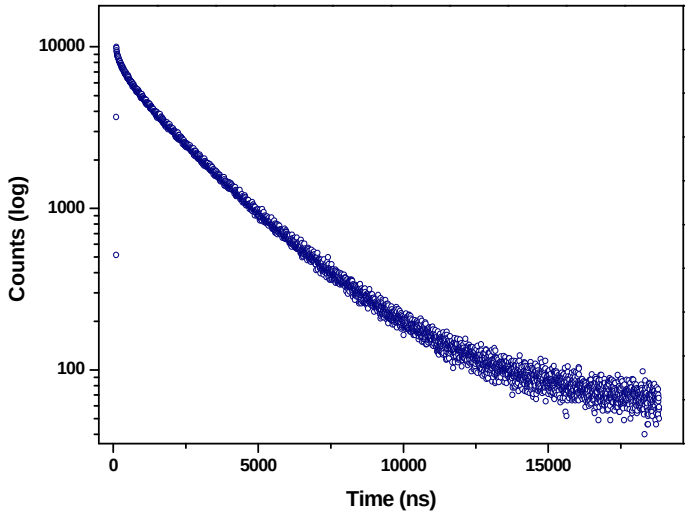

Figure 24. Time-resolved emission decay of **1@GSNP** in degassed water (λ_{ex}= 379 nm, $\lambda_{monitored}$= λ_{em}= 510 nm). Fitting results (χ^2 = 1.14): τ_1 = 6.83 x 10^{-7} ± 1.42 x 10^{-8} s; α_1= 9.80%; τ_2 = 2.61 x 10^{-6} ± 3.57 x 10^{-9} s; α_2= 90.20%.

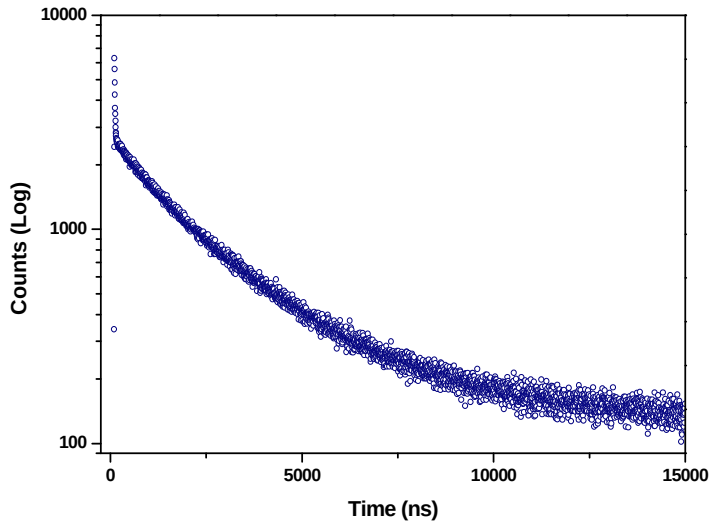

Figure 25. Time-resolved emission decay of **2@GSNP** in degassed water (λ_{ex}= 379 nm, $\lambda_{monitored}$= λ_{em}= 510 nm). Fitting results (χ^2 = 1.02): τ_1 = 1.04 x 10^{-6} ± 3.58 x 10^{-8} s; α_1= 17.14%; τ_2 = 2.82 x 10^{-6} ± 1.30 x 10^{-8} s; α_2= 82.86%.

Nanoparticles entrapping Ru complexes **3** and **4**, *i.e.* **3@GSNP** and **4@GSNP**, respectively, show an emission spectrum (Fig. 26 and 27) almost superimposable to that of the corresponding complex in solution (§3.4.2.2), except a slight blue-shift of **3@GSNP**, attributed to the more rigid environment experienced in the silica rigid matrix. Instead, **4@GSNP** emission spectrum is red-shifted respect to **4**. The intensity of the spectra is little diminished in air-equilibrated solution, due to the quenching effect of the oxygen. The O_2 sensitation is demonstrated by collecting the 1270 nm $^1O_2$ phosphorescence in D_2O solution of **3@GSNP** and **4@GSNP** (not reported for the bad signal-to-noise ratio, due to the extremely low concentration of the samples, obtained dissolving in D_2O a little amount of the H_2O solution of the nanoparticles).

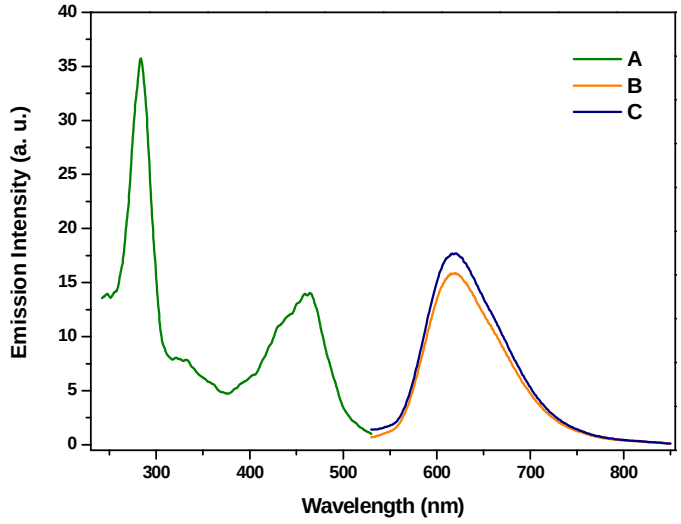

Figure 26. Excitation spectrum (**A**) in air-saturated water (λ_{em}= 630 nm) and emission spectra of **3@GSNP** at room temperature in air-saturated (**B**) or in degassed (**C**) water (λ_{ex}= 430 nm).

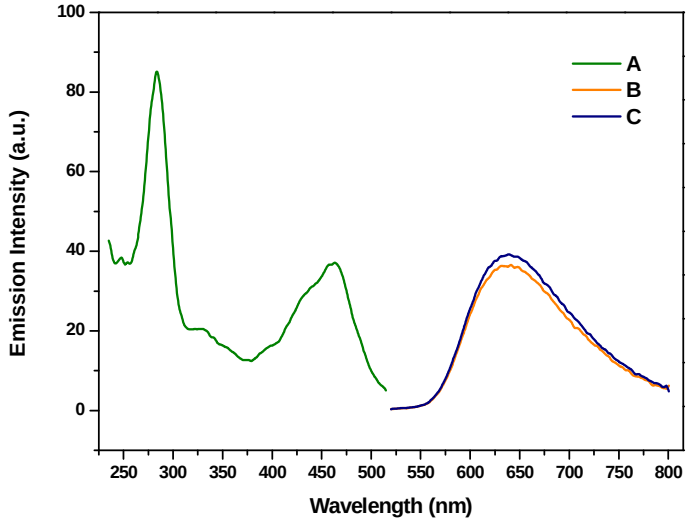

Figure 27. Excitation spectrum (**A**) in air-saturated water (λ_{em}= 640 nm) and emission spectra of **4@GSNP** at room temperature in air-saturated (**B**) or in degassed (**C**) water (λ_{ex}= 460 nm).

Ru complex-containing nanoparticles follow a bi-exponential lifetime decay, in presence as well as in absence of O_2 (Fig. 28 and 29; see § Appendix A.3 where the time profiles of air-equilibrated solutions emission are reported). Likewise for the free Ru complexes (properly fitted by a mono-exponential function), also for the complexes-containing nanoparticles it was tried to fit lifetime decays by a mono-

exponential function, but the obtained χ^2-value were unacceptable. By comparing lifetime values of **3@GSNP** and **4@GSNP** with the correspondent values of **3** and **4**, it can be noted only a small enhance, in accordance with the more rigid environment experienced into the nanoparticles. Moreover, respect to **1@GSNP** and **2@GSNP**, the emission intensity difference between Ar-equilibrated and air-equilibrated solutions of **3@GSNP** and **4@GSNP** is very small, especially for the latter; this is due to the scarce emission intensity of the Ru respect to Ir complexes, which is maintained when the complexes are encapsulated into GSNPs, but, in the case of **4@GSNP** the extremely low value of $k_q[O_2] = 2.97 \times 10^3\ s^{-1}$ (obtained by means of the eq. 5 § 3.4.2.2 using the average lifetimes) must be taken into account. This low value is attributed to the scarce oxygen concentration inside the nanoparticles, if we suppose that, differently from the other complex-entrapping GSNPs, the silicon functionalization of the complex **4** facilitates the loading into NP silica matrix, resulting in a deeper localization of the complex, so preserving an its relevant fraction from oxygen contact.

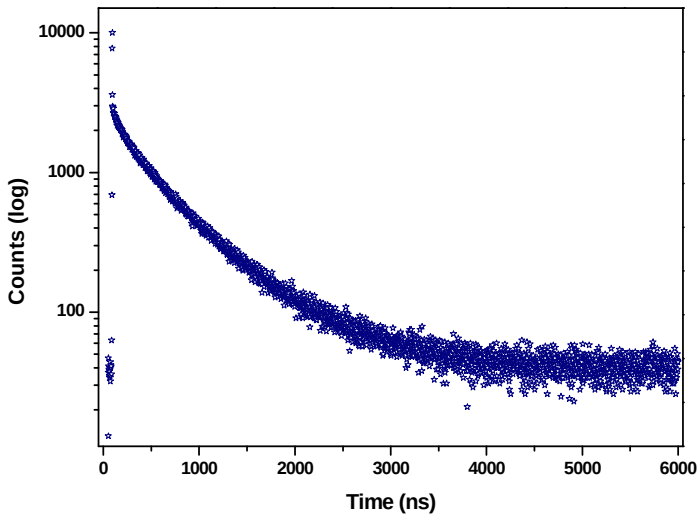

Figure 28. Time-resolved emission decay of **3@GSNP** in degassed water (λ_{ex}= 460 nm, $\lambda_{monitored}$= λ_{em}= 630 nm). Fitting results (χ^2 = 1.08): $\tau_1 = 2.62 \times 10^{-7} \pm 7.93 \times 10^{-9}$ s; α_1= 24.78%; $\tau_2 = 7.18 \times 10^{-7} \pm 3.59 \times 10^{-9}$ s; α_2= 75.22%.

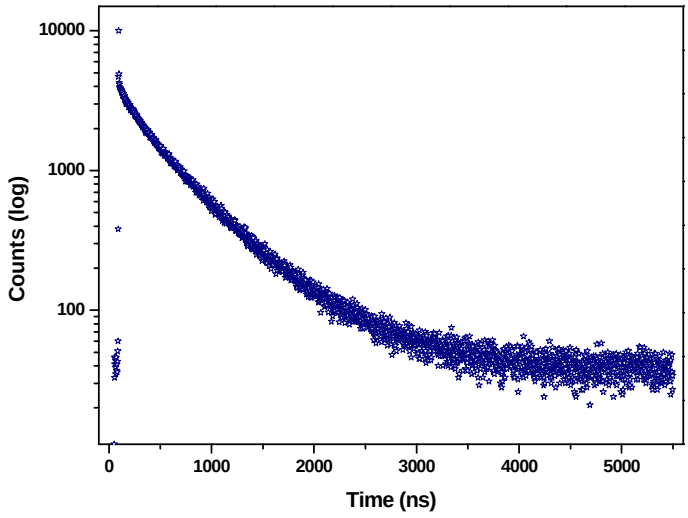

Figure 29. Time-resolved emission decay of **4@GSNP** in degassed water (λ_{ex}= 460 nm, $\lambda_{monitored}$= λ_{em}= 640 nm). Fitting results (χ^2 = 1.06): τ_1 = 2.60 x 10^{-7} ± 6.65 x 10^{-9} s; α_1= 30.08%; τ_2 = 6.37 x 10^{-7} ± 2.57 x 10^{-9} s; α_2= 69.92%.

4.3.3 GSNPs entrapping other TMCs

The method of synthesis previously described was used to incorporate within the silica matrix several platinum complexes (Fig. 30), which had been previously tested the photosensitizing capability. Nevertheless, the obtained GSNPs do not emit. This can be due to a sort of unknown quenching of the complexes luminescence in the silica matrix (with or without oxygen), or, more trivial, to an unsuccessful loading of the fluorophore into GSNPs. As reported in literature (Bagwe 2004), the hydrophilic environment of silica does not favor entrapment of hydrophobic dye molecules. To successfully entrap dye molecules inside a silica matrix, polar or cationic dye molecules should be used to increase the electrostatic attraction of the dye with the negatively charged silica matrix and the size of the dye molecules should be large to prevent dye leakage from pores of the silica matrix.

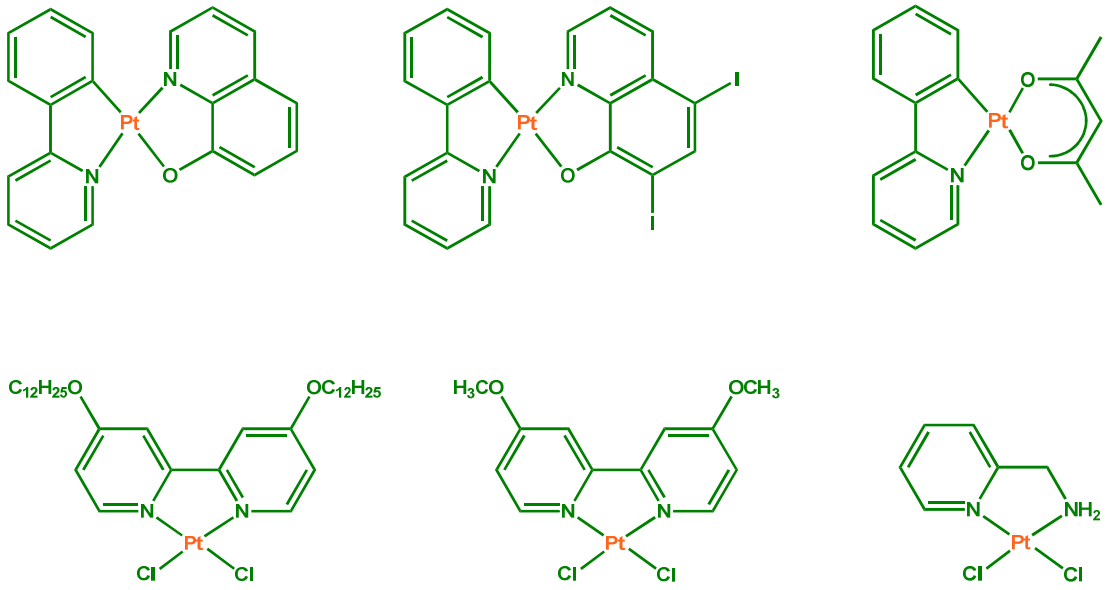

Figure 30. Structures of Pt(II) complexes with photosensitizing capability tested to be incorporated into GSNPs.

4.3.4 *In-vitro* test of nanoparticles cytotoxicity

Several assays are in use to determine the effect of a drug on cells *in vitro*. The "dye exclusion test" is a rapid method to evaluate cell viability in response to environmental insults. It is based on the ability of viable cells to be impermeable to trypan blue, naphthalene black, erythrosine, and other dyes. When the membrane integrity of the cells is compromised, there is a dye uptake into the cells; in this way, viable cells, which are unstained, appear clear with a refractive ring around them, while unviable cells appear dark blue colored (Longo-Sorbello 2006).
The mentioned method was applied to assess the viability of murine mammary adenocarcinoma cells (TS/A-pc), after incubation with gold nanoparticles containing the photosensitizer Ru complex **3**, **3@GSNP**, followed or not by irradiation and using the trypan blue as dye.

Protocol

Murine mammary adenocarcinoma cells (TS/A-pc) were plated in 96-wells plates (1.5×10^4 per well) 24 hours before the experiment, maintained in minimum essential medium (Roswell Park Memorial Institute medium, RPMI) supplemented with 10% fetal bovine serum and penicillin and streptomycin antibiotics (1%). Cells were incubated with the indicated concentration of complex for 24 hours, exposed to irradiation with light at 470 nm (FWHM = 30 nm, irradiance at 100mm = 25 W/m^2) or kept in the dark for 1 hour and placed at 37°C in a humidified 95% air / 5% CO_2 atmosphere, for another 24 hours. For trypan blue assay, the medium was removed and cells were wash once with phosphate buffered saline (PBS), then a solution (1:10) trypan blue/PBS was added by wells. The results were expressed as percentage of viable cells for one hundred cells counted by well. Experiments were carried out in triplicates.

Results

As shown in Figure 31, *in dark conditions* the treatment of murine mammary adenocarcinoma cells with nanoparticles containing the photosensitizer show a slight toxicity for concentrations ranging from 5 to 20 μM (purple trace), while the naked

photosensitizer displayed practically no cytotoxic effect for all concentrations tested (red trace). *After light exposure*, NPs with the encapsulated complex significantly show an enhanced photodynamic activity with a surviving cell fraction lower than 20% for concentrations up to 5 µM (green trace), while to obtain analogous results with the naked photosensitizer are required concentrations up to 20 µM (blue trace).

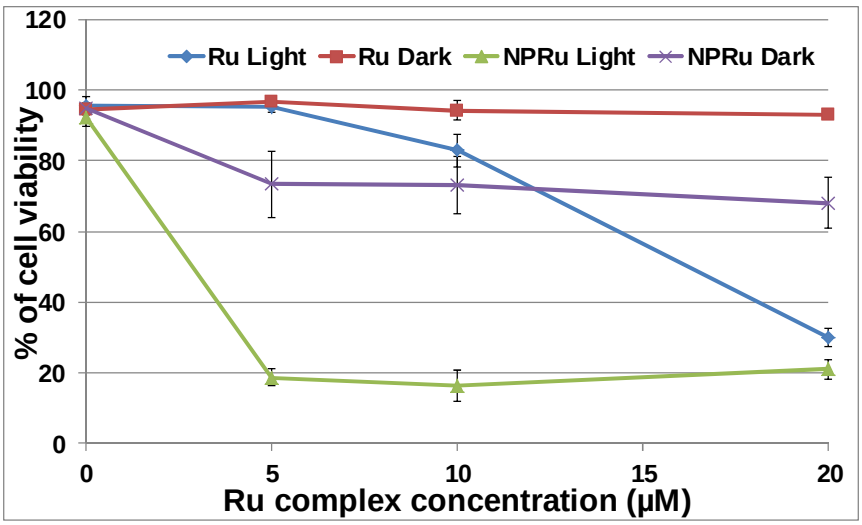

Figure 31. Dark cytotoxicity and photodynamic activity of the photosensitizer **3@GSNP** at different concentrations, in solution or entrapped within gold nanoparticles.

4.3.5 Gold-Dye Silica Nanoparticles and imaging

Confocal fluorescence microscopy was used to determine the uptake and the intracellular localization of the photosensitizer **3@GSNP**.

Settings and protocol

U87MG (Human glioblastoma) and HEK293 (Human kidney) cells were grown in Dulbecco's Modified Eagle Medium (DMEM) enriched with 4.5 g/L glucose and supplemented with 1% L-glutamine, 10% fetal bovine serum. TS/A-pc cells were grown in RPMI supplemented with 10% fetal bovine serum (FBS). All the cell lines were cultured at 37 °C in a humidified 95% air / 5% CO_2 atmosphere.

Cells were grown for 24 hours on a 8-wells lab-Tek chamber I (Nunc). Immediately before running the experiment, cells were incubated for one hour in phenol red and FBS free DMEM alone or containing 3 µM of the NPs with the encapsulated Ru complex at 37°C, 5% CO_2. Following incubation, the cells were rinsed and images were collected.

Confocal microscopy was performed on the Leica TCS SP5 (Wetzlar, Germany) microscope using a 40x oil immersion objective of 1.2 Numeric Aperture (N.A.), pinhole 100 micrometers. The 488 nm laser intensity was set up at 3% of its maximum intensity and the emission was collected at 625-740 nm. For enhanced contrast images, the maximum intensity of the lut was decreased from 255 to 100 for all conditions allowing the comparison between cells alone or containing the NP.

Results

Fluorescence microscopies showed clear uptake of nanoparticles containing the luminescent Ru complex U87MG, HEK293 and TS/A-pc cells. Nanoparticles were internalized into cells after 2 hours-incubation at 3µM. They were mainly observed in the cytoplasm, but an uptake in the cellular vesicles can not be excluded. In the experimental conditions, autofluorescence of the vesicles was observed, leading to a strong signal that hide a part of the nanoparticles signal.

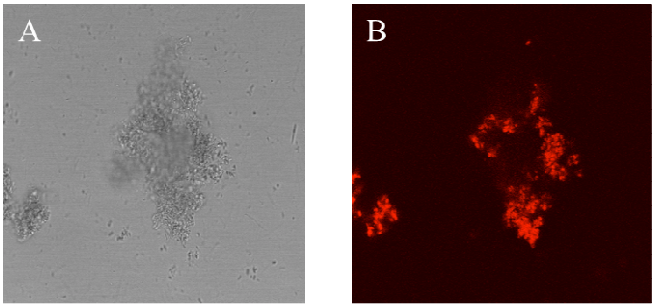

Figure 32. Bright field image (**A**) and confocal fluorescence imaging (**B**) of gold-silica nanoparticles with the incorporated complex **3@GSNP**.

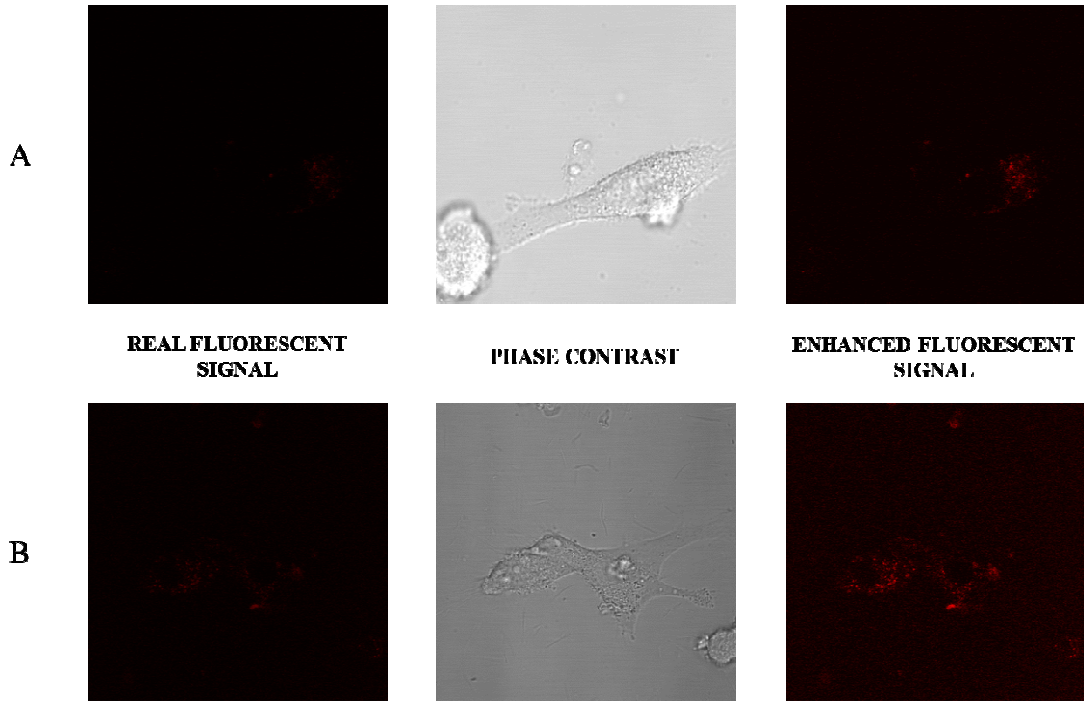

Figure 33. Bright field image and confocal fluorescence imaging corresponding to U87MG cells (**A**) and to U87MG cells after incubation with gold-silica nanoparticles 3µM (**B**).

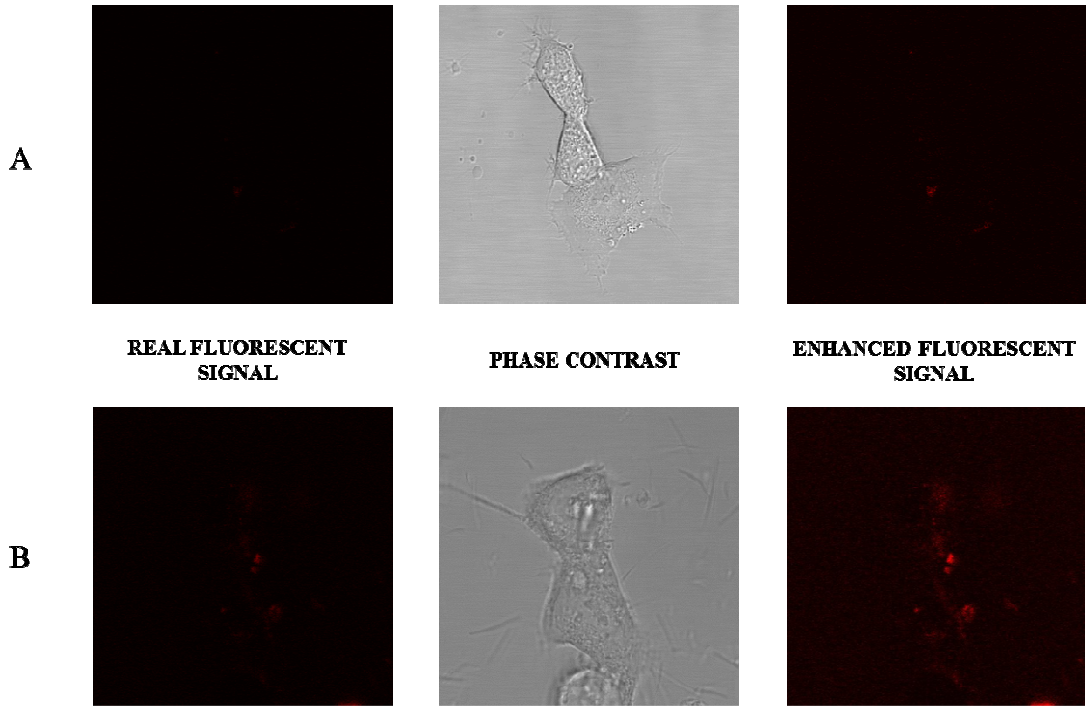

Figure 34. Bright field image and confocal fluorescence imaging corresponding to HEK293 cells (**A**) and to HEK293 cells after incubation with gold-silica nanoparticles 3µM (**B**).

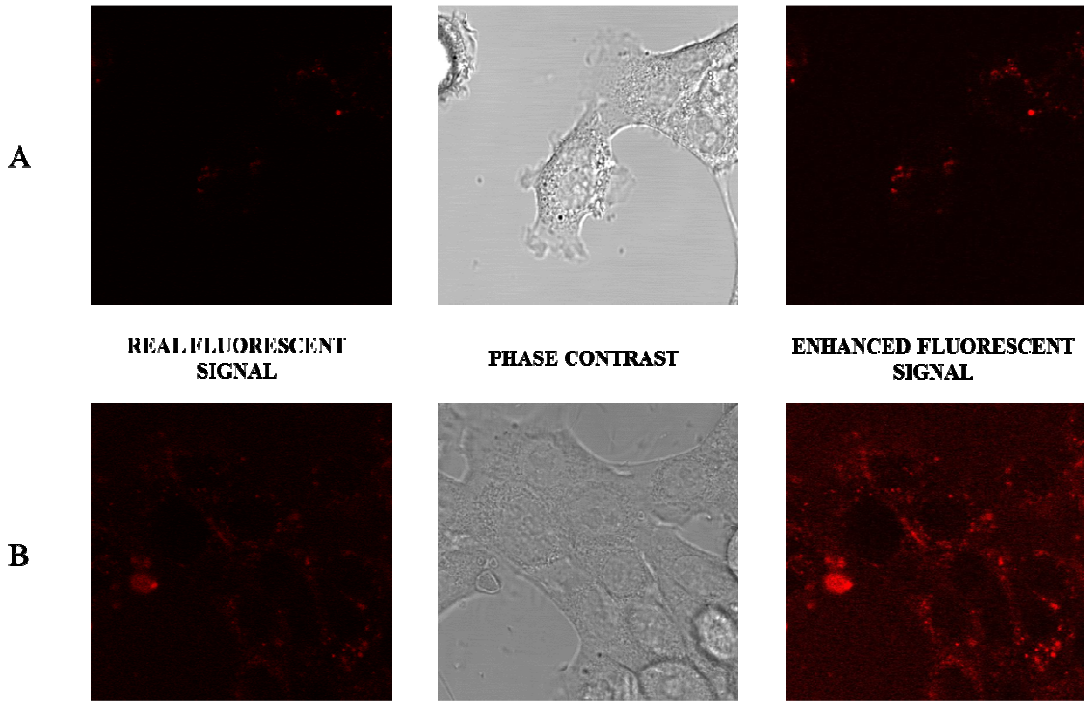

Figure 35. Bright field image and confocal fluorescence imaging corresponding to TS/A-pc cells (**A**) and to TS/A-pc cells after incubation with gold-silica nanoparticles 3µM (**B**).

4.4 Conclusion

Combining diagnosis and therapy in one process is an emerging biomedical method referred to as theranostics. The primary goal of theranostics is to selectively target-specific diseased tissues or cells to increase diagnostic and therapeutic accuracy. With the help of theranostics, we can bring together key stages of a medical treatment, such as diagnosis and therapy, and make a treatment shorter, safer and more efficient. Several theranostic methods have employed nanoparticles as the carriers of diagnostic agents and drugs. Biocompatible nanoparticles are currently under development as cancer theranostic agents that would enable noninvasive diagnosis and precise cancer therapy. Based on these premises, we achieved the synthesis of gold silica-based nanoparticles doped with ionic octahedral complexes of transition metals, with the idea to evaluate their multifunctionality in the field of biomedical applications, on the basis of the photosensitizing properties of the complexes coupled to their intrinsic luminescence.

The gold-silica nanoparticles (GSNPs) entrapping transition metal complexes (TMCs) have been synthesized by adapting the sol-gel method, in a quaternary water/oil microemulsion, and using $HAuCl_4$ as source of gold, APTES and TEOS as silica source, $NaBH_4$ and a thiol as reducing and coating gold agents. Summarizing, the water to surfactant ratio gives the number of droplets; the thiolate surface of gold clusters interacts strongly with APTES precursors that coated physically the surface and exhibit the silanol group to the subsequent condensation of TEOS molecules; the polysiloxane precursors are distributed in all micelles and the thickness of polysiloxane shell was due to the amount of silanes. By adding TMCs solution at the microemulsion, GSNPs entrap them into the silica matrix. Finally, the following scheme illustrates the sequence of steps of nanoparticles synthesis.

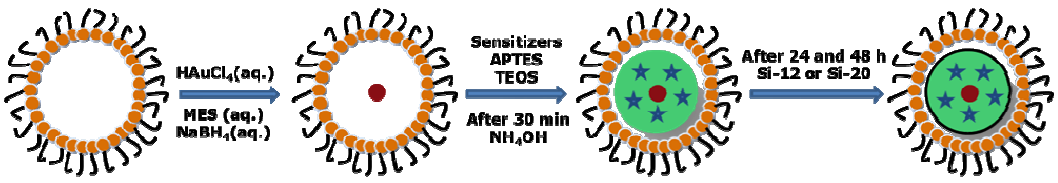

The hybrid gold core/silica shell nanoparticles constitute a perfect example of multifunctional structures; the microemulsion is a versatile synthesis method that permits to incorporate several nanometric object of different nature, confined into a closed volume. The combination between sol-gel process and microemulsion system results in the total control of the growth of core shell structures from nucleation step to the coating process and, eventually, the particle stabilization. Transmission electron microscope images show clearly the obtained GSNPs, and it is possible to recognize with great accuracy the structure of the gold core. Due to the emissive properties of the encapsulated TMCs, it was possible to test the successful of the synthesis.

The synthetic method was used to incorporate within the silica matrix several neutral platinum complexes, which had been previously tested the photosensitizing capability. Nevertheless, the obtained GSNPs do not emit. This can be due to a sort of unknown quenching of the complexes luminescence in the silica matrix (with or without oxygen), or, more trivial, to an unsuccessful loading of the fluorophore into GSNPs. A possible explanation of the failed Pt(II) compounds loading could be recognized in the charge of the complexes: positive in the successfully incorporated ruthenium and iridium complexes, neutral in platinum ones. The hydrophilic environment of silica does not favor entrapment of hydrophobic dye molecules. To successfully entrap dye molecules inside a silica matrix, polar or cationic dye molecules should be used to increase the electrostatic attraction of the dye with the negatively charged silica matrix and the size of the dye molecules should be large to prevent dye leakage from pores of the silica matrix.

GSNPs entrapping TMCs have been characterized in order to indentify qualitatively their capability of sensitizing dioxygen; the sample containing the Ir and Ru complexes previously tested free in solution, showed photosensitizing ability, more pronounced for Ir complexes. In particular, GSNPs entrapping ruthenium complex functionalized with silica alkyl chain, has a negligible O_2 sensitivity. This was attributed to the scarce oxygen concentration inside the nanoparticles, if we suppose that, differently from the other complex-entrapping GSNPs, the silicon functionalization of the complex facilitates the loading into NP silica matrix, resulting in a deeper localization of the complex, so preserving an its relevant fraction from oxygen contact. Nevertheless, a preliminary *in vitro* test of GSNPs entrapping another

ruthenium complex was performed on cell tumor culture, to evaluate the dark *vs.* light cytotoxicity. The promising results encourage us to continue on this path, functionalizing the surface of the nanoparticles with specific molecules that address the GSNP towards target organs.

Finally, thanks to the high radiative rate constant of the iridium complexes, GSNPs entrapping these compounds maintains luminescence also in presence of oxygen. This special feature allows to have a material that generates oxygen and simultaneously emits. This double function was observed in living matter, in particular in tested cell culture, observed by fluorescent microscope, making these NPs a beautiful example of theranostic materials.

Moreover, taking into account the superimposition of the iridium complexes emission band with the gold plasmonic band, it is reasonable to suppose an energy-transfer process that, although partially quenches emission, actives thermal de-exciting paths in gold core, which, in turn, could be useful in photothermal therapy

.

Final conclusions and *perspectives*

We have pointed out some of the richness in the photophysics of metal complexes in relation to biomedical issues, following the fate of an excited state, along a non-radiative and/or radiative path.

In principle, a sensor is based on the radiative deactivation of a species: emitted light, or a modulation of it, is the signal that a process has taken place or that the species experienced a new environment. If emission is topologically detected, as example by means of a fluorescence microscopy, an image can be recorded. On the other side, non-radiative deactivation of the energy-rich excited states can be used to promote other processes; in other words, by means of non-radiative path, radiant energy of the electromagnetic field can be canalized towards desired targets, as example to generate highly-reactive species. But as often happens in Nature, what appears opposite in fact it is not, and even in the case of the decay of molecular excited states, radiative and non-radiative pathways are not competitive, but can be simultaneous.

Metal complexes are a sort of "*in nuce*" nano-multifunctional material: a proper choice of metal joined to one or more ligands can afford various functions, and light can act as function driving force and/or a way of communication between the nanoworld and macroworld. We have tried to explore potential of the photophysics of some metal complexes in biomedical applications, keeping in mind simultaneous radiative and non-radiative relaxation pathways of electronically excited-states, that in our application field become sensoristic and therapeutics; or, by using an emphatic neologism, theranostics.

Gold-silica nanoparticles entrapping Ir(III) or Ru(II) complexes have been successfully synthesized, and they are simultaneously phosphorescent and able to generate singlet oxygen. These nanoparticles were administered to tumor cell culture, and it was possible to:

- visualize, by fluorescent microscope, the nanoparticles localization inside the cell compartments;

- verify, by cytotoxical test, the effectiveness of photogenerated singlet oxygen to destroy tumor cells.

Thanks to the versatility of nanoparticles synthesis, it is possible to functionalize the nanoparticles surfaces with specific group to address them towards a specific target; recent studies demonstrate that breast tumor cells show an increased glucose up-take: masking nanoparticles by glucose could make achievable a specific accumulation into these cells.

A very cheap and fast way to make water soluble a compound is to graft it to a hydrosoluble polymer. We have synthesized and characterized a Pt(II) complex-containing polymethacrylate polymer, which show oxygen photosensitizing ability.

Thanks to the high-oxygen permeabilityof the polymer matrix, similar materials can be used to disinfect wastewater, making these materials good candidates in Antimicrobial Photodynamic Therapy.

In drug research, “in vitro” test is the first way to evaluate the efficacy of a molecule. However, in living organism, drug bioavailability is a key factor for the success. Scarcely water soluble drugs take great advantage to interact with bloodstream serum protein, such as Human Serum Albumin, a carrier for lipophilic species.

Medicinal inorganic chemistry is a field of increasing prominence as metal-based compounds offer possibilities for the design of therapeutic agents not readily available to organic compounds. The wide range of coordination numbers and geometries, accessible redox states, thermodynamic and kinetic characteristics, and the intrinsic properties of the cationic metal ion and ligand itself offer the medicinal chemist a wide spectrum of reactivities that can be exploited. Unfortunately, a lot of useful metal complexes are scarcely water soluble, so the binding to the serum albumin becomes of capital relevance.

In this light, fluorescence spectroscopy offers the advantage of sensitivity, simplicity and wealth of molecular information concerning protein-drug interactions. Besides the classical studies of intrinsic protein fluorescence quenching (due to a binding interaction), to have luminescent meta-based drug, represents a way to better characterize the protein binding.

We have studied the spectroscopic properties of a new zinc complex with interesting antitumoral properties, to evaluate the binding to Human Serum Albumin from a dual point of view: protein fluorescence quenching, and complex fluorescence modulation.

Thanks to the availability of the data concerning the different distribution of the Zinc complex drug into protein or extra-protein environment, obtained by means of the solvatochromic properties, it should be possible to introduce substituent groups on the ligands to study their effect on the protein binding.

Metals ions have been traditionally included in therapy to exploit their reactivity and have been particularly attractive because of the exceptionally wide range of reactivities available. On the other hand, metals can also be used as building blocks for well-defined, three-dimensional constructs. In this way, the availability of many different coordination geometries allows for the synthesis of structures with unique stereochemistry and orientation of organic ligands and structures which are not accessible through purely organic, carbon-based compounds. The kinetic inertness of the coordination/organometallic bonds make these compounds in principle behave like organic compounds. This approach immensely expands our ability to chart biologically-relevant chemical space.

Targeted delivery and/or controlled prodrug activation, be it by light, intracellular reduction or other means, hold the promise of more selective and effective drug administration.

The concept of the metal as scaffold for the construction of unique, yet well-defined three-dimensional structures, rather than reactive centre, holds much promise.

Finally, the advent of medicinal bioorganometallic chemistry has further expanded the toolbox of the medicinal inorganic chemist. The nature of the research will rely ever more heavily on interdisciplinary collaboration, but many exciting discoveries and applications almost certainly lie ahead.

Appendix MATERIALS, METHODS, EXPERIMENTAL APPARATUS AND SUPPLEMENTARY PHOTOPHYSICAL DATA

A.1 Photophysical Measurements

Spectrofluorimetric grade solvents were used for the photophysical investigations in solution.

1) ***Absorption***

A Perkin Elmer Lambda 900 spectrophotometer was employed to obtain the absorption spectra.

2) ***Emission***

Steady-state emission spectra were recorded on a HORIBA Jobin-Yvon Fluorolog-3 FL3-211 spectrometer (Fig. 1) equipped with a 450 W xenon arc lamp (**L**), double-grating excitation ($\mathbf{M_{ex}}$) and single-grating emission ($\mathbf{M_{em}}$) monochromators (2.1 nm/mm dispersion; 1200 grooves/mm), and a Hamamatsu R928 photomultiplier tube (**PM**) or a TBX-04-D single-photon-counting detector ($\mathbf{D_{TCSPC}}$) or a InGaAs liquid nitrogen-cooled solid-state detector ($\mathbf{D_{InGaAs}}$). Emission and excitation spectra were corrected for source intensity (lamp and grating) and emission spectral response (detector and grating) by standard correction curves.
Deaerated samples were prepared by bubbling argon into.

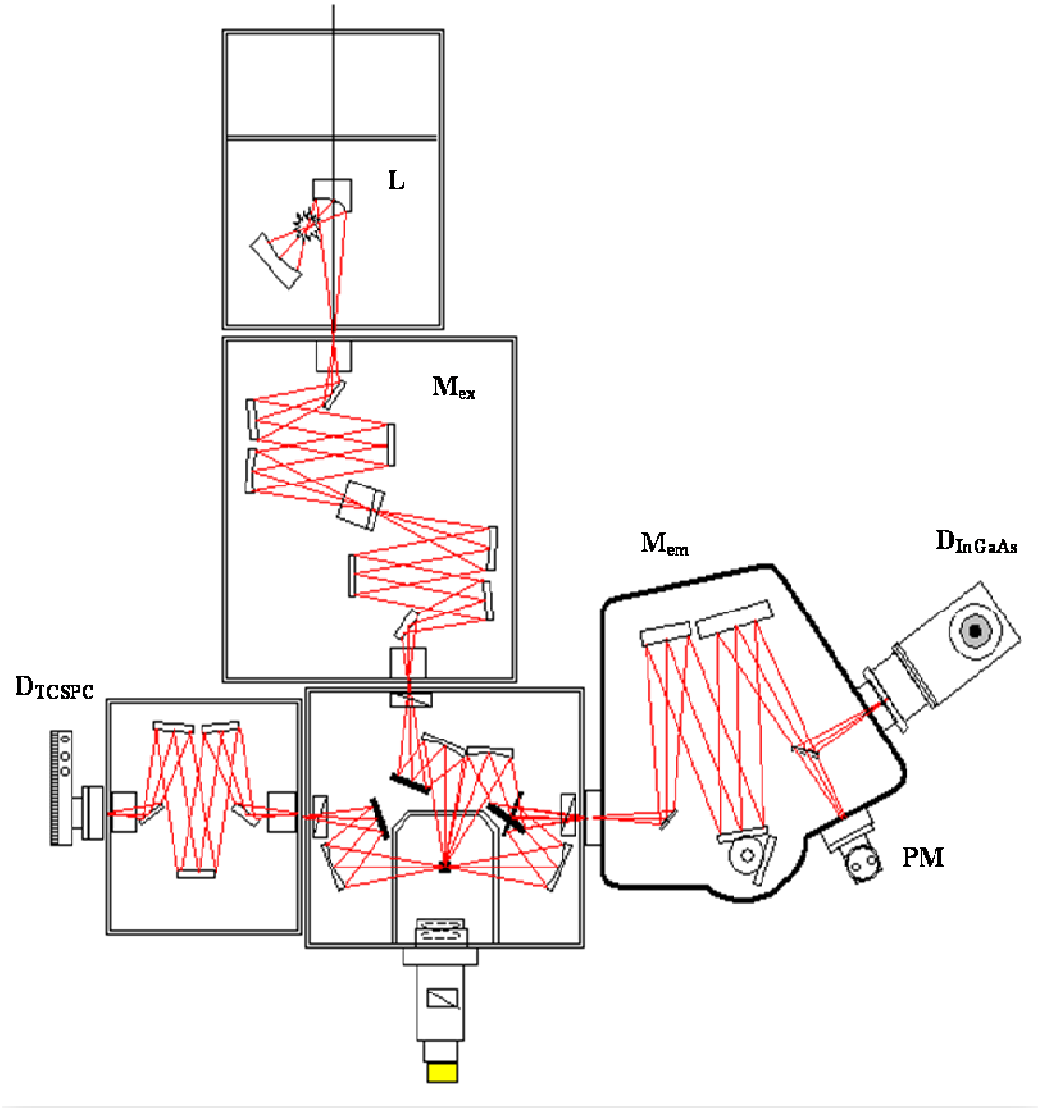

Figure 1. FluoroLog3-2iHR1-TCSPC-IGA, optical configuration.

3) ***Lifetimes***

Time-resolved measurements were performed using the time-correlated single-photon counting (TCSPC) option on the Fluorolog 3.

Excitation sources (Table 1) were mounted directly on the sample chamber at 90° to a single-grating emission monochromator and collected with a TBX-04-D single-photon-counting detector. The photons collected at the detector are correlated by a time-to-amplitude converter (TAC) to the excitation pulse.

Source	λ_{em}	Duration	Power	Repetition rate
Nanoled	265 nm	1.2 ns	0.2 pJ	1 MHz
Laser Nanoled	379 nm	750 ps	63 pJ	1 MHz
Nanoled	461 nm	1.3 ns		1 MHz

Table 1. Excitation sources used.

Signals were collected using an IBH Data Station Hub photon counting module, and data analysis was performed using the commercially available DAS6 software (HORIBA Jobin Yvon IBH). The fitting procedure of the emission intensity decays I(t) uses a multi-exponential model according to the expression

$$I(t) = \Sigma_i \alpha_i \exp(-t/\tau_i)$$

where τ_i are the decay times and α_i represent the amplitudes of the components at t=0. Goodness of fit was assessed by minimizing the reduced Chi squared function (χ^2) and visual inspection of the weighted residuals. When using the multi-exponential decay law it is often valuable to determine the average lifetime ($< \tau >$), which is given by

$$< \tau > = \Sigma_i \alpha_i \tau_i^2 / \Sigma_i \alpha_i \tau_i$$

4) ***Emission quantum yields (EQY)***

Emission quantum yields values (Φ) in solution were determined by using the optically dilute method (Demas 1971) on aerated and deaerated solutions which absorbance at excitation wavelengths was < 0.1 according to the formula (where the superscript text R refers to the reference standard):

$$\Phi = \Phi^R (A_{em}/ A^R_{em}) (Abs/Abs^R) (n/n^R)$$

where A_{em} is the integrated corrected emission area obtained exciting the sample at the wavelength λ_{ex}, *Abs* is the absorbance measured at the λ_{ex}, *n* is the refractive index

of the solvent. $Ru(bipy)_3Cl_2$ (bipy = 2,2'-bipyridine) in water (Φ = 0.028) (Nakamaru 1982) and aminopyridine in ethanol (Φ = 0.37) (Mutai 2002) were used as standard. The experimental uncertainty on the molar extinction coefficients is 10%, while on the emission quantum yields is 20%. The examined compounds are fairly stable in solution, as demonstrated by the constancy of their absorption spectra over a week.

A.2 Synthetic Procedures

Grafting insertion of the (pam)Pt(Cl)$_2$ complex into polymethacrylic acid

Procedure. The (pam)Pt(Cl)$_2$ complex (§ 3.4) (0.01 g) was dissolved in chloroform and the resulting solution was deposited as a thin film in a round bottom flask by solvent evaporation. Then, 10 ml of a 1.0 M H_2O_2 water solution containing 2.0 g of methacrylic acid was added, and, successively, 0.25 g of ascorbic acid was introduced in the reaction flask. The mixture was maintained at 25 °C for 24 h under atmospheric air and, in an excess volume of acetone (5:1), a precipitate was obtained. The precipitate was purified by dissolution in ethanol and precipitation in diethylether (5:1) three times and finally was dried under vacuum for 24 h at room temperature. The polymer was checked to be free of unreacted complex by the absorption spectra of the washing media; the molecular weight distribution of the polymer was determined by GPC/SEC analyses and corresponds to an average value of 97 000 Da, with $M_w/M_n < 1.6$. The reaction mechanism involved the radical insertion of the (pam)Pt(Cl)$_2$ complex into the growing chain of polymethacrylic acid (Puoci 2008). In the first step of the reaction, a radical species is formed on the Pt complex, which then reacts with the polymer growing chain.

Materials and Instruments. Polymethacrylic acid (pMAA) standard samples for size-exclusion chromatography (M_n= 600 - 500000; M_w/M_n = 1.06-1.10) were obtained from Sigma-Aldrich (Sigma Chemical Co., St Louis, MO, USA).

M_n and M_w/M_n were measured by Gel Permeation Chromatography (GPC) using water as eluent at 45°C and at flow rate, 1.0 mL min^{-1} on Waters Ultrahydrogel-1000 column connected to a Jasco PU-2089 pump and a Jasco 930-RI refractive-index detector. The columns were calibrated using as standard pMAA samples.

^{1}H NMR spectra were acquired on a Bruker Advance DRX-300 spectrometer in DMSO-d6 or D_2O solution, with tetramethylsilane as internal standard. Infrared spectra were recorded with a Spectrum One FT-IR Perkin-Elmer spectrometer. Elemental analyses were performed with a Perkin-Elmer 2400 microanalyzer.

A.3 Supplementary Photophysical Data

Table 1. Photophysical data for complexes **1-4** in solution at room temperature.

	air-equilibrated solution			deaerated solution		
	χ^2	τ/μs (α/%)	$\langle\tau\rangle$/μs	χ^2	τ/μs (α/%)	$\langle\tau\rangle$/μs
1[a]	1.10	τ_1 = 0.273 (17.8); τ_2 = 0.409 (82.2)	0.39	1.01	τ_1 = 1.220 (10.5); τ_2 = 2.250 (89.5)	2.18
2[a]	1.15	τ_1 = 0.307 (22.1); τ_2 = 0.447 (77.9)	0.42	1.01	τ_1 = 1.030 (10.8); τ_2 = 1.860 (89.2)	1.81
3[b]	1.05	τ_1 = 0.260 (13.4); τ_2 = 0.403 (86.5)	0.39	1.01	τ_1 = 0.487 (10.7); τ_2 = 0.914 (89.3)	0.88
4[b]	1.02	τ_1 = 0.313 (42.0); τ_2 = 0.411 (58.0)	0.37	1.03	τ_1 = 0.491 (10.5); τ_2 = 0.896 (89.5)	0.87

[a]H_2O solution; [b]CH_2Cl_2 solution.

Complex 1

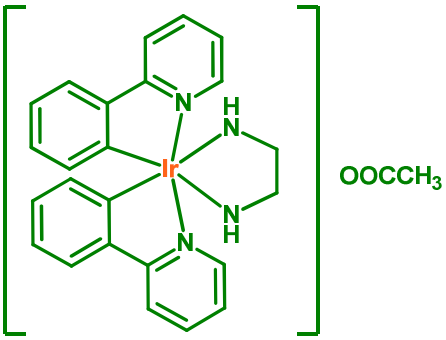

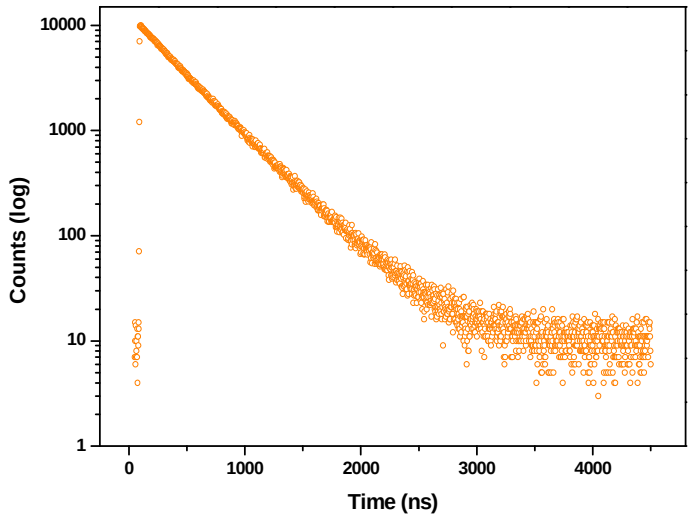

Figure 2. Time-resolved emission decay of **1** in air-equilibrate water (λ_{ex}= 379 nm, $\lambda_{monitored}$= λ_{em}= 510 nm). Fitting results (χ^2 = 1.19): τ = 0.388 x 10^{-6}s.

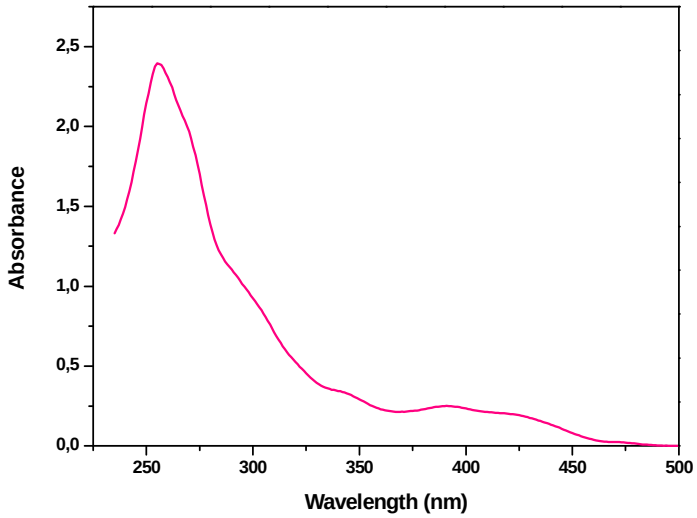

Figure 3. Absorption spectrum of **1** in D_2O at room temperature.

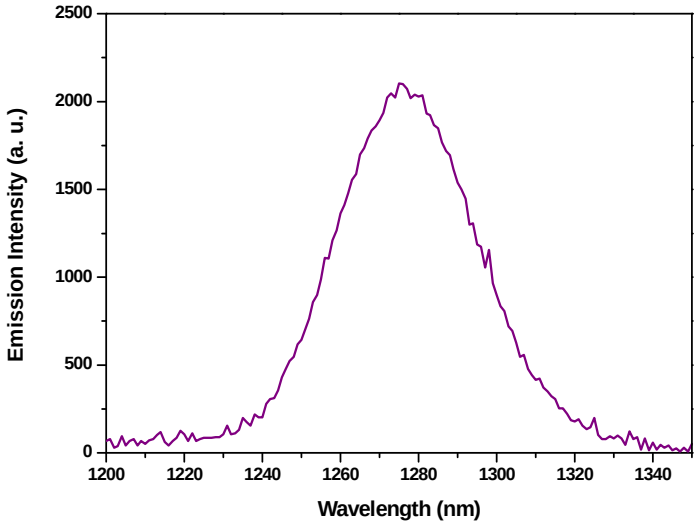

Figure 4. Singlet oxygen phosphorescence upon irradiation at 390 nm of **1** in air-saturated D_2O.

Complex 2

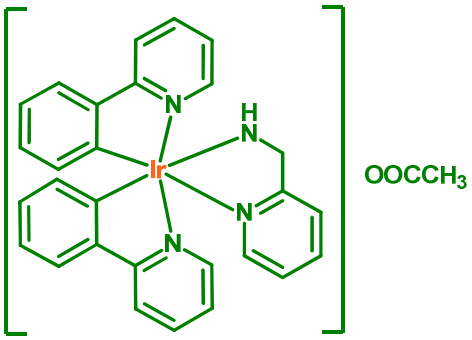

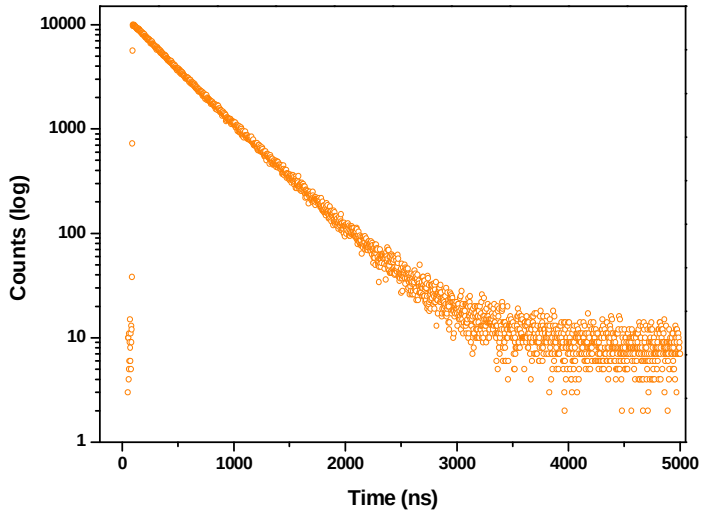

Figure 5. Time-resolved emission decay of **2** in air-equilibrated water (λ_{ex}= 379 nm, $\lambda_{monitored}$= λ_{em}= 510 nm). Fitting results (χ^2 = 1.27): τ = 0.420 x 10^{-6} s.

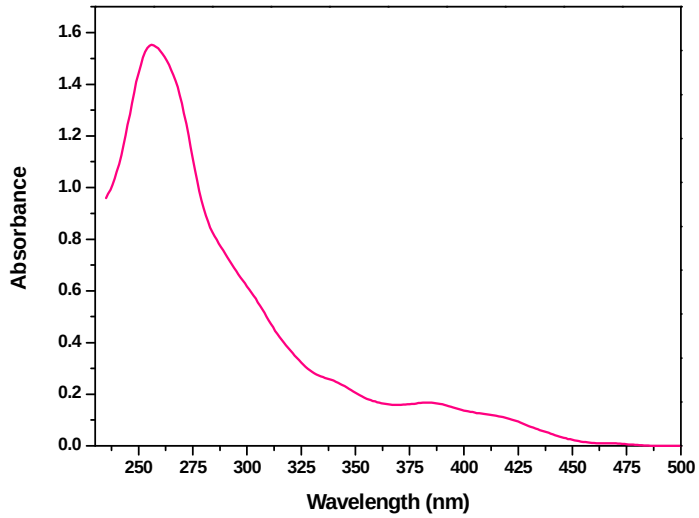

Figure 6. Absorption spectrum of **2** in D_2O at room temperature.

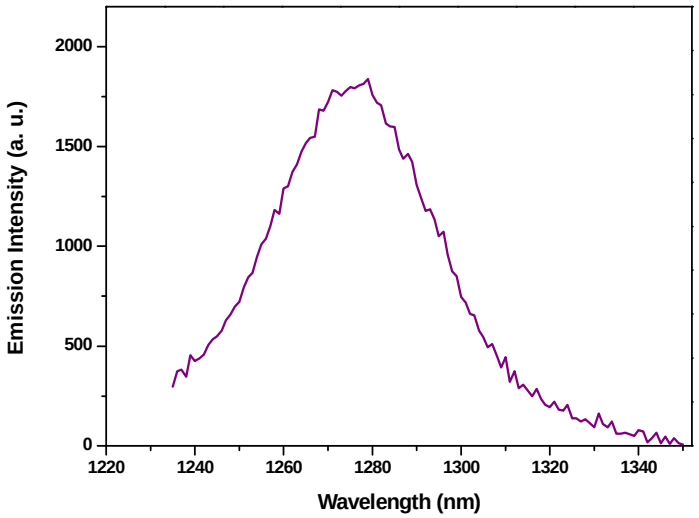

Figure 7. Singlet oxygen phosphorescence upon irradiation at 400 nm of **2** in air-saturated D_2O.

Complex 3

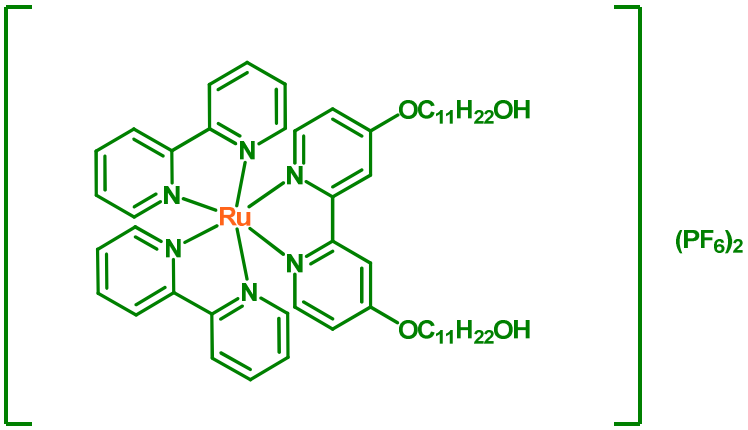

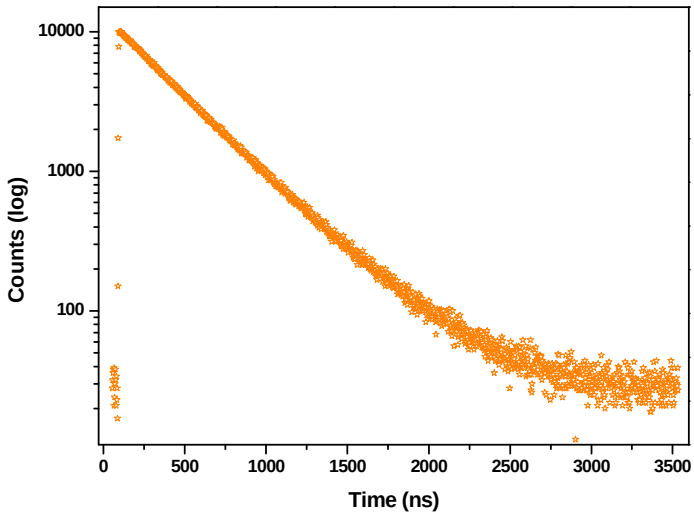

Figure 8. Time-resolved emission decay of **3** in air-equilibrated dichloromethane (λ_{ex}= 460 nm, $\lambda_{monitored}$= λ_{em}= 630 nm). Fitting results (χ^2 = 1.08): τ = 0.385 x 10^{-6} s.

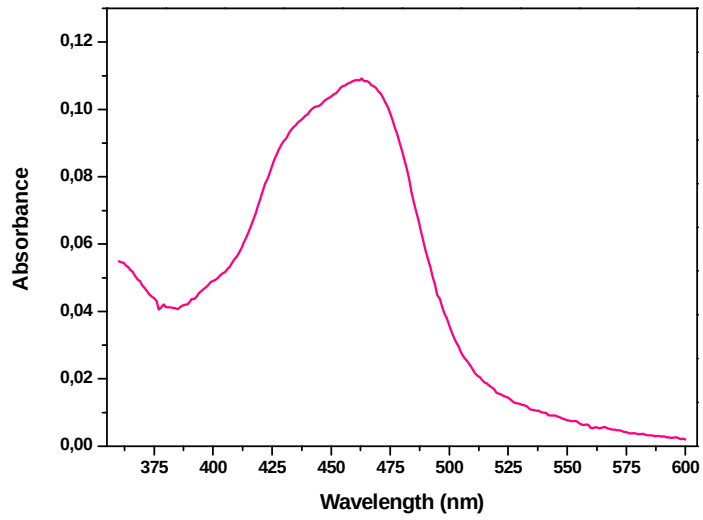

Figure 9. Absorption spectrum of **3** in THF at room temperature.

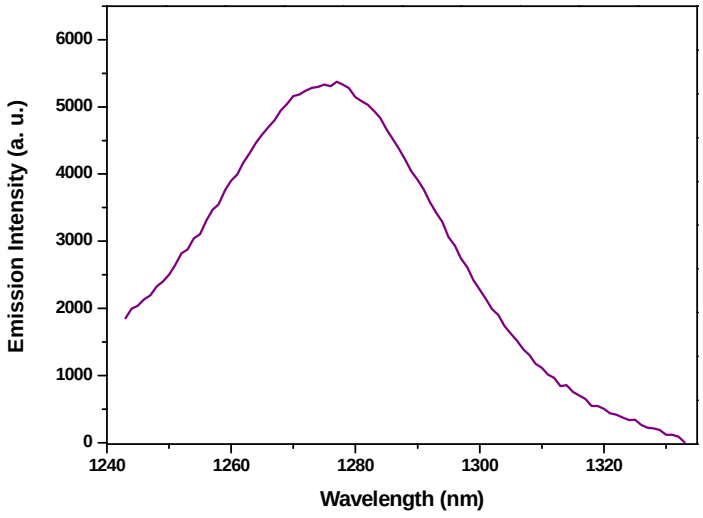

Figure 10. Singlet oxygen phosphorescence upon irradiation at 465 nm of **3** in air-saturated THF.

Complex 4

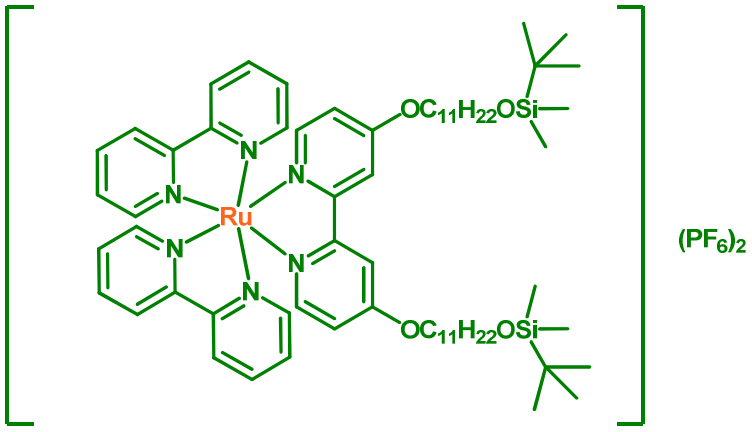

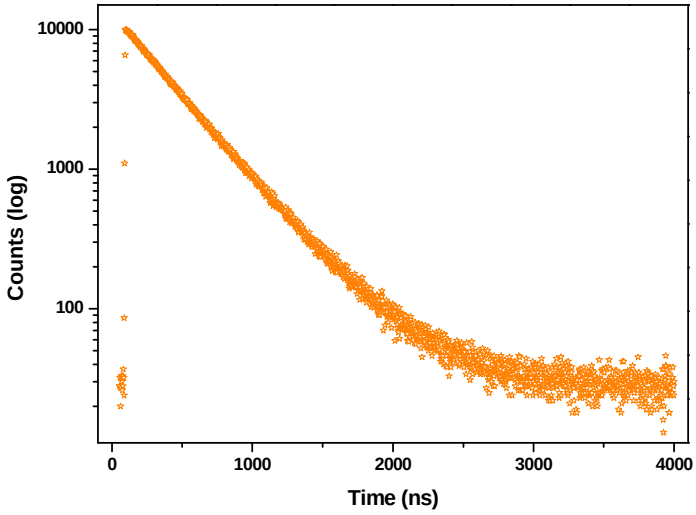

Figure 11. Time-resolved emission decay of **4** in air-equillibrated dichloromethane (λ_{ex}= 460 nm, $\lambda_{monitored}$= λ_{em}=630 nm). Fitting results (χ^2 = 1.07): τ = 0.368 x 10^{-6} s.

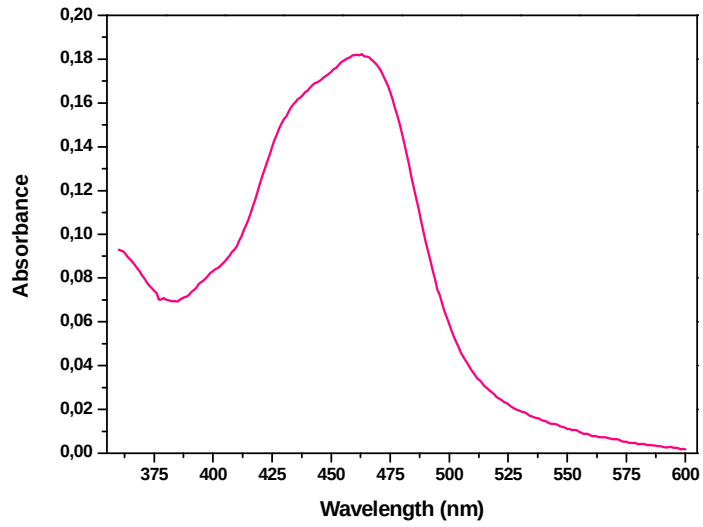

Figure 12. Absorption spectrum of **4** in THF at room temperature.

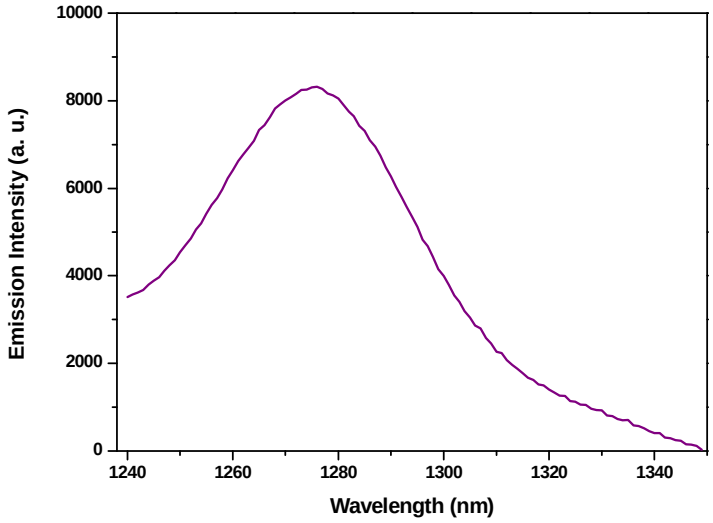

Figure 13. Singlet oxygen phosphorescence upon irradiation at 460 nm of **4** in air-saturated THF.

1@GSNP

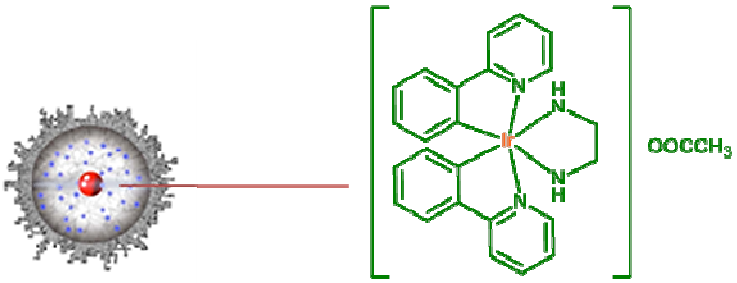

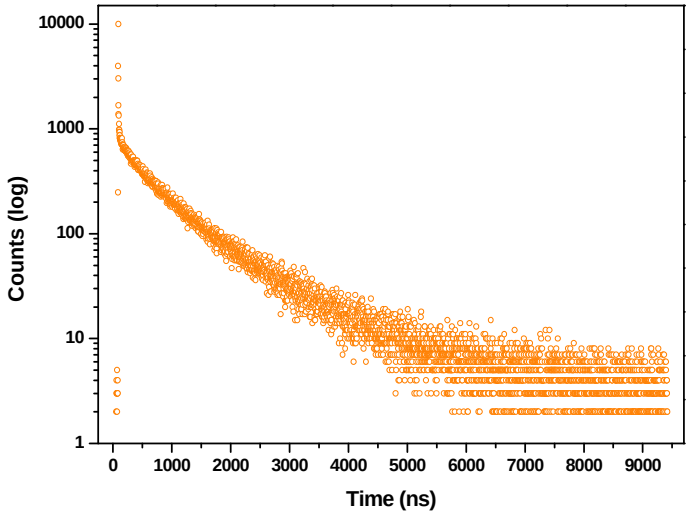

Figure 14. Time-resolved emission decay of **1@GSNP** in water (λ_{ex}= 379 nm). Fitting results (χ^2 = 1.19): τ_1 = 4.08 x 10^{-7} ± 1.19 x 10^{-8} s; α_1= 31.90%; τ_2 = 1.21 x 10^{-6} ± 8.40 x 10^{-9} s; α_2= 68.10%.

2@GSNP

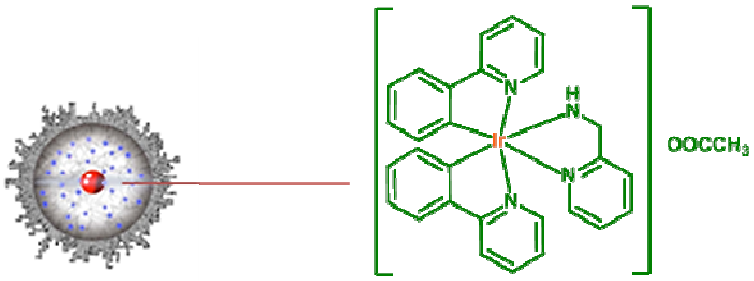

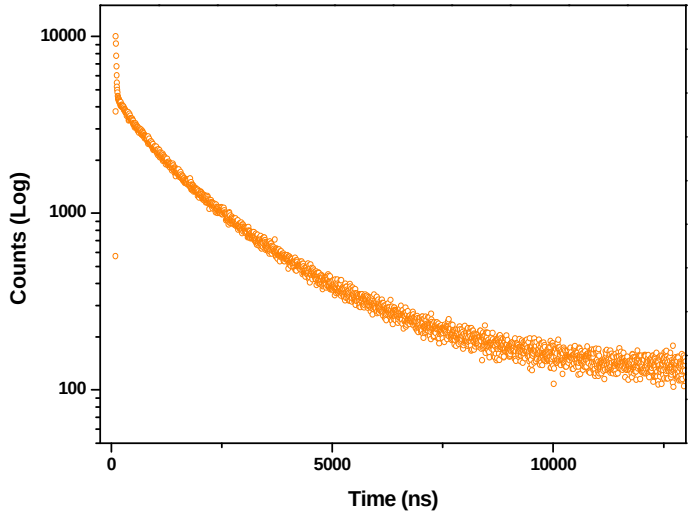

Figure 15. Time-resolved emission decay of **2@GSNP** in water (λ_{ex}= 379 nm, $\lambda_{monitored}$= λ_{em}= 510 nm). Fitting results (χ^2 = 1.02): τ_1 = 8.09 x 10^{-7} ± 1.22 x 10^{-8} s; α_1= 26.08%; τ_2 = 2.39 x 10^{-6} ± 8.23 x 10^{-9} s; α_2= 73.92%.

3@GSNP

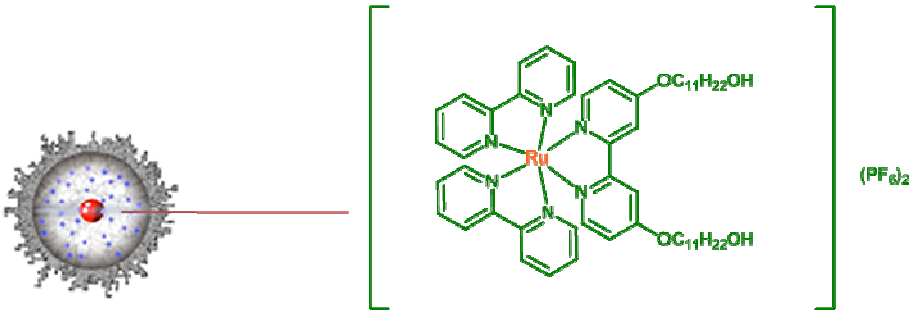

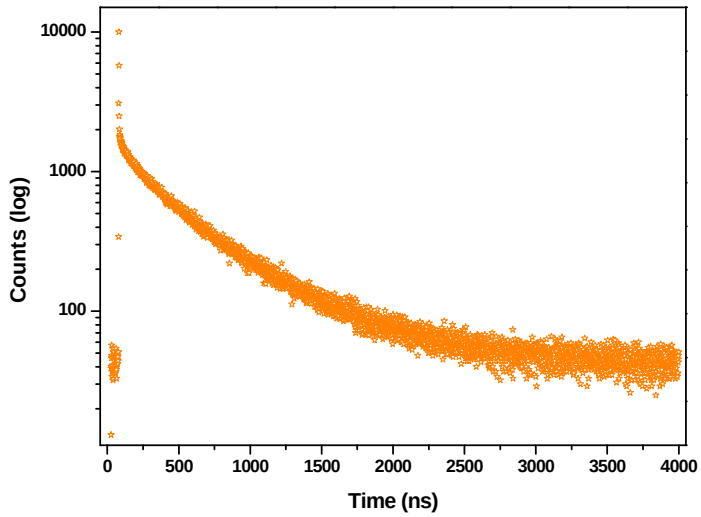

Figure 16. Time-resolved emission decay of **3@GSNP** in water (λ_{ex}= 460 nm, $\lambda_{monitored}$= λ_{em}= 630 nm). Fitting results (χ^2 = 1.05): τ_1 = 1.73 x 10^{-7} ± 6.16 x 10^{-9} s; α_1= 17.02%; τ_2 = 5.85 x 10^{-7} ± 2.71 x 10^{-9} s; α_2= 82.98%.

4@GSNP

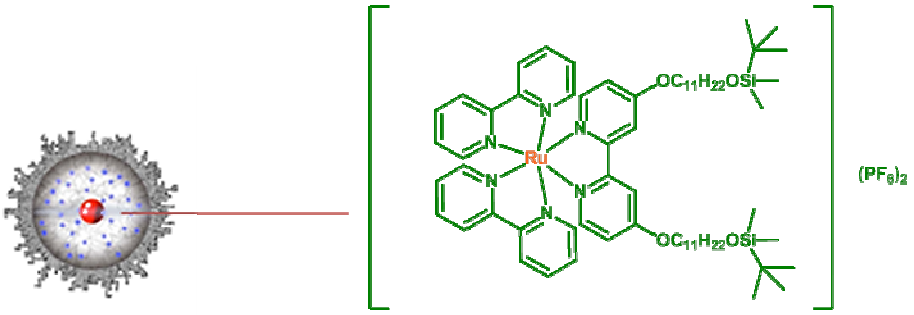

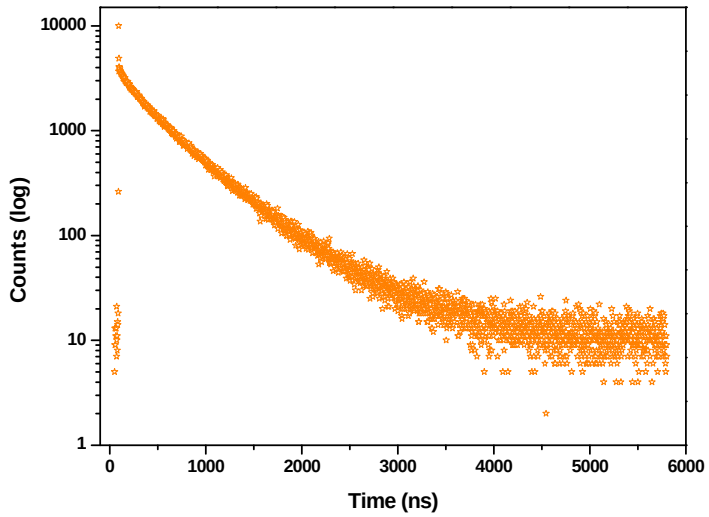

Figure 17. Time-resolved emission decay of **4@GSNP** in water (λ_{ex}= 460 nm, $\lambda_{monitored}$= λ_{em}= 640 nm). Fitting results (χ^2 = 1.08): τ_1 = 2.69 x 10^{-7} ± 6.14 x 10^{-9} s; α_1= 28.73% τ_2 = 6.34 x 10^{-7} ± 2.39 x 10^{-9} s; α_2= 71.27%.

References

- Ali, H., J. E. van Lier, (1999) *Metal complexes as Photo- and Radiosensitizers*. Chem. Rev. 99, 2379-2450.
- Allison, R. R., G. H. Downie, R. Cuenca, X. H. Hu, C. J. H. Childs, C. H. Sibata, (2004) *Photosensitizers in clinical PDT*. Photodiagn. Photodyn. 1, 27-42.
- Allison, R. R., H. C. Mota, V. S. Bagnato and C. H. Sibata, (2008) *Bio-nanotechnology and photodynamic therapy-State of the art review*. Photodiagn. Photodyn. Ther. 5, 19-28.
- Arriagada, F. J., K. Osseo-Asare, (1999) *Synthesis of nanosize silica in a nonionic water-in-oil microemulsion: Effects of the water/surfactant molar ratio and ammonia concentration*. J. Colloid Interface Sci. 211, 210–220.
- Badley, R. D., T. F. Warren, F. J. McEnroe, R. A. Assink, (1990) *Surface modification of colloidal silica*. Langmuir 6, 792-801.
- Baggaley, E., J. A. Weinstein, J. A. G. Williams, (2012) *Lighting the way to see inside the live cell with luminescent transition metal complexe*s. Coord. Chem. Rev. 256, 1762-1785.
- Bagwe, R. P., Y. L. R. Hilliard, W. Tan, (2004) *Optimization of dye-doped silica nanoparticles prepared using a reverse microemulsion method*. Langmuir 20, 8336-8342.
- Bechet, D., P. Couleaud, C. Frochot, M. L. Viriot, F. Guillemin, M. Barberi-Heyob, (2008) *Nanoparticles as vehicles for delivery of photodynamic therapy agents*. Trends biotechnol. 11, 612-621.
- Bellus, D., (1978) *Quenchers of singlet oxygen in singlet oxygen: reactions with organic compounds and polymer*, John Wiley and Sons, New York.
- Boca S. C., M. Four, A. Bonne, B. van der Sanden, S. Astilean, P. L. Baldeck and G. Lemercier, (2009) *An ethylene-glycol decorated ruthenium(II) complex for two photon photodynamic therapy*. Chem. Commun. 30, 4590-4592.
- Brasseur, N., R. Ouellet, C. La Madeleine, J. E. Van Lier, (1999) *Water soluble aluminium phthalocyanine-polymer conjugates for PDT:*

photodynamic activities and pharmacokinetics in tumour-bearing mice. Br. J. Cancer 80, 1533-1541.

- Brinker, C. J., (1988) *Hydrolysis and condensation of silicates: effects on structure*. J. Non-Cryst. Solids 100, 31-50.
- Brown, S. B., E. A. Brown, and I. Walker (2004) *The present and future role of photodynamic therapy in cancer treatment*. Lancet Oncol. 5, 497-508.
- Bruijnincx, P. C. A., P. J. Sadler, (2008) *New Trends for Metal Complexes with Anticancer Activity*. Curr. Opin. Chem. Biol. 12, 197-206.
- Brust, M., M. Walker, D. Bethell, D. J. Schiffrin, R. J. Whyman, (1994) *Synthesis of thiol-derivatized gold nanoparticles in a two-phase liquid-liquid system*. J. Chem. Soc., Chem. Commun. 801-802.
- Capek, I., (2004) *Preparation of metal nanoparticles in water-in-oil (w/o) microemulsions*. Adv. Colloid Interface Sci. 110, 49-74.
- Carter, D., J. X. Ho, (1994) *Advances in Protein Chemistry*. Academic Press, New York, 45, 153-203.
- Celli, J. P., B. Q. Spring, I. Rizvi, C. L. Evans, K. S. Samkoe, S. Verma, B. W. Pogue and T. Hasan, (2010) *Imaging and Photodynamic Therapy: Mechanisms, Monitoring, and Optimization*. Chem. Rev. 110, 2795-2838.
- Choi, M. T. M., P. P. S. Li and D. K. P. Ng, (2000) *A direct comparison of the aggregation behavior of phthalocyanines and 2,3-naphthalocyanines.* Tetrahedron 56, 3881-3887.
- Choi, Y., J. R. McCarthy, R. Weissleder and C. H. Tung, (2006) *Conjugation of a photosensitizer to an oligoarginine-based cell-penetrating peptide increases the efficacy of photodynamic therapy*. ChemMedChem 1, 458-463.
- Cobley, C. M., J. Chen, E. C. Cho, L. V. Wang, Y. Xia, (2011) *Gold nanostructures: a class of multifunctional materials for biomedical applications*. Chem. Soc. Rev. 1, 44-56.
- Connick, W. B., L. M. Henling, R. E. Marsh, H. B. Gray, (1996) *Emission spectroscopic properties of the red form of dichloro(2,2'-bipyridine)platinum(ii). Role of intermolecular stacking interactions*, Inorg. Chem. 35, 6261-6265.
- Costa, R. D., E. Ortì, H. J. Bolink, F. Monti, G. Accorsi, N. Armaroli, (2012) *Luminescent ionic transition-metal complexes for light-emitting*

electrochemical cells. Angew. Chem. Int. Ed. 51, 8178-8211.

- Curri, M. L., A. Agostiano, L. Manna, M. Della Monica, M. Catalano, L. Chiavarone, V. Spagnolo, M. Lugara, (2000) *Synthesis and characterization of CdS nanoclusters in a quaternary microemulsion: the role of the cosurfactant*. J. Phys. Chem. B 104, 8391-8397.
- Daniel, M. C., D. Astruc, (2004) *Gold nanoparticles: assembly, supramolecular chemistry, quantum-size-related properties, and applications toward biology, catalysis, and nanotechnology*. Chem. Rev. 104, 293-346.
- Davies, M. J., (2003) *Singlet oxygen-mediated damage to proteins and its consequences*. Biochem. Biophys. Res. Commun. 305, 761–770.
- De Rosa, M. C., R. J. Crutchley, (2002) *Photosensitized singlet oxygen and its applications.* Coord. Chem. Rev. 233, 351-371.
- Demas, J. N., G. A. Crosby, (1971) *Measurement of photoluminescence quantum yields. Review*. *J. Phys. Chem.* 75, 991-1024.
- Derycke, A. S. L. and P. A. M. de Witte, (2004) *Liposomes for photodynamic therapy.* Adv. Drug Deliv. Rev. 56, 17-30.
- Divsalar, A., M. J. Bagheri, A. A. Saboury, H. Mansoori-Torshizi, M. Amani, (2009) *Investigation on the interaction of newly designed anticancer Pd(II) complexes with different aliphatic tails and Human Serum Albumin*. J. Phys. Chem. B 113, 14035-14042.
- Djurovich, P. I., D. Murphy, M. E. Thompson, B. Hernandez, R. Gao, P. L. Hunt and M. Selke, (2007) *Cyclometalated iridium and platinum complexes as singlet oxygen photosensitizers: quantum yields, quenching rates and correlation with electronic structures.* Dalton Trans. 34, 3763-3770.
- Dougherty, T. J., C. J. Gomer, B. W. Henderson, G. Jori, D. Kessel, M. Korbelik, J. Moan, Q. Peng, (1998) *Photodynamic Therapy*, J. Nat. Cancer Inst. 12, 889-905.
- Dreaden. E. C., A. M. Alkilany, X. Huang, C. J. Murphy, M. A. El-Sayed, (2012) *The golden age: gold nanoparticles for biomedicine*. Chem. Soc. Rev. 41, 40-79.
- Dugaiczyk, A., S. W. Law, O. E. Dennison, (1982) *Nucleotide sequence and the encoded amino acids of human serum albumin mRNA.* Proc. Natl. Acad. Sci. U.S.A. 79, 71-75.

- Edelson, M. F., (1988) *Light-activated drugs*. Sci. Am. 259, 68-75.
- Faridbod, F., M. R. Ganjali, B. Larijani, S. Riahi, A. A. Saboury, M. Hosseini, P. Norouzi, C. Pillip, (2011) *Interaction study of pioglitazone with albumin by fluorescence spectroscopy and molecular docking*. Spectrochim. Acta, Part A. 78, 96-101.
- Farrer, N. J., L. Salassa and P. J. Sadler, (2009) *Photoactivate chemotherapy (PACT): the potential of excited-state d-block metals in medicine.* Dalton Trans. 48, 10690-10701.
- Fernández-Moreira, V., F. L. Thorp-Greenwood, M. P. Coogan, (2010) *Application of d^6 transition metal complexes in fluorescence cell imaging*. Chem. Commun. 46, 186-202.
- Flamigni, L., A. Barbieri, C. Sabatini, B. Ventura, F. Barigelletti, (2007) *Photochemistry and photophysics of coordination compounds: Iridium*. Top Curr. Chem. 281, 143-203.
- Franklin, R. B. and L. C. Costello, (2007) *Zinc as an anti-tumor agent in prostate cancer and in other cancers*. Arch. Biochem. Biophys. 463, 211-217.
- Franklin, R. B. and L. C. Costello, (2009) *The important role of the apoptotic effects of zinc in the development of cancers*. J. Cell. Biochem. 106, 750-757.
- Fujii, M., S. Minobe, M. Usui, S. Hayashi, E. Gross, J. Diener and D. Kovalev, (2004) *Generation of singlet oxygen at room temperature mediated by energy transfer from photoexcited porous Si.* Phis. Rev. B 70, 085311.
- Galanski, M., M. A. Jakupec, B. K. Keppler, (2005) *Update of the preclinical situation of anticancer platinum complexes: novel design strategies and innovative analytical approaches*. Curr. Med. Chem. 12, 2075-2094.
- Gao, R., D. G. Ho, B. Hernandez, M. Selke, D. Murphy, P. I. Djurovich, and M. E. Thompson, (2002) *Bis-cyclometalated Ir(III) complexes as efficient singlet oxygen sensitizers.* J. Am. Chem. Soc. 124, 14828-14829.
- Garcia-Fresnadillo, D., Y. Georgiadou, G. Orellana, A. M. Braun, E. Oliveros, (1996) *Singlet-oxygen ($'\Delta_g$) production by rutheniurn(II) complexes containing polyazaheterocyclic ligands in methanol and in water*. Helv. Chem. Acta 79, 1222-1238.
- Glomm, W. R., J. S. Moses, M. K. Brennaman, J. M. Papanikolas, S. Franzen, (2005) *Detection of adsorption of Ru(II) and Os(II) Polypyridyl complexes on*

gold and silver nanoparticles by single-photon counting emission measurements. J. Phys. Chem. B 109, 804-810.

- Gomes, A. J., L. O. Lunardi, J. M. Marchetti, C. N. Lunardi, A. C. Tedesco, (2005) *Photobiological and ultrastructural studies of nanoparticles of poly(lactic-co-glycolic acid)-containing bacteriochlorophyll-a as a photosensitizer useful for PDT treatment*. Drug Deliv. 12, 159–164.
- Goze, C., J. C. Chambron, V. Heitz, D. Pomeranc, X. J. Salom-Roig, J. P. Sauvage, A. F. Morales, F. Barigelletti, (2003) *Long-lived MLCT excited states-RuII complexes with a helical bis-phen ligand*. Eur. J. Inorg. Chem., 3752-3758.
- Guerrero-Martínez, A., Y. Vida, D. Domínguez-Gutiérrez, R. Q. Albuquerque, L. De Cola, (2008) *Tuning emission properties of Iridium and Ruthenium metallosurfactants in micellar systems*. Inorg. Chem. 47, 9131-9133.
- Guldi, D. M., T. D. Mody, N. N. Gerasimchuk, D. Magda and J. L. Sessler, (2000) *Influence of large metal cations on the photophysical properties of texaphyrin, a rigid aromatic chromophore*. J. Amer. Chem. Soc. 34, 8289-8298.
- Guo, Z., P. J. Sadler, (1999) *Metals in Medicine*. Angew. Chem. Int. Ed. 38, 1512-1531.
- Halliwell, B. and J. M. C. Gutteridge (2007) *Free radical in biology and medicine. Fourth Edition.* Oxford University Press.
- Hambley, T. W., (2007) *Developing new metal-based therapeutics: challenges and opportunities*. Dalton Trans. 43, 4929-4937.
- He, G. S., L.-S. Tan, Q. Zheng and P. N. Prasad, (2008) *Multiphoton absorbing materials: molecular designs, characterizations, and applications*. Chem. Rev. 108, 1245-1330.
- He, X. M. and D. C. Carter, (1992) *Atomic structure and chemistry of human serum albumin*. Nature. 358, 209-215.
- He, X., X. Wu, K. Wang, B. Shi, L. Hai, (2009) *Methylene blue-encapsulated phosphonate-terminated silica nanoparticles for simultaneous in vivo imaging and photodynamic therapy*. Biomaterials 30, 5601–5609.
- Holzer, W., A. Penzkofer, T. Tsuboi, (2005) *Absorption and emission*

spectroscopic characterization of Ir(ppy)$_3$. Chem. Phys. 308, 93-102.

- Hong, S. Y., G. Tobias, K. T. Al-Jamal, B. Ballesteros, H. Ali-Boucetta, S. Lozano-Perez, P. D. Nellist, R. B. Sim, C. Finucane, S. J. Mather, M. L. H. Green, K. Kostarelos and B. G. Davis, (2010) *Filled and glycosylated carbon nanotubes for in vivo radioemitter localization and imaging.* Nature Materials 9, 485-490.
- Huang, X., W. Qian, I. H. El-Sayed, M. A. El-Sayed, (2007) *The potential use of the enhanced nonlinear properties of gold nanospheres in photothermal cancer therapy*. Laser Surg. Med. 39, 747–753.
- Ingram, R. S., M. J. Hostetler, R. W. Murray (1997) *Poly-hetero-ω-functionalized alkanethiolate-stabilized gold cluster compounds*. J. Am. Chem. Soc. 119, 9175-9178.
- Iyer, A. K., G. Khaled, J. Fang, H. Maeda, (2006) *Exploiting the enhanced permeability and retention effect for tumor targeting*. Drug Discovery Today 11, 812-818.
- Jain, P. K., I. H. El-Sayed, M. A. El-Sayed, (2007) *Au nanoparticles target cancer*. Nano Today 2, 18-29.
- Jain, P. K., K. S. Lee, I. H. El-Sayed, M. A. El-Sayed, (2006) *Calculated absorption and scattering properties of gold nanoparticles of different size, shape, and composition: applications in biological imaging and biomedicine*. J. Phys. Chem. B 110, 7238-7248.
- Jamieson, E. R., S. J. Lippard, (1999) *Structure, recognition, and processing of cisplatin-DNA adducts*. Chem. Rev. 99, 2467-2498.
- Josefsen, L. B. and R. W. Boyle, (2008) *Photodynamic therapy and the development of metal-based photosensitizers.* Met.-Based Drugs 2008: 276109.
- Jung, Y., S. J. Lippard, (2007) *Direct cellular responses to platinum-induced DNA damage*. Chem Rev. 107, 1387-1407.
- Juris, A., V. Balzani, F. Barigelletti, P. Belser, A. Von Zelewsky, (1988) *Ru(II) polypyridine complexes: photophysics, photochemistry, electrochemistry, and chemiluminescence*. Coord. Chem. Rev. 84, 85-277.

- Katrahalli, U., S. Jaldappagari, S. S. Kalanur, (2010) *Probing the binding of fluoxetine hydrochloride to human serum albumin by multispectroscopic techniques*. Spectrochimica Acta Part A 75, 314-319.
- Kelland, L., (2007) *The resurgence of platinim-based cancer chemotherapy*. Nat. Rev. Cancer 7, 573-584.
- Kennedy, L. C., L. R. Bickford, N. A. Lewinski , A. J. Coughlin, Y. Hu , E. S. Day , J. L. West , R. A. Drezek, (2011) *A new era for cancer treatment: gold-nanoparticle-mediated thermal therapies*. Small 7, 169-183.
- Kim, S., T. Y. Ohulchanskyy, H. E. Pudavar, R. K. Pandey, P. N. Prasad, (2007) *Organically modified silica nanoparticles co-encapsulating photosensitizing drug and aggregation-enhanced two photon absorbing fluorescent dye aggregates for two photon photodynamic therapy*. J. Am. Chem. Soc. 129, 2669–2675.
- Konan, Y. N., M. Berton, R. Gurny, E. Allemann, (2003) *Enhanced photodynamic activity of meso-tetra(4-hydroxyphenyl)porphyrin by incorporation into sub-200 nm nanoparticles*. Eur. J. Pharm. Sci. 18, 241-249.
- Konan, Y. N., R. Gurny and E. Allemann, (2002) *State of the art in the delivery of photosensitizers for photodynamic therapy*. J. Photochem. Photobiol. B. Biol. 66, 89-106.
- Koo, H., H. Lee, S. Lee, K. H. Min, M.S. Kim, D. S. Lee, Y. Choi, I. C. Kwon, K. Kim, S. Y. Jeong, (2010) *In vivo tumor diagnosis and photodynamic therapy via tumoral pH-responsive polymeric micelles*. Chem. Commun. 46, 5668–5670.
- Kratz, F., (2008) *Albumin as a drug carrier: design of prodrugs, drug conjugates and nanoparticles*. J. Control. Release 132, 171-183.
- Kreibirg, U., M. Vollmer, (1995) *Optical properties of metal clusters*. Springer Series in Material Science 25, Springer, Berlin, 1995.
- Kreimer-Birnbaum, M., (1989) *Modified porphyrins, chlorins, phthalo-cyanines, and purpurins: second generation photosensitizers for photo-therapy*. Semin. Hematol. 26, 157-173.
- Kuimova, M. K., H. A. Collins, M. Balaz, E. Dahlstedt, J. A. Levitt, N. Sergent, K. Suhling, M. Drobizhev, N. S. Makarov, A. Rebane, H. L. Anderson and D. Phillips, (2009) *Photophysical properties and intracellular*

imaging of water-soluble porphyrin dimers for two-photon excited photodynamic therapy. Org. Biomol. Chem. 7, 889-896.

- Kunkely, H., A. Vogler, (1990), *Photoluminescence of platinum complex [PtII(4,7-diphenyl-1,10-phenanthroline)(CN)2] in solution*. J. Am. Chem. Soc. 112, 5625-5627.
- Lai, C. W., Y. H. Wang, C. H. Lai, M. J. Yang, C. Y. Chen, P. T. Chou, C. S. Chan, Y. Chi, Y. C. Chen, J. K. Hsiao, (2008) *Iridium-complex-functionalized Fe_3O_4/SiO_2 core/shell nanoparticles: a facile three in one system in magnetic resonance imaging, luminescence imaging, and photodynamic therapy*. Small 4, 218-224.
- Lakowicz, J. R., (1999) *Principles of fluorescence spectroscopy*. Kluwer Academic/Plenum, New York, NY.
- Lal, M., L. Levy, K. S. Kim, G. S. He, X. Wang, Y. H. Min, S. Pakatchi, P. N. Prasad, (2000) *Silica nanobubbles containing an organic dye in a multilayered organic/inorganic heterostructure with enhanced luminescence*. Chem. Mater. 12, 2632-2639.
- Lal, S. L., S. E. Clare, N. J. Halas, (2008) *Nanoshell-enabled photothermal cancer therapy: impending clinical impact*. Acc. Chem. Res., 41, 1842-1851.
- Lang, K., Mosinger, J., Wagnerova, D. M. (2004) *Photophysical properties of porphirinoid sensitizers non-covalently bound to host molecules; model for photodynamic therapy.* Coord. Chem. Rev. 248, 321-350.
- Leznoff , C. C., A. B. P. Lever, (1996) *Phtalocyanines: properties and applications*, VCH Publishing, New York.
- Lin, S. Y., M. J. Li, Y. S. Wei, (2004) *Ethanol or/and captopril-induced precipitation and secondary conformational changes of human serum albumin*. Spectrochim. Acta, Part A. 60, 3107-3111.
- Liu, X., Y. Du, W. Sun, J. Kou, B. Yu, (2009) *Study on the interaction of levocetirizine dihydrochloride with human serum albumin by molecular spectroscopy*. Spectrochim. Acta A Mol. Biomol. Spectrosc. 74, 1189-1196.
- Liu, Y., R. Hammitt, D.A. Lutterman, L.E. Joyce, R.P. Thummel and C. Turro, (2009) *Ru(II) complexes of new tridentate ligands: unexpected high yield of sensitized $^1O_2$*. Inorg. Chem. 48, 375-385.

- Longo-Sorbello, G. S. A., G. Saydam, D. Banerjee, J. R. Berniti, (2006) *Cytotoxicity and cell growth assays*. In: Celis, J. E. (Ed.), Cell Biology: a Laboratory Handbook, Academic Press, San Diego, pp. 315-324.
- Love, J., L. Estroff, J. Kriebel, R. Nuzzo, G. Whitesides, (2005) *Self-assembled monolayers of thiolates on metals as a form of nanotechnology*. Chem. Rev. 105, 1103-1170.
- Macdonald, I. J. and T. Dougherty, (2001) *Basic principles of photodynamic therapy.* J. Phorphyrins Phthalocyanine 5, 105-129.
- Mandeville, J. S., E. Froehlich, H. A. Tajmir-Riahi, (2009) *Study of curcumin and genistein interactions with human serum albumin*. J. Pharmaceut. Biomed. Anal. 49, 468-474.
- Martin, M.; M.-B. Krogh-Jespersen, M. Hsu, J. Tewksbury, M. Laurent, K. Viswanath, H. Patterson, (1983) *Multistate luminescence, absorption, and MCD studies of the relative energies of d-d, d-□*, and n, □-□* transitions for the cis and trans isomers of dichlorobis(pyridine) platinum(II)*. Inorg. Chem. 22, 647-652.
- Martin, P. C., M. Gouterman, B.V. Pepich, G. E. Renzoni, D. C. Schindele, (1991) *Effects of ligands, solvent, and variable sulfonation on dimer formation of aluminum and zinc phthalocyanine sulfonates.* Inorg. Chem. 30, 3305-3309.
- Martini, M., P. Perriat, M. Montagna, R. Pansu, C. Julien, O. Tillement and S. Roux, (2009) *How gold particles suppress concentration quenching of fluorophores encapsulated in silica beads*. J. Phys. Chem. C 113, 17669-17677.
- Miller, J. M., U. Schmidt-Erfurth, M. Sickenberg, C. J. Pournaras, H. Laqua, I. Barbazetto, L. Zografos, B. Piguet, G. Donati, A.-M. Lane, R. Birngruber, H. van den Berg, H. A. Strong, U. Manjuris, T. Gray, M. Fsadni, N. M. Bressler, E. S. Gragoudas (1999) *Photodynamic therapy with verteporfin for choroidal neovascularization caused by age-related degeneration*. Arch. Ophthalmol. 117, 1161-1173.
- Moan, J., and P. Juzenas, (2004). *Photostability of Drugs and Drug Formulations, 2nd edition*. ed. H. H. Tonnesen. CRC Press, Boca Raton, FL, 189-211.

- Montalti, M., A. Credi, L. Prodi, M. T. Gandolfi, (2006) *Handbook of photochemistry, 3rd edition.* Taylor & Francis Group.
- Munk, V. P., C. I. Diakos, L. T. Ellis, R. R. Fenton, B. A. Messerle and T. W. Hambley, (2003) *Investigations into the interactions between DNA and conformationally constrained pyridylamineplatinum(II) analogues of AMD473*. Inorg. Chem. 42, 3582-3590.
- Mutai, T., J.-D. Cheon, G. Tsuchiya, K. Araki, (2002) *6-Amino-2,2':6',2''-terpyridines as highly fluorescent compounds-effect of the number of pyridine rings on fluorescence properties*. J. Chem. Soc. Perkin Trans. 2, 862-865.
- Nakamaru, K., (1982) *Luminescence quantum yields, and lifetimes of trischelated ruthenium(II) mixed-ligand complexes including 3,3'-dimethyl-2,2'-bipyridyl*. Bull. Soc. Chem. Jpn. 5, 2697-2705.
- Nanda, R. K., N. Sarkar, R. Banerjee, (2007) *Probing the interaction of ellagic acid with human serum albumin: A fluorescence spectroscopic study*. J. Photochem. Photobiol., A. 192, 152-158.
- Nyman, E. S. and P. H. Hynninen, (2004) *Research advances in the use of tetrapyrrolic photosensitizers for photodynamic therapy*. J. Photochem. Photobiol. B 73, 1-28.
- Oar, M. A., J. M. Serin, W. R. Dichtel, J. M. J. Fréchet, T. Y. Ohulchanskyy and P. N. Prasad, (2005) *Photosensitization of singlet oxygen via two-photon excited FRET in aqueous media.* Chem. Mater. 17, 2267-2275.
- Ogilby, P. R., (2010) *Singlet oxygen: there is indeed something new under the sun.* Chem. Soc. Rev. 39, 3181-3209.
- Olenick, N. L., A. K. Antunez, M. E. Clay, B. D. Rihter, M. E.Kenney, (1993) *New phthalocyanine photosensitizers for photodynamic therapy*. J. Photochem. Photobiol. 57, 242-247.
- Oppenländer, T., (2003) *Photochemical Purification of Water and Air*, Weinheim, Germany: Wiley-VCH Verlag.
- Orvig, C., M. J. Abrams, (1999) *Medicinal inorganic chemistry: introduction*. Chem Rev. 99, 2201-2203.
- Paszko, E., C. Ehrhardt, M. O. Senge, D. P. Kelleher and J. V. Reynolds, (2011) *Nanodrug applications in photodynamic therapy.* Photodiagn. Photodyn. Ther. 8, 14-29.

- Peacock, A. F. A., Sadler, (2008) *Medicinal Organometallic Chemistry: Designing Metal Arene Complexes as Anticancer Agents*. Chem. Asian J. 3, 1890-1899.
- Peng, C. L., L.Y. Yang, T. Y. Luo, P. S. Lai, S. J. Yang, W. J. Lin and M. J. Shieh, (2010) *Development of pH sensitive 2-(diisopropylamino)ethyl methacrylate based nanoparticles for photodynamic therapy*. Nanotechnology 21, 155103.
- Perez-Juste, J., I. Pastoriza-Santos, L. M. Liz-Marzan, P. Mulvaney, (2005) *Gold nanorods: synthesis, characterization and applications*. Coord. Chem. Rev. 249, 1870-1901.
- Peters, T., (1996) *All about albumin: biochemistry, genetics and medical applications*. Academic Press, San Diego (CA).
- Pucci, D., T. Bellini, A. Crispini, I. D'Agnano, P.F. Liguori, P. Garcia-Orduña, S. Pirillo, A. Valentini and G. Zanchetta, (2012) *DNA binding and cytotoxicity of fluorescent curcumin-based Zn(II) complexes*. Med. Chem. Commun. 3, 462-468.
- Puoci, F., F. Iemma, M. Curcio, O. I. Parisi, G. Cirillo, U. G. Spizzirri and N. Picci, (2008) *Synthesis of methacrylic-ferulic acid copolymer with antioxidant properties by single-step free radical polymerization.* J. Agric. Food Chem. 56, 10646-10650.
- Qi, Z. D., B. Zhou, Q. Xiao, C. Shi, Y. Liu, J. Dai, (2008) *Interaction of rofecoxib with human serum albumin: Determination of binding costants and the binding site by spectroscopic methods*. J. Photochem. Photobiol., A. 193, 81-88.
- Qiu, W., L. Zhang, O. Okobiah, Y. Yang, L. Wang, D. Zhong, A. H. Zewail, (2006) *Ultrafast solvation dynamics of human serum albumin: correlations with conformational transitions and site-selected recognition*. J. Phys. Chem. 110, 10540-10549.
- Ramachandra, S., F. Polo, F. Edafe, K. C. Schuermann, C. A. Nijhuis, P. Belser, W. F. Reus, G. M. Whitesides, L. De Cola, (2011) *Luminescent acetylthiol derivative tripodal osmium(II) and iridium(III) complexes: Spectroscopy in solution and on surfaces*. Pure Appl. Chem. 83, 779-799.

- Redmond, R. W., J. N. Gamlin, (1999) *A compilation of singlet oxygen yields from biologically relevant molecules*. Photochem. Photobiol. 70, 391-475.
- Ricciardi, L., F. Puoci, G. Cirillo, M. La Deda, (2012) *A new member of the oxygen-photosensitizers family: a water-soluble polymer binding a platinum complex*. Dalton Trans. 41, 10923-1925.
- Ricci-Junior, E., J. M. Marchetti, (2006) *Preparation, characterization, photocytotoxicity assay of PLGA nanoparticles containing zinc (II) phthalocyanine for photodynamic therapy use*. J. Microencapsul. 23, 523-538.
- Rosenthal, I., (1985) *Singlet oxygen,* ed. A. A. Frimer, CRC Press, Boca Raton, vol.I, 13-38.
- Roy, I., T. Y. Ohulchanskyy, H. E. Pudavar, E .J. Bergey, A. R. Oseroff, J. Morgan, T. J. Dougherty, P. N. Prasad, (2003) *Ceramic-based nanoparticles entrapping water-insoluble photosensitizing anticancer drugs: a novel drug-carrier system for photodynamic therapy*. J. Am. Chem. Soc. 125, 7860-7865.
- Ruggi, A., F. W. B. van Leeuwen, A. H. Velders, (2011) *Interaction of dioxygen with the electronic excited state of Ir(III) and Ru(II) complexes: Principles and biomedical applications*. Coord. Chem. Rev. 255, 2542-2554.
- Schaap A.P, A.L Thayer, E.C Blossey, D.C Neckers, (1975) *Polymer-based sensitizers for photooxidations.* J. Am. Chem. Soc., 97, 3741-3745.
- Schaffner-Hamann, C., A. Von Zelewsky, A. Barbieri, F. Barigelletti, G. Muller, J. P. Riehl, A. Neels, (2004) *Diastereoselective formation of chiral tris-cyclometalated Iridium (III) complexes: characterization and photophysical properties*. J. Am. Chem. Soc. 126, 9339-9348.
- Schmidt, R., (1989) *Influence of heavy atoms on the deactivation of singlet oxygen* $^1\Delta_g$ *in solution.* J. Am. Chem. Soc. 111, 6983-6987.
- Schmidt, R., (2006) *Photosensitized generation of singlet oxygen.* Photochem. Photobiol. 82, 1161-1177.
- Sharman, W. M., G. M. Allen, J. E. VanLier, (1999) *Photodynamic therapeutics: basic principles and clinical applications.* Drug Discov. Today 4, 507-517.
- Shavaleev, N. M., H. Adams, J. Best, R. Edge, S. Navaratnam and J. A. Weinstein, (2006) *Deep-red luminescence and efficient singlet oxygen generation by cyclometalated platinum(II) complexes with 8-*

hydroxyquinolines and quinoline-8-thiol. Inorg. Chem. 45, 9410-9415.

- Soukos, N. S., M. R. Hamblin, T. Hasan, (1997) *The effect of charge on cellular uptake and phototoxicity of polysine chlorin(e) conjugate*. Photochem. Photobiol. 65, 723-729.
- Sternberg, E. D., D. Dolphin and C. Brückner, (2001) *Porphyrin-based photosensitizers for use in photodynamic therapy*. Tetrahedron 47, 9513-9547.
- Sudlow, G., D. J. Birkett, D. N. Wade, (1975) *The characterization of two specific drug binding sites on human serum albumin*. Mol. Pharmacol. 11, 824-832.
- Sudlow, G., D. J. Birkett, D. N. Wade, (1976) *Further characterization of specific drug binding sites on human serum albumin*. Mol. Pharmacol. 12, 1052-1061.
- Sulkowska, A., (2002) *Interaction of drugs with bovine and human serum albumin*. J. Mol. Struct. 614, 227-232.
- Sumer, B., J. Gao, (2008) *Theranostic nanomedicine for cancer*. Nanomedicine 3, 137-140.
- Szacilowski, K., W. Macyk, A. Drzewiecka-Mutuszek, M. Brindell and G. Stochel, (2005) *Bioinorganic Photochemistry: Frontiers and Mechanisms*. Chem. Rev. 105, 2647-2694.
- Tarushi, A., C. P. Raptopoulou, V. Psycharis, A. Terzis, G. Psomas, D. P. Kessissoglou, (2010) *Zinc(II) complexes of the second-generation quinolone antibacterial drug enrofloxacin: structure and DNA or albumin interaction*. Bioorg Med. Chem. 18, 2678-2685.
- Templeton, A. C., W. P. Wuelfing, R. W. Murray, (2000) *Monolayer-Protected Cluster Molecules*. Acc. Chem. Res. 33, 27-36.
- Thompson, K. H., C. Orvig, (2006) *Metal complexes in medicinal chemistry: new vistas and challenges in drug design*. Dalton Trans. 6, 761-764.
- Tijerina, M., K. D. Fowers, P. Kopeckova`, J. Kopecek, (2000) *Chronic exposure of human ovarian carcinoma cells to free or HPMA copolymer-bound mesochlorin e does not induce p-glycoprotein-mediated multidrug resistance*. Biomaterials 21, 2203-2210.

- Trnková, L., I. Boušová, V. Staňková, J. Dršata, (2011) *Study on the interaction of catechins with human serum albumin using spectroscopic and electrophoretic techniques*. J. Mol. Struct. 985, 243-250.
- Trynda-Lemiesza, L., K. Wiglusza, (2010) *Interactions of human serum albumin with meloxicam. Characterization of binding site*. J. Pharm. Biomed. Anal. 52, 300-304.
- Tu, H. L., Y. S. Lin, H. Y. Lin, Y. Hung, L. W. Lo, Y. F. Chen and C. Y. Mou, (2009) *In-vitro studies of functionalized mesoporous silica nanoparticles for photodynamic therapy*. Adv. Mater. 21, 172-177.
- van Nostrum, C. F., (2004) *Polymeric micelles to deliver photosensitizers for photodynamic therapy*. Adv. Drug Deliv. Rev. 56, 9-16.
- van Zutphen, S., J. Reedijk, (2005) *Targeting platinum anti-tumour drugs: Overview of strategies employed to reduce systemic toxicity*. Coord Chem Rev. 249, 2845-2853.
- Vivero-Escoto, J. L., Y. T. Huang, (2011) *Inorganic-organic hybrid nanomaterials for therapeutic and diagnostic imaging applications*. Int. J. Mol. Sci. 12, 3888-3927.
- Wang, D., S. J. Lippard, (2005) *Cellular processing of platinum anticancer drugs*. Nat. Rev. Drug Discovery 4, 307-320.
- Wang, H., R., Shen, J. Wu, N. Tang, (2009) *Antitumor activity and dna-binding investigations of the Zn(ii) and Cu(ii) complexes with isoeuxanthone*. Chem. Pharm. Bull. 57, 814-818.
- Wang, L., W. Tan, (2006) *Multicolor FRET silica nanoparticles by single wavelength excitation*. Nano. Lett. 6, 84-88.
- Westermann, P., T. Glanzmann, S. Andrejevic, D. R. Braichotte, M. Van Lier, M. Forrer, G. A. Wagnieres, Ph. Monnier, H. van den Berg, J.-P. Mach, S. Follio, (1998) *Long circulating half-life and high tumor selectivity of the photosensitizer meta-tetrahydroxyphenylchlorin conjugated to poly-ethylene gylcol in nude mice grafted with a human colon carcinoma*. Int. J. Cancer 76, 842-850.
- Wieder, M. E., D. C. Hone, M. J. Cook, M. M. Handsley, J. Gavrilovic, D. A. Russell, (2006) *Intracellular photodynamic therapy with photosensitizer-nanoparticle conjugates: cancer therapy using a 'Trojan horse'*, Photochem.

Photobiol. Sci. 5, 727-734.

- Wilkinson, F., W. P. Helman, A. B. Ross, (1993) *Quantum yields for the photosensitized formation of the lowest electronically excited singlet-state of molecular oxygen in solution.* J. Phys. Chem. Ref. Data. 22, 113-262.
- Williams, J. A. G., (2007) *Photochemistry and Photophysics of Coordination Compounds: Platinum.* Top. Curr. Chem. 281, 205-268.
- Wu, F. Y., L.-N. Zhang, Z.-J. Ji, X.-F. Wan, (2010) *Spectroscopic investigation of the interaction between thiourea-zinc complex and serum albumin*. J. Lumin. 130, 1280-1284.
- Wu, Q., C. Li, Y. J. Hu, Y. Liu, (2009) *Study of caffeine binding to human serum albumin using optical spectroscopic methods*. Sci. China Ser. B-Chem. 52, 2205-2212.
- Wu, S., C. Zhu, C. Zhang, Z. Yu, W. He, Y. He, Y. Li, J. Wang, Z. Guo, (2011) *In vitro and in vivo fluorescent imaging of a monofunctional chelated platinum complex excitable using visible light*. Inorg. Chem. 50, 11847-11849.
- Wu, S.-S., W.-B. Yuan, H.-Y. Wang, Q. Zhang, M. Liu, K.-B. Yu, (2008) *Synthesis, crystal structure and interaction with DNA and HSA of (N,N'-dibenzylethane-1,2-diamine) transition metal complexes*. J. Inorg. Biochem. 102, 2026-2034.
- Xu, H., C. Liu, J. Mei, C. Yao, S. Wang, J. Wang, Z. Li, Z. Zhang, (2012) *Effects of light irradiation upon photodynamic therapy based on 5-aminolevulinic acid-gold nanoparticle conjugates in K562 cells via singlet oxygen generation*. Int. J. Nanomedicine. 7, 5029-5038.
- Yang, F., C. Bian, L. Zhu, G. Zhao, Z. Huang, M. Huang, (2007) *Effect of human serum albumin on drug metabolism: structural evidence of esterase activity of human serum albumin*. J. Struct. Biol. 157, 348-355.
- Yi, D. K., I. C. Sun, J. H. Ryu, H. Koo, C. W. Park, I. C. Youn, K. Choi, I. C. Kwon, K. Kim, C. H. Ahn, (2010) *Matrix metalloproteinase sensitive gold nanorod for simultaneous bioimaging and photothermal therapy of cancer*. Bioconjug. Chem. 21, 2173-2177.

- Yu, M., Q. Zhao, L. Shi, F. Li, Z. Zhou, H. Yang, T. Yia, C. Huanga, (2008) *Cationic iridium(III) complexes for phosphorescence staining in the cytoplasm of living cells*. Chem. Commun. 18, 2115-2117.
- Yue, Y., X. Chen, J. Qin, X. Yao, (2009) *Spectroscopic investigation on the binding of antineoplastic drug oxaliplatin to human serum albumin and molecular modeling*. Colloids Surf., B. 69, 51-57.
- Zhang, G., Q. Que, J. Pan, J. Guo, (2008) *Study of the interaction between icariin and human serum albumin by fluorescence spectroscopy*. J. Mol. Struct. 881, 132-138.
- Zhang, J., L. D. Sun, C. Qian, C. S. Liao, C. H. Yan, (2001) *Synthesis and optical properties of nanosized CdS prepared in a quaternary CTAB/ n-hexanol/n-heptane/water reverse micelle*. Chin. Sci. Bull. 46, 1873-1877.
- Zhang, S. J., M. Hosaka, T. Yoshihara, K. Negishi, Y. Iida, S. Tobita, T. Takeuchi, (2010) *Phosphorescent light-emitting iridium complexes serve as a hypoxia-sensing probe for tumor imaging in living animals*. Cancer Res. 70, 4490-4498.
- Zhao, L. (2001) *Singlet Oxygen*; Free Radical and Radiation Biology Graduate Program, The University of Iowa: Iowa City, IA.
- Zhou, B., Z. D. Qi, J. X. Dong, Y. Z. Zhang, Y. Liu, (2007) *Interaction of loratadine with serum albumins studied by fluorescence quenching method*. J. Biochem. Biophys. Methods. 70, 743-747.
- Zimcik, P., M. Miletin, K. Kopecky, Z. Musil, P. Berka, V. Horakova, H. Kucerova, J. Zbytovska and D. Brault, (2007) *Influence of aggregation on interaction of lipophilic, water-insoluble azaphthalocyanines with DOPC vesicles.* Photochem. Photobiol. 1497-1504.

Acknowledgments

First of all, I would like to express my gratitude to Dr. Massimo La Deda for being an excellent supervisor and extraordinary professor, a great example that I hope to match in the future.

I am grateful to Prof. Mauro Ghedini, Prof. Alessandra Crispini, Prof. Daniela Pucci and Dr. Iolinda Aiello for their valuable scientific support.

I would like to thank Prof. Olivier Tillement and his research team (Laboratoire de Physico-Chimie des Matériaux Luminescents, Université Claude Bernard Lyon 1) for collaboration and hospitality, with special thanks to Matteo Martini and Lucie Sancey Galliot, it was a pleasure working with them on this project.

I would also like to thank Dr. Elisabeta I. Szerb, Dr. Anna Maria Talarico, Dr. Paola Liguori, Dr. Sante Pirillo for their contribution, and my colleagues Yogesh Yadav, Andreea Ionescu and Barbara Sanz for all the good moments spent together.

This dissertation is dedicated to my grandparents ... their joy would have been without measure.